Hashemite Kingdom of Jordan

Scientific Research Support Fund

Hashemite University

Jordan Journal of Earth and Environmental Sciences

JJEES

An International Peer-Reviewed Scientific Journal

Financed by the Scientific Research Support Fund

http://jjees.hu.edu.jo/

Volume (7) Number (1) ISSN 1995-6681 June 2015 / Shaban 1436

The Jordan Journal of Earth and Environmental Sciences (JJEES)

JJEES is an international peer-reviewed research journal, issued by the Deanship of Academic Research and Graduate Studies, the Hashemite University, in corporation with, the Jordanian Scientific Research Support Fund, the Ministry of Higher Education and Scientific Research.

SUBMISSION ADDRESS:

Professor **Eid A. Al-Tarazi**
Deanship of Academic Research and Higher Studies
Hashemite University, P.O. Box 150458, Postal Code 13115, Zarqa, Jordan.
Phone: +962-5-3903333 ext.4229
E-Mail: jjees@hu.edu.jo

Hashemite Kingdom of Jordan

Scientific Research Support Fund

Hashemite University

Jordan Journal of Earth and Environmental Sciences

JJEES

An International Peer-Reviewed Scientific Journal

Financed by the Scientific Research Support Fund

Volume 7 Number (1)

http:// jjees.hu.edu.jo/

ISSN 1995-6681

المجلة الأردنية لعلوم الأرض والبيئة
Jordan Journal of Earth and Environmental Sciences (JJEES)
http://jjees.hu.edu.jo

Hashemite University

Deanship of Scientific Research and Graduate Studies

TRANSFER OF COPYRIGHT AGREEMENT

Journal publishers and authors share a common interest in the protection of copyright: authors principally because they want their creative works to be protected from plagiarism and other unlawful uses, publishers because they need to protect their work and investment in the production, marketing and distribution of the published version of the article. In order to do so effectively, publishers request a formal written transfer of copyright from the author(s) for each article published. Publishers and authors are also concerned that the integrity of the official record of publication of an article (once refereed and published) be maintained, and in order to protect that reference value and validation process, we ask that authors recognize that distribution (including through the Internet/WWW or other on-line means) of the authoritative version of the article as published is best administered by the Publisher.

To avoid any delay in the publication of your article, please read the terms of this agreement, sign in the space provided and return the complete form to us at the address below as quickly as possible.

Article entitled:----------

Corresponding author: ----------

To be published in the journal: Jordan Journal of Earth & Environmental Sciences (JJEES)

I hereby assign to the Hashemite University the copyright in the manuscript identified above and any supplemental tables, illustrations or other information submitted therewith (the "article") in all forms and media (whether now known or hereafter developed), throughout the world, in all languages, for the full term of copyright and all extensions and renewals thereof, effective when and if the article is accepted for publication. This transfer includes the right to adapt the presentation of the article for use in conjunction with computer systems and programs, including reproduction or publication in machine-readable form and incorporation in electronic retrieval systems.
Authors retain or are hereby granted (without the need to obtain further permission) rights to use the article for traditional scholarship communications, for teaching, and for distribution within their institution.

☐ **I am the sole author of the manuscript**

☐ **I am signing on behalf of all co-authors of the manuscript**

☐ **The article is a 'work made for hire' and I am signing as an authorized representative of the employing company/institution**

Please mark one or more of the above boxes (as appropriate) and then sign and date the document in black ink.

Signed:_____ **Name printed:** _____

Title and Company (if employer representative) : _____

Date: _____

Data Protection: By submitting this form you are consenting that the personal information provided herein may be used by the Hashemite University and its affiliated institutions worldwide to contact you concerning the publishing of your article.

Please return the completed and signed original of this form by mail or fax, or a scanned copy of the signed original by e-mail, retaining a copy for your files, to:

Hashemite University
Deanship of Scientific Research and Graduate Studies
Zarqa 13115 Jordan
Fax: +962 5 3903338
Email: jjees@hu.edu.jo

Subscription

Jordan Journal of Earth & Environmental Sciences (ISSN 1995-6681)
An International Peer- Reviewed Research Journal
Published by the deanship of Research and Graduate Studies- The Hashemite University

Name:	الاســـــــــــم:
Specialty:.....	التخصـــــــــص:
Address:.....	العنـــــــــوان:
P.O. Box:.....	صنـــدوق البريـــــد:
City & Postal Code:	المدينة: الرمز البريدي:
Country:.....	الـــــــــــدولة:
Phone:.....	رقـــم الهاتـــــف:
Fax No:.....	رقـــم الفاكـــــس:
E-mail:.....	البريـــد الإلكترونـــي:
Method of payment:	طريقـــــة الدفـــع:
Amount Enclosed:.....	المبلـــــغ المرفـــق:
Signature:.....	التوقيـــــــــع:

Cheques should be paid to Deanship of Research and Graduate Studies- The Hashemite University

I would like to subscribe to the Journal:

For

- ☐ One year
- ☐ Two years
- ☐ Three years

One year Subscription Rates		
	Inside Jordan	Outside Jordan
Individuals	10JD	70$
Students	5JD	35$
Institutions	20JD	90$

Correspondence

Subscriptions and sales:

Prof. Dr. Eid Al-Tarazi
The Hashemite University
P.O. Box 330127- Zarqa 13115 - Jordan
Tel. +962-(0) 795651567 (mobile)
+962-5-3903333 - 4229 (office)
Fax: +962 5 3903338
Email: jjees@hu.edu.jo

JJEES
Jordan Journal of Earth and Environmental Sciences

JJEES
Jordan Journal of Earth and Environmental Sciences

Volume 7, (Number 1), June, 2015
ISSN 1995-6681
Pages 1 - 9

Studies on Adsorptive Removal of Some Heavy Metal Ions by Calix[4]Resorcine

Salah A. Al-Trawneh*

Assistant Professor, Department of Chemistry, Mutah University, P.O. BOX 7, Mutah 61710, AlKarak

Received 17 March, 2015; Accepted 23 April, 2015

Abstract

Removal of heavy metal ions (Mn(II), Cu(II), Co(II), Zn(II), and Pb(II)) from aqueous solutions was carried out using C-4-hydroxyphenylcalix[4]resorcinarene as adsorbent surface. The effect of various parameters, such as solution pH, contact time and temperature on the adsorption capacity of C-4-hydroxyphenylcalix[4]resorcinarene for the selected heavy metal ions, was investigated and optimized. The experimental data were investigated using three kinetic models: Santosa first order, Largergen pseudo second order and Ho pseudo second order. Ho pseudo second order model described the adsorption process with high correlation coefficient (R^2) compared to the other two models. The selectivity of the adsorbent toward a mixture of heavy metal ions was studied and revealed that the removal percentage of the heavy metal ions in a mixture is ranked differently from the separate heavy metal ions. Three adsorption equilibrium isotherm models - Freundlich, Langmuir and Temkin - were applied on the adsorption experimental data. It was found that the Langmuir model well described the adsorption process much better than the other isotherm models. In addition, the thermodynamic parameters of the adsorption processes for the heavy metal ions were calculated and found to be as follows: negative ΔH^o indicating exothermic processes; negative ΔG^o indicating spontaneous processes.

Keywords: C-4-Hydroxyphenylcalix[4]resorcinarene, adsorption, heavy metal ions, kinetic, isotherm, atomic absorption spectroscopy.

1. Introduction

Organic and inorganic pollutants are discharged into the environment from different sources, especially industrial wastes. Heavy metal ions, such as (Pd, Cu, Cd, Zn, Ni, etc.), are considered one of the main sources of water pollutants (Samiey et. al., 2014; Tuama and Mohammed, 2014). Most of the heavy metal ions are highly toxic, non-biodegradable and easily accumulative to toxic levels. The bio-accumulation of these ions in human bodies may damage or reduce the central nervous system, or may cause a kidney and a liver damage (Ahmad et. al., 2013). According to the World Health Organization (WHO), the regular limits of specific heavy metal ions in drinking water should not exceed 0.01, 2.0, 0.007, 0.003 and 5.0 mg/L for Pd, Cu, Ni, Cd and Zn, respectively (W.H.O., 1996). Therefore, such heavy metal ions must be removed from wastewater before discharging it into the ecosystem.

Among the various contaminants, which are found in water, heavy metal ions require special techniques for their removal, due to their toxicity, even though the environment has low concentrations (Harris, 1996). Several methods, such as precipitation (Esalah et. al., 2000), solvent extraction (Lertlapwasin et. al., 2010), coagulation/flotation (Rubio et. al., 2002; Ghurye et. al., 2004), ultrafiltration (Yurloval et. al., 2002), reverse osmosis (Greenlee et. al., 2009; Benit and Ruiz, 2002), electrochemical treatment (Emamjomeh and Sivakumar, 2009), and ion-exchange methods (Mahmoud and Hoadley, 2012) investigated wastewater treatment. However, most of these techniques are very expensive, with a low efficiency and are inapplicable to treat low concentration levels of heavy metal ions in wastewater (Tuama and Mohammed, 2014).

The adsorption technique is a well-known separation method which is considered to be a promising alternative for environmental control (Ren et. al., 2008) and is considered to be an economic and efficient method for the removal of pollutants from water pollutant. In addition, the adsorbent can be regenerated by a suitable desorption procedure (Pan et. al., 2009). Different kinds of conventional and non-conventional adsorbents, such as activated carbon (Uzun and Güzel, 2000), zeolites (Biskup and Subotic, 2004; Cincotti et. al., 2006), clays (Gier and Johns, 2000; Koppelman and Dillard, 1977), polymers and agricultural wastes (O'Connell et. al., 2008; Dang et. al., 2009; Zewail and El-Garf, 2010) were used for the removal of heavy metal ions.

Recently, macromolecules have attracted the attention of chemists due to their use as baskets for trapping molecules or ions (Gutsche, 1988). The unique geometry of calixarenes, which are a family of macrocyclic oligophenols, and the presence of active sites - mainly OH groups - will allow them to form host-guest complexes with neutral molecules and ions (Kunsagi et. al., 2005). A number of calix[n]arene derivatives, such as calix[4]arene (Tabakci et. al., 2006), calix(aza)crown and its oligomeric analog (Akkus et. al.,

* Corresponding author. e-mail: salah_trawneh@yahoo.com

2009), calix[6]-Na-hexasulphonate (Kunsagi et. al., 2005) etc, were successfully shown to adsorb toxic heavy metal ions. In addition, calix[n]arene derivatives can be also used to adsorb dye waste (Ming et. al., 2011).

The present study is focused on the investigation of the adsorption efficiency of the synthesized C-4-hydroxyphenylcalix[4]resorcinarene as adsorbent surface for the heavy metal ions (Mn(II), Cu(II), Co(II), Zn(II), and Pb(II)). Moreover, isotherm models, kinetic modeling, thermodynamic, and selectivity studies of the adsorption of the selected heavy metal ions onto C-4-hydroxyphenylcalix[4] resorcinarene were carried out, calculated and presented.

2. Experimental

Apparatus and instrumentation

The pH measurements were done using glass electrode pH meter model pH 525 (WTW®, Weilheim, Germany). The pH meter was calibrated using pH 4, pH 7 and pH 10 buffer solutions at 25°C according to a standard method (Andrew et. al., 2005). Heavy metal ions concentrations were measured using an Atomic Absorption Spectrophotometer (AAS) Model AA-6200 (Shimadzu®, Kyoto, Japan). The AAS was equipped with a hollow cathode lamp and a 10 cm long slot-burner head and air/acetylene flame. The operating conditions adjustments in the spectrophotometer were carried out according to the standard guidelines of the manufacturer. The hollow cathode lamp and emission wavelength, slit width, the correct coefficient for the calibration straight line, the working linear range and detection limit were determined for each heavy metal ions. The optimum parameters for AAS used to determine the concentrations of different heavy metals are listed in Table 1. Figure 1 shows the linear calibration curve for each heavy metal ion used in the present study. Standard solutions of each heavy metal ion were prepared in order to obtain these calibration curves for the five heavy metal ions used in this study.

Table 1. Standard parameters used in determination of different heavy metal ions using Atomic Absorption Spectrophotometer (Shimadzu, AA-6200)

Heavy metal ion	Wave length (nm)	Slit width (nm)	Flow of fuel (L/min)	Lamp current (mA)	Flame description
Pb(II)	217.0	0.7	2.0	12	Air-Acetylene
Cu(II)	324.7	0.7	1.8	6	Air-Acetylene
Mn(II)	280.1	0.2	2.0	10	Air-Acetylene
Zn(II)	213.9	0.7	2.0	8	Air-Acetylene
Co(II)	240.7	0.2	2.2	12	Air-Acetylene

Adsorbent

As illustrated in scheme 1, C-4-hydroxyphenylcalix[4] resorcinarene 3 adsorbent was synthesized according to the previously published method (Weinelt and Schneider,1991).

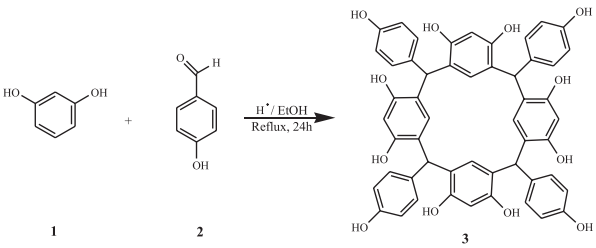

Scheme 1. Preparation of C-4-hydroxyphenylcalix[4]resorcinarene adsorbent 3

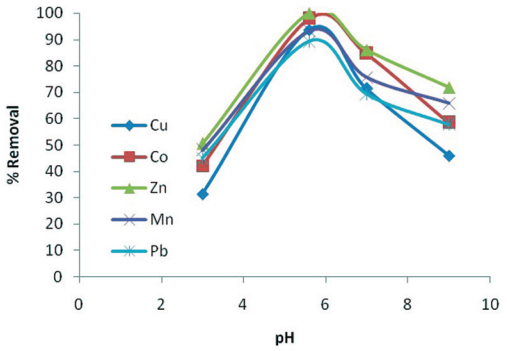

Figure 1. Linear calibration curves for selected heavy metal ions Cu(II); Mn(II); Zn(II); Pb(II); and Co(II)

Effect of pH

The adsorption experiments were carried out at different pH values. A 0.1 g sample of the C-4-hydroxyphenylcalix[4] resorcinarene adsorbent 3 was added to a 100 mL of each heavy metal ion solution with initial concentration of 1 ppm. The adsorption was investigated at pH = 3.0; 5.6; 7.0, 9.0. The mixtures were mechanically agitated at room temperature for 30 min. The solid adsorbent was filtered and the absorbance of the filtrate was measured using AAS spectrometry to determine the final heavy metal ion concentration.

Effect of contact time

The effect of the contact time on the adsorption efficiency was investigated by running a different agitation time in the range of 2–30 min. A 0.1 g sample of the C-4-hydroxyphenylcalix[4]resorcinarene adsorbent 3 was added into 100 mL of each metal ion solution with initial concentration of 1 ppm at the measured optimum pH. The contents of the flask were agitated at 25°C for time intervals of 2, 5, 7, 10, 15, 20, 25, 30 min .The residual concentration of the heavy metal ion in the blank and solution samples was determined using AAS. Blank solution serves as a controller for the presence of the heavy metal ion, which was precipitated after treatment.

Selectivity and competition study

A 0.1 g sample of the C-4-hydroxyphenylcalix[4] resorcinarene adsorbent 3 was added to a 100 mL of an aqueous solution containing a mixture of heavy metal ions with initial concentration of 1 ppm of each heavy metal ion at optimum pH. After shaking in a thermostatic system (25°C) for 10 min; the adsorbent was filtered and the concentration of the heavy metal ions in the filtrate was determined using AAS through dilution with distilled water.

Data Analysis

The removal of the selected heavy metal ions used in this study was calculated from the mass balance, which was stated as the amount of metal ions adsorbed onto the C-4-hydroxyphenylcalix[4]resorcinarene adsorbent 3. The amount of Cu(II), Co(II), Zn(II), Mn(II), and Pb(II) that is removed from the solution is expressed by Equation (1) (Al-Ghezawi et. al., 2010):

$$q_e = (C_i - C_e)/S \quad (1)$$

where q_e is the heavy metal ion concentration adsorbed at equilibrium (mg of heavy metal ion per g of adsorbent), C_i is the initial concentration of metal ions in the solution (ppm), C_e is the equilibrium concentration or final concentration of metal ions in the solution (ppm), S is the dosage (slurry) concentration and it is expressed by the following Equation (2):

$$S = m/V \quad (2)$$

where (V) is the initial volume of metal ion solutions used and m is the mass of adsorbent. The adsorption percentage is calculated using the following Equation (3):

$$\% \text{ adsorption} = [(C_i - C_e) / C_i] \times 100 \% \quad (3)$$

3. Results and Discussion

Adsorption of the selected heavy metal ions Pb(II), Cu(II), Co(II), Mn(II), and Zn(II) under different pH and contact time was investigated to determine the maximum adsorption percentage of these heavy metal ions and to determine the kinetic mechanism applied for this study.-

Effect of pH

In the adsorption process, the pH of the solution may affect the adsorbent surface charge, the distribution of metal species, and the level of dissociation of functional groups on the active sites of adsorbent. The effect of pH on the adsorption of heavy metal ions in the present study was investigated at different pH ranging from 3 to 9. Figure 2 shows the effect of solution pH on the amount of Cu(II), Co(II), Zn(II), Mn(II), and Pb(II) adsorbed onto C-4-hydroxyphenylcalix[4]resorcinarene 3. It was found that the heavy metal ions adsorption capacity reached its maximum value at pH = 5.6 for all investigated heavy metal ions onto adsorbent 3. C-4-hydroxyphenylcalix[4] resorcinarene 3 contains 8 phenolic-OH groups that may serve as active binding sites. At pH = 3, hydroxyl (-OH) groups of the C-4-hydroxyphenylcalix[4]resorcinarene 3 will be protonated to make these active sites positively charged. Thus, in highly acidic solutions electrostatic repulsion interactions between the adsorbent and the adsorbate will most likely occur due to similar positive characters. In other words, there was an adsorption competition between the proton (H^+) and metal ions Cu(II), Co(II), Zn(II), Mn(II), and Pb(II)) that causes the least amount of metal ions adsorbed by the resorcinarene.

The concentration of protons in the solution decreases with increasing pH so the adsorption competition between H^+ with Cu(II), Co(II), Zn(II), Mn(II), and Pb(II) is reduced, resulting in an escalating adsorption of heavy metal ions by C-4-hydroxyphenylcalix[4]resorcinarene adsorbent 3. Moreover, at pH=7 the deprotonation of the phenolic hydroxyl group of C-4-hydroxyphenylcalix[4]resorcinarene adsorbent 3 converts them into negative charged phenoxide ions which are huge and labile, other competitive smaller anions (anions accompanied with the transitions metal cations used) will selectively chelate to the heavy metal ions, thus resulting in reduction of % removal of the heavy metal ions by the adsorbent.

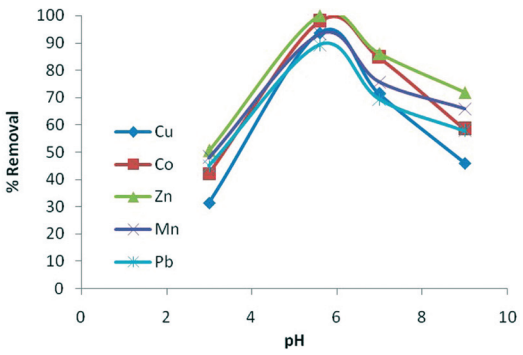

Figure 2. Effect of solution pH on the adsorption of the selected heavy metal ions on C-4-hydroxyphenylcalix[4]resorcinarene adsorbent 3

Effect of contact time

Investigating the uptake amount of the heavy metal ions vs. agitating time is a necessary parameter for determining the adsorption equilibrium and the adsorption rate constant based on the kinetic model adopted. The removal percentage of the heavy metal ions Cu(II), Co(II), Zn(II), Mn(II), and Pb(II) vs. agitating time using C-4-hydroxyphenylcalix[4]resorcinarene adsorbent 3 is shown in Figure 3. The optimum contact time that leads to the maximum adsorption of each heavy metal ion was 30 min. When the adsorption equilibrium is reached, increasing contact time will not affect the amount of adsorbed heavy metal ions. At initial adsorption stage, the surface of the adsorbent was empty, so the adsorption of heavy metal ions onto the adsorbent surface was rapid. Later, the adsorption rate decreased with time, indicating that the saturation on the active sites of the adsorbent is reached.

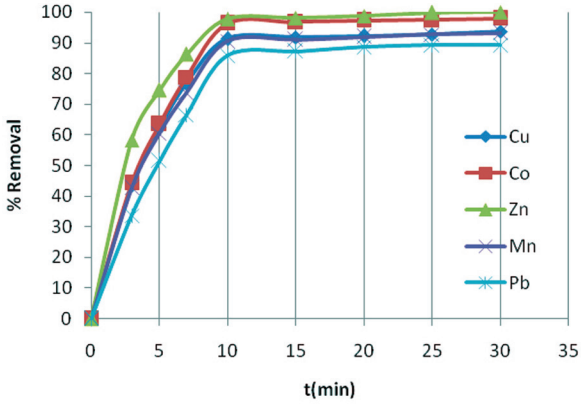

Figure 3. Effect of contact time on the amount of heavy metal ions onto C-4-methoxyphenylcalix[4]resorcinol 3; conditions: initial concentration 1 ppm; pH 5.6; T = 298±1 K

Adsorption kinetics

Several models are available to understand and rationalize the mechanism of heavy metal ions sorption onto the adsorbent. In order to investigate the mechanism of sorption, Santosa et. al. (2007) introduced a kinetic equation model for a single heavy metal ion adsorption onto the adsorbent surface with an overview of the concentration of adsorbate in the aqueous phase. Mathematical equation for such single ion adsorption is expressed by equation (4):

$$\ln (C_o/C_t)/C_t = k_1 t/C_t + K \quad (4)$$

where C_0 is the initial metal concentration (mg/L), C_t is the concentration of heavy metal ions in solution at time t (mg/L), t is the contact time (min), k_1 is the first-order rate adsorption constant (min^{-1}), and K is adsorption-desorption equilibrium constant $(mg/L)^{-1}$.

The approach to the second order kinetics model is reviewed based on the concentration of adsorbate in solid phase (the adsorbent). In order to distinguish the kinetic equation based on the concentration of solution and adsorption capacity of the adsorbent, Lagergren's (Lagergren, 2007) first order and Ho's (Ho and Mckay, 2000) second order rate equations are called pseudo-1st order and pseudo-second order, respectively. The pseudo 1st order equation is generally expressed by equation (5) (Lagergren, 2007):

$$\log (q_e - q_t) = \log q_e - k_1 t \quad (5)$$

and the pseudo 2nd order kinetic model, which was reviewed by Ho and Mckay (2000), is expressed by equation 6:

$t/q_t = 1/k_2q_e^2 + t/q_e$ (6)

where q_e and q_t (mg.g^{-1}) are the adsorption capacities at equilibrium and contact time t, while k_1 and k_2 are the rate constants of pseudo-1st order and pseudo-second order adsorption, respectively.

The rate constant (k_1) was determined from the slope of the plot of log (q_e-q_t) vs. t and k_2 was obtained from the plot of t/q_t vs. t. The time-dependent experimental adsorption data presented in Figure 3 were used for kinetic modeling. In order to study the adsorption kinetics of Cu(II), Co(II), Zn(II), Mn(II), and Pb(II) onto C-4-methoxyphenylcalix[4] resorcinarene adsorbent 3, the 1st order heavy metal ion adsorption of Santosa et. al. (2007) pseudo-1st order of Lagergren (2007) and pseudo-2nd order of Ho and Mckay (2000) models, were applied and used to process and treat the experimental adsorption data.

Based on Figure 4, the plotted curve has the highest level of linearity comparing with the 1st order heavy metal ions adsorption showed in Figure 5 and pseudo-1st order adsorption showed in Figure 6. The results obtained from the kinetic study, including the rate constant value for each heavy metal ion adsorption kinetic, are presented in Table 2. Thus, it can be concluded that the adsorption of Cu(II), Co(II), Zn(II), Mn(II), and Pb(II) onto C-4-hydroxyphenylcalix[4] resorcinarene adsorbent 3 follows pseudo-2nd order kinetic model.

Table 2. Kinetic modeling and adsorption parameters of Cu(II), Co(II), Zn(II), Mn(II), and Pb(II) onto C-4-hydroxycalix[4] resorcinarene

Kinetic models	Rate constant k		Correlation coefficient, R^2
1st order of Santosa	Cu (II)	0.094 (min^{-1})	0.859
	Co (II)	0.134 (min^{-1})	0.905
	Zn (II)	0.226 (min^{-1})	0.957
	Mn (II)	0.093 (min^{-1})	0.877
	Pb (II)	0.080 (min^{-1})	0.871
Pseudo 1st order of Lagergren	Cu (II)	0.085 (mg.g^{-1} min^{-1})	0.870
	Co (II)	0.105 (mg.g^{-1} min^{-1})	0.896
	Zn (II)	0.109 (mg.g^{-1} min^{-1})	0.942
	Mn (II)	0. 093 (mg.g^{-1} min^{-1})	0.930
	Pb (II)	0.112 (mg.g^{-1} min^{-1})	0.957
Pseudo 2nd order of Ho &Mc Kay	Cu (II)	0.519 (g.mg $^{-1}$ min^{-1})	0.988
	Co (II)	0.458 (g.mg $^{-1}$ min^{-1})	0.986
	Zn (II)	0.760 (g.mg $^{-1}$ min^{-1})	0.995
	Mn(II)	0.473 (g.mg $^{-1}$ min^{-1})	0.987
	Pb(II)	0.335 (g.mg $^{-1}$ min^{-1})	0.973

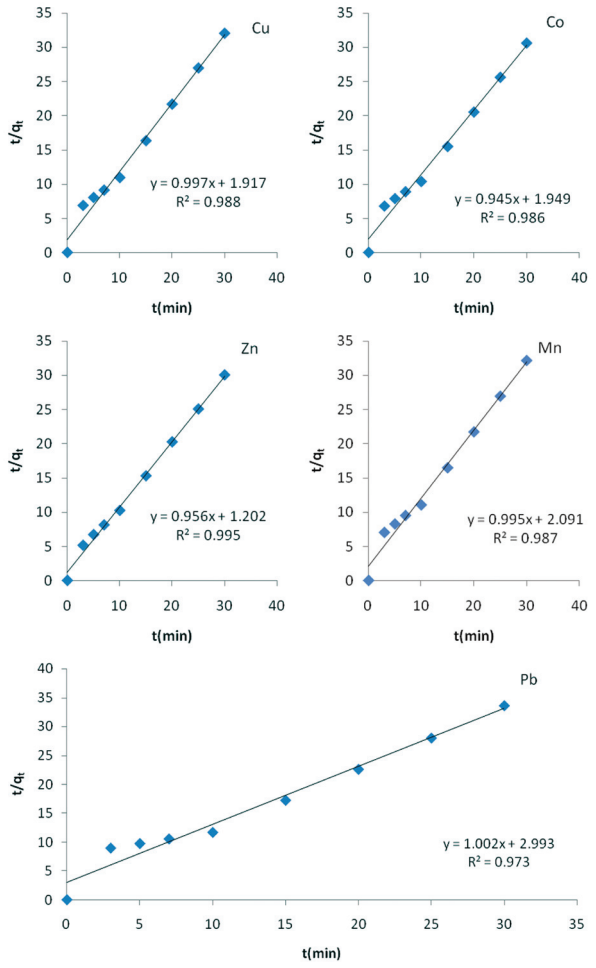

Figure 4. Pseudo second order kinetics of selected heavy metal ions adsorbed onto the C-4-hydroxyphenylcalix[4]resorcinarene adsorbent 3

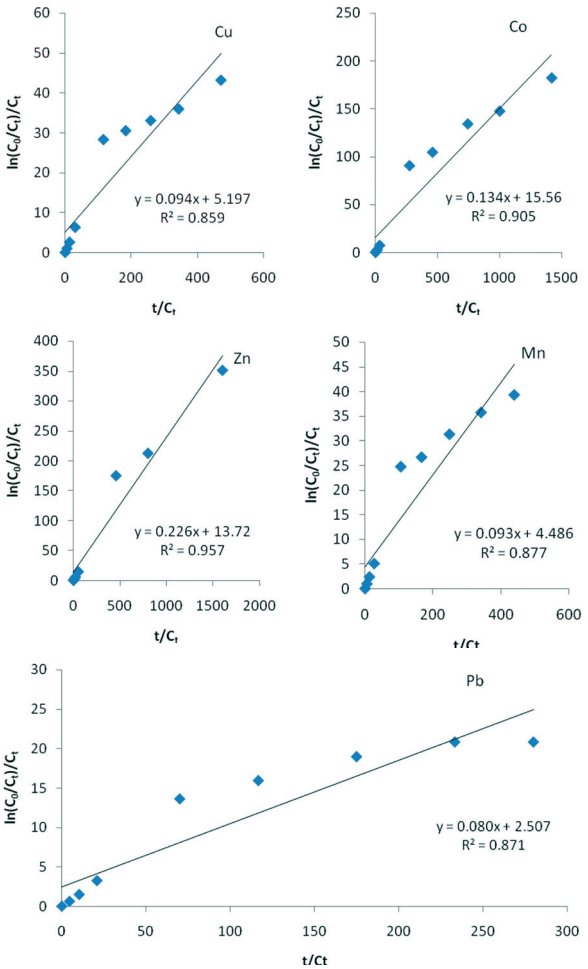

Figure 5. First order kinetics of selected heavy metal ions adsorption onto C-4-hydroxyphenylcalix[4]resorcinarene adsorbent 3

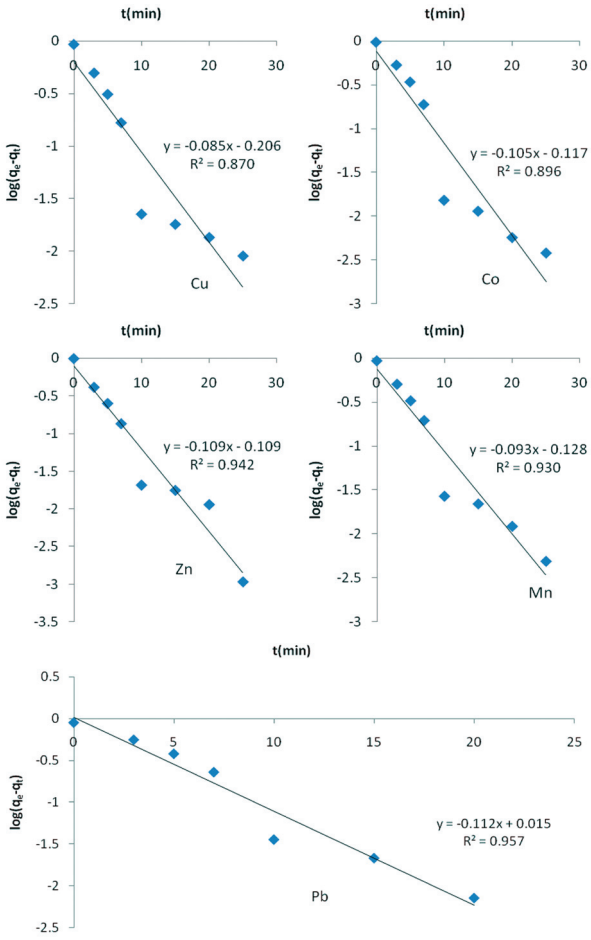

Figure 6. Pseudo first order kinetics of selected heavy metal ions adsorption onto the C-4-hydroxyphenylcalix[4]resorcinarene adsorbent 3

Selectivity and competition study

The adsorption selectivity experiments of adsorbent 3 towards a mixture of heavy metal ions Cu(II), Co(II), Zn(II), Mn(II), and Pb(II) were conducted at pH = 5.6 and shacking time of 10 min. The adsorption efficiency of C-4-hydroxyphenyl-calix[4]resorcinarene 3 against separate heavy metal ions is shown in Figure 7 with a removal capacity in the order: Zn(II) > Co(II) > Cu(II) > Mn(II) > Pb(II), and with a removal percentage of 97.81%, 96.35%, 91.36%, 90.49%, 85.71%, respectively. On the other hand, the removal percentage of a mixture of heavy metal ions was affected and differed from those of the separated heavy metal ions. The removal percentage of a mixture of initial concentration of 1 ppm was Zn(II) > Cu(II) > Co(II) > Mn(II) > Pb(II), with a percentage removal 33.13%, 24.10%, 18.08%, 15.12%, 7.86%, respectively, as illustrated in Figure 8.

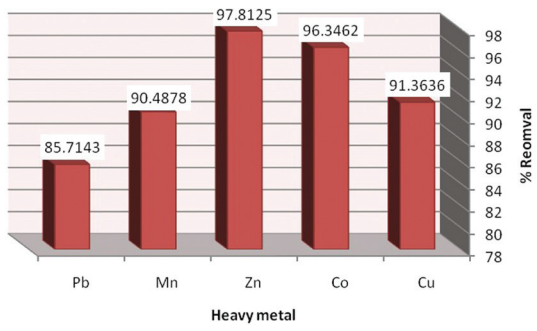

Figure 7. Adsorption efficiency of C-4-hydroxyphenylcalix[4] resorcinarene adsorbent 3 towards separate heavy metal ions

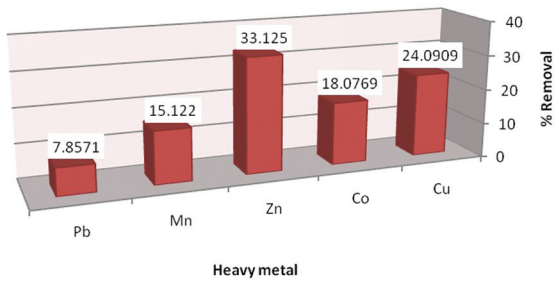

Figure 8. Selectivity of C-4-hydroxyphenylcalix[4]resorcinarene 3 towards a mixture of heavy metal ions

Effect of temperature

The temperature effect on the adsorption of the heavy metal ions Cu(II), Co(II), Zn(II), Mn(II), and Pb(II) onto C-4-hydroxyphenylcalix[4]resorcinarene 3 was studied by performing the adsorption experiments at temperatures of 298, 303, 308, and 318 K. The influence of temperature on the adsorption of the heavy metal ions on C-4-hydroxyphenylcalix[4]resorcinarene 3 at optimum pH and contact time is illustrated in Figure 9.

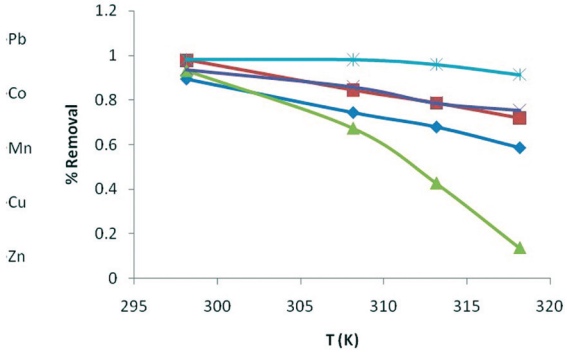

Figure 9. Temperature effect on the removal efficiency of the heavy metal ions Cu(II), Co(II), Zn(II), Mn(II), and Pb(II)

Adsorption isotherms

To understand the mechanism of the adsorption systems, the equilibrium adsorption isotherms were studied in details. The adsorption process was examined against different isotherm models, such as Langmuir, Freundlich, and Temkin.

The Langmuir isotherm

This isotherm model describes the adsorbate-adsorbent system, assuming that each adsorbate molecule occupies only one site, surface is homogenous and adsorption on surface is not delocalized (Thajeel, 2013). The linear form of the Langmuir isotherm equation is expressed as:

$$(C_e/q_e) = 1/q_{max}b + (1/q_{max})C_e \quad (7)$$

where q_{max} is the maximum metal ions uptake per unit mass of adsorbent (mg/g), b is the Langmuir constant (L/mg) which is related to the free energy of adsorption.

A plot of C_e/q_e vs. C_e gives a straight line with a slope of $1/q_{max}$ and intercept of $1/q_{max}b$ as shown in Figure 10. The calculated constants obtained from Langmuir isotherm are listed in Table 3. The characteristic of the Langmuir isotherm is expressed in terms of dimensionless equilibrium parameter (R_L) (Surchi, 2011) which is represented in equation 8 where K = bM and M is the atomic mass of the selected heavy metal ion:

$$R_L = 1/(1+KC_o) \quad (8)$$

The correlation coefficient (R^2) values for the heavy metal ions Pb(II), Co(II), Cu(II), and Zn(II) are high (0.981-0.999), which might be due to the fact that the adsorption of these heavy metal ions can be well described using the Langmuir isotherm model. In addition, the R_L values for the adsorption of the selected heavy metal ions are above 0 and below 1, which confirmed that the adsorption process is favorable for all the selected heavy metal ions. The relation between standard free energy (ΔG^o) and the Langmuir constant (K) is given by the following equation 9 (T. J., 1997; Y. Liu, 2006)

$$\Delta G^o = - RT \ln K \quad (9)$$

Based on the data listed in Table 3, the ΔG^o value for each heavy metal ion is calculated using equation 9 and presented in Table 3 for each heavy metal ion, and found to be negative, which confirmed that the adsorption process is spontaneous.

The Freundlich isotherm

This isotherm model assumes a heterogonous adsorption surface with sites that have different energies of adsorption and are not equally available (Freundlich, 1906; Tadjarodi et. al., 2013; Moradi et. al., 2012). It is more widely used but provides no information on the monolayer adsorption capacity and its linear equation form can be expressed as:

$$\log q_e = \log K + 1/n \log C_e \quad (10)$$

where K ($mg^{1-1/n}L^{1/n}$) and n (dimensionless) are the Freundlich adsorption constants. These constants and correlation coefficients were calculated and presented in Table 4. The calculations were performed by plotting log q_e vs. log c_e as shown in Figure 11.

The Temkin isotherm

This linear form of Temkin isotherm equation (Chwdhury et. al., 2010) is given and presented in equations 11-12:

$$q_e = B_T \ln K_T + B_T \ln C_e \quad (11)$$

$$b_T = (RT) / (B_T) \quad (12)$$

where K_T is Temkin adsorption potential (L/g), B_T and b_T are Temkin constants, R is the universal gas constant and T is the temperature.

Figure 12 illustrates the plotting of q_e vs. ln C_e. Table 5 listed K_T, B_T and b_T for each of the selected heavy metal ions. The Enthalpy change (ΔH^o) and Entropy change (ΔS^o) are related with the Gibbs free energy by equation 13 which can be expressed as:

$$\log K = \Delta S^o / 2.303 R - \Delta H^o / 2.303 RT \quad (13)$$

So plotting log K vs. 1/T will produce a straight line with slope equal to $-\Delta H^o/2.303R$ and intercept equal to $\Delta S^o/2.303R$. Figure 13 represents the plotting of log K vs. 1/T for each heavy metal ion used in this study. The calculated thermodynamic parameters obtained from Figure 13 are listed in Table 6.

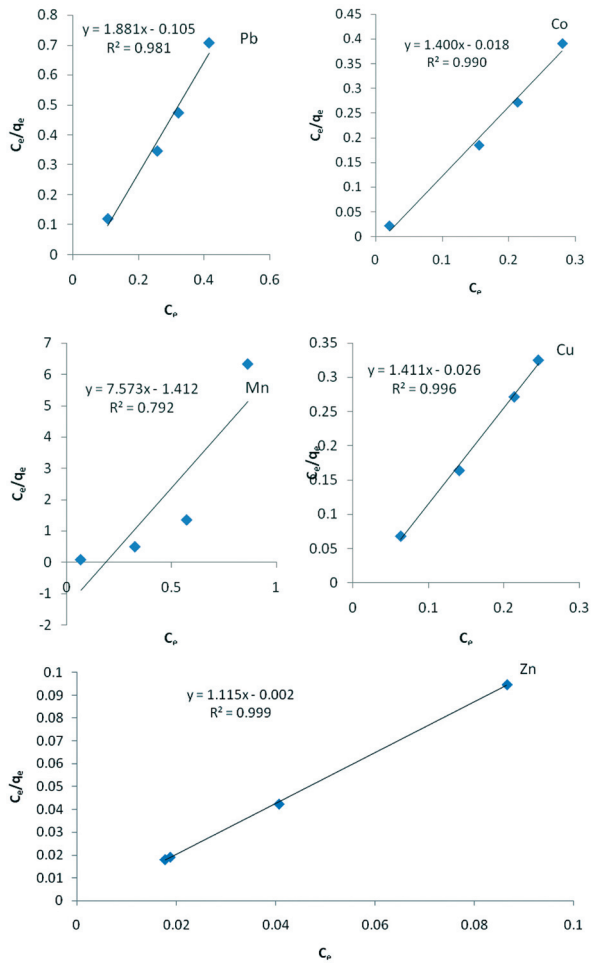

Figure 10. The linear Langmuir adsorption isotherms for the heavy metal ions Cu(II), Co(II), Zn(II), Mn(II), and Pb(II)

Table 3. The calculated Langmuir adsorption constants and thermodynamic parameters for the heavy metal ions Cu(II), Co(II), Zn(II), Mn(II), and Pb(II) at 298 K

Heavy metal ion	q_{max} (mg/g)	b / K (L/mol)	R_L	ΔG^o (KJ/ mol)
Pb(II)	0.53	17.9 / 3708.8	$2.7x10^{-4}$	-20.37
Co(II)	0.71	78.25 / 4626.0	$2.16x10^{-4}$	-20.92
Mn(II)	0.13	5.45 / 299.4	$3.33x10^{-3}$	-14.13
Cu(II)	0.71	54.17 / 3442.3	$2.90x10^{-4}$	-20.19
Zn(II)	0.9	555.6 / 36330	$2.74x10^{-5}$	-26.03

Table 4. The calculated Freundlich adsorption constants and correlation coefficients for the heavy metal ions Cu(II), Co(II), Zn(II), Mn(II), and Pb(II) at 298 K

Heavy metal ion	K	n	R^2
Pb(II)	0.48	3.45	0.936
Co(II)	0.66	9.52	0.899
Mn(II)	0.22	1.59	0.691
Cu(II)	0.62	6.45	0.959
Zn(II)	0.82	22.73	0.958

Table 5. The calculated Temkin adsorption constants and correlation coefficients for the heavy metal ions Cu(II), Co(II), Zn(II), Mn(II), and Pb(II) at 298 K

Heavy metal ion	K (L/g)	B_T	b_T	R^2
Pb(II)	0.14	-0.216	$-1.15x10^4$	0.965
Co(II)	$8.25x10^{-4}$	-0.090	$-2.75x10^4$	0.925
Mn(II)	0.47	-0.288	$-8.6x10^3$	0.887
Cu(II)	0.01	-0.131	$-1.89x10^4$	0.970
Zn(II)	$3.83x10^{-9}$	-0.042	$-5.9x10^4$	0.962

Table 6. The calculated thermodynamic parameters for the heavy metal ions Cu(II), Co(II), Zn(II), Mn(II), and Pb(II) at 298 K

Heavy metal ion	ΔS° (J/mol)	ΔH° (KJ/mol)	ΔG° (KJ/mol)	R^2
Pb(II)	-54.86	-16.11	-20.37	0.965
Co(II)	-40.30	-11.97	-20.92	0.925
Mn(II)	-229.38	-6.88	-14.13	0.887
Cu(II)	-29.83	-8.75	-20.19	0.970
Zn(II)	-8.63	-2.56	-26.03	0.962

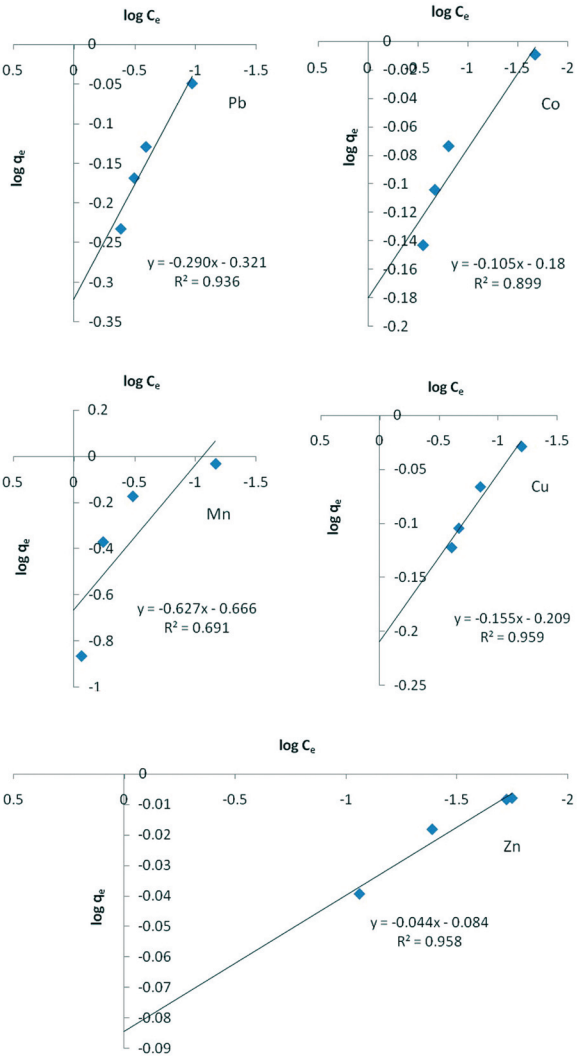

Figure 11. The linear Freundlich adsorption isotherms for the heavy metal ions Cu(II), Co(II), Zn(II), Mn(II), and Pb(II)

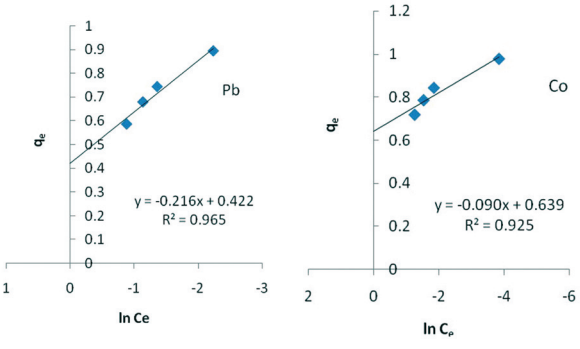

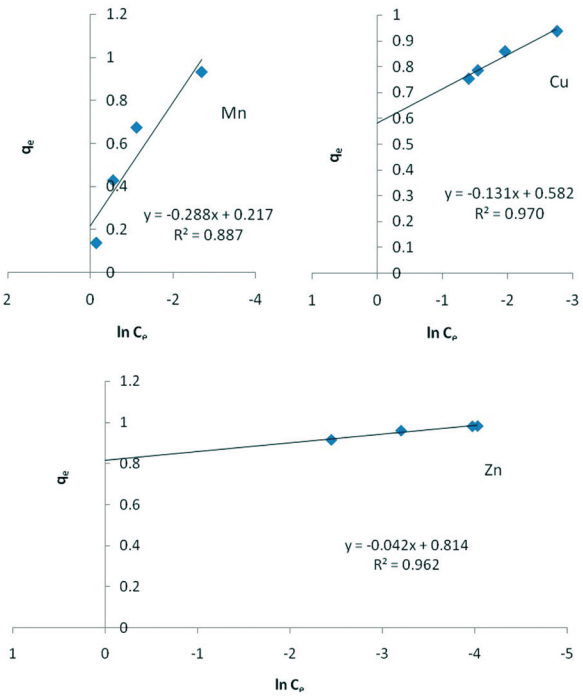

Figure 12. The linear Temkin adsorption isotherms for the heavy metal ions Cu(II), Co(II), Zn(II), Mn(II), and Pb(II)

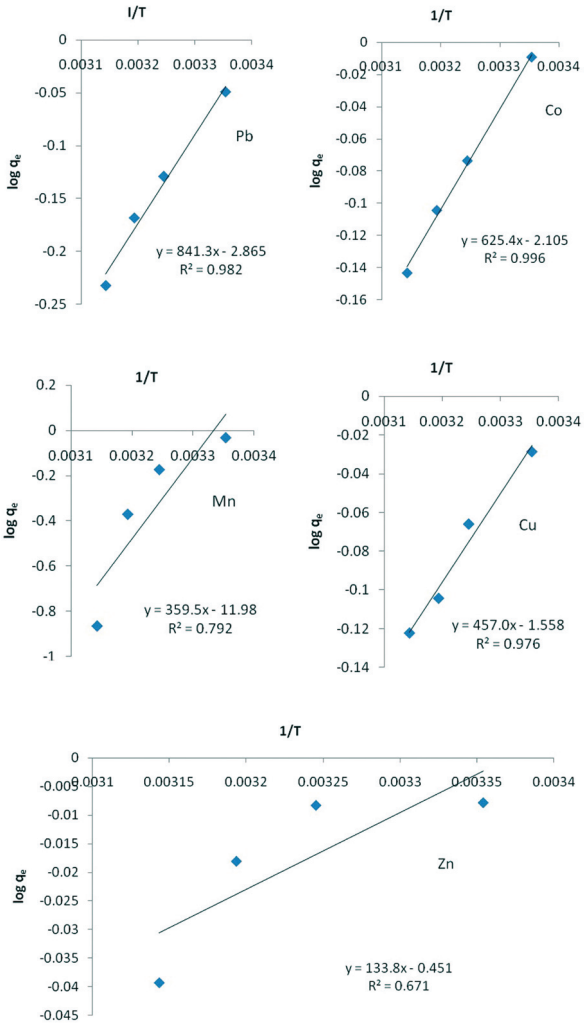

Figure 13. The linear plotting of log K vs. 1/T for the heavy metal ions Cu(II), Co(II), Zn(II), Mn(II), and Pb(II)

4. Conclusions

The adsorption experimental data obtained from the current study confirmed that C-4-hydroxyphenylcalix[4] resorcinarene 3 is an effective adsorbent for the removal of heavy metal ions (Mn(II), Cu(II), Co(II), Zn(II), and Pb(II)) from aqueous solutions. The adsorption capacity increases with the increase of the contact time until equilibrium is reached at contact time of 30 min. In addition, it has been found that the adsorption capacity increases with increasing the pH of the heavy metal ions solution with optimum results achieved at pH = 5.6; this is because the active binding sites (OH groups) become more negatively charged at higher pH values.

The experimental data for the adsorption of the selected heavy metal ions were adopted by Langmuir isotherm model ($0 < R_L < 1$) and followed pseudo second order kinetic model.

The calculated thermodynamic parameters values of Gibbs free energy (ΔG^o) and heat of enthalpy (ΔH^o) indicated that the adsorption processes were favorable, spontaneous, and exothermic. Future work could be extended to include studying the other adsorption variables, such as initial concentration of the heavy metal ion, amount of adsorbent, and other toxic heavy metal ions.

Acknowledgments

The financial support of this work by Mu'tah University is highly appreciated and acknowledged.

References

[1] Ahmad, R., Kumar, R., and Lasker, M.A., 2013. Adsorptive removal of Pb2+ form aqueous solution by macrocyclic calix[4] naphthalene: kinetic, thermodynamic, and isotherm analysis, Environ. Sci. Pollut. Res, 20, 219-226.

[2] Akkus, G. U., Memon, S., Sezgin, M., and Yilmaz, M., 2009. Synthesis of Calix(aza)crown and its Oligomeric Analogue for the Extraction of Selected Metal Cations and Dichromate Anions, Clean, 37:109–114.

[3] Al-Ghezawi, N., Al-Anber, M. A., Al-Anber, Z. A., El-Hasan, T., Al-Momani, I., 2010. Decontamination and adsorption modelling of aqueous Pb2+ and Co2+ ions using natural inorganic materials: tripoli (NT) and bentonite (NB) ,Desal. Wat. Treat, 24, 336-343.

[4] Andrew, D., Lenore, S., Eugene, W., Arnold, E., and Mary Ann, H., 2005. Standard Methods for the Examination of Water & Wastewater., 21th edition, Borntobescientist .

[5] Benit, Y., and Ruiz, M.L., 2002. Reverse osmosis applied to metal finishing wastewater, Desalination, 142, 229–234.

[6] Biskup, B., and Subotic, B., 2004. Kinetic analysis of the exchange processes between sodium ions from zeolite A and cadmium, copper and nickel ions from solutions ,Sep. Purif. Technol, 37,17–31.

[7] Chwdhury, S., Mishra, R., Saha, P., and Kushwaha, P., 2010. Adsorption thermodynamics, kinetics and isosteric heat of adsorption of malachite green onto chemically modified rice husk, Desalination, 265, 159-168.

[8] Cincotti, A., Mameli, A., Locci, A.M., Orru, R., and Cao, G., 2006. Heavy Metals Uptake by Sardinian Natural Zeolites: Experiment and Modeling , Ind. Eng. Chem. Res, 45, 1074–1084.

[9] Dang, V.B.H., Doan, H.D., Dang-Vuc, T., and Lohi, A., 2009. Equilibrium and kinetics of biosorption of cadmium(II) and copper(II) ions by wheat straw, Bioresour. Technol, 100, 211–219.

[10] Emamjomeh, M.M., and Sivakumar, M., 2009. Review of pollutants removed by electrocoagulation and electrocoagulation/flotation processes, J. Environ. Manag, 90, 1663–1679.

[11] Esalah, O.J., Weber, M.E., and Vera, J.H., 2000. Removal of lead, cadmium and zinc from aqueous solutions by precipitation with sodium Di-(n-octyl) phosphinate, Can. J. Chem. Eng, 78, 948– 954.

[12] Freundlich, H. M. F., 1906. Z. Phys. Chem, 57, 385-470.

[13] Ghurye, G., Clifford, D., and Tripp, A., 2004. Iron Coagulation and Direct Microfiltration to Remove Arsenic from Groundwater, AWWA, 96, 143–152.

[14] Gier, S., and Johns, W.D., 2000. Heavy metal-adsorption on micas and clay minerals studied by X-ray photoelectron spectroscopy, Appl. Clay Sci, 16, 289–299.

[15] Greenlee, L.F., Lawler, D.F., Freeman, B.D., Marrot, B., and Moulin, P., 2009. Reverse osmosis desalination: Water sources, technology, and today's challenges, Water Res, 43, 2317–2348.

[16] Gutsche, C. D., 1998. Calixarenes Revisited, the Royal Society of Chemistry: Cambridge.

[17] Harris, S., 1996. Economics of the environment: a survey, Econ. Rec, 72 (217): 154–171.

[18] Ho, Y. S., and Mckay, G., 2000. The kinetics of sorption of divalent metal ions onto sphagnum moss peat, Water Research, 34, 735–742.

[19] Koppelman, M.H., and Dillard, J.G.,1977. A study of the adsorption of Ni(II) and Cu(II) by clay minerals, Clays Clay Miner, 25, 457–462.

[20] Kunsagi, Mate., Szabo, K., Lemli, B., Bitter, I., Nagy, G., and Kollar, L., 2005. Host–guest interaction between water-soluble calix[6]arene hexasulfonate and p-nitrophenol,Thermochim. Acta, 425, 121-126.

[21] Lagergren, S., 2007. Comments on ''An adsorption and kinetic study of lac dyeing on silk'', Zur theorie der sogenannten, Dyes Pigments, 72, 134-136.

[22] Lertlapwasin, R., Bhawawet, N., Imyim, A., and Fuangswasdi, S., 2010. Ionic liquid extraction of heavy metal ions by 2-aminothiophenol in 1-butyl-3-methylimidazolium hexafluorophosphate and their association constants, Sep. Purif. Technol, 72, 70–76.

[23] Liu, Y., 2006. Some consideration on the Langmuir isotherm equation , Coll. Surf. A: Physicochem. Eng. Aspects, 274, 34-36.

[24] Mahmoud, A., and Hoadley, A.F., 2012. An evaluation of a hybrid ion exchange electrodialysis process in the recovery of heavy metals from simulated dilute industrial wastewater, Water Res, 46, 3364–3376.

[25] Ming, Chen., Ting, Shang., Wei, Fang., and Guowang, Diao., 2011. Study on adsorption and desorption properties of the starch grafted p-tert-butyl-calix[n] -arene for butyl Rhodamine B solution, J. Hazard. Mater, 185, 914–921.

[26] Moradi, O., Mirza, B., Norouzi, M., and Fakhri, A., 2012. Removal of Co(II), Cu(II) and Pb(II) ions by polymer based 2-hydroxyethyl methacrylate: thermodynamics and desorption studies, J. Environ. Health Sci. & Eng, 9, 31.

[27] O'Connell, D.W., Birkinshaw, C., and O'Dwyer, T.F., 2008. Heavy metal adsorbents prepared from the modification of cellulose: A review, Bioresour. Technol, 99, 6709–6724.

[28] Pan, B.J., Pan, B.C., Zhang, M.W., Lv, L., Zhang, Q.X., and Zheng, S.R., 2009. Development of polymeric and polymer-based hybrid adsorbents for pollutants removal from waters, Chem. Eng. J, 151, 19–29.

[29] Ren, Y., Zhang, M., and Zhao, D., 2008. Synthesis and properties of magnetic Cu(II) ion imprinted composite adsorbent for selective removal of copper, Desalination, 228 (1–3): 135–149.

[30] Rubio, J., Souza, M.L., and Smith, R.W., 2002. Overview of flotation as a wastewater treatment technique, Miner. Eng, 15, 139–155.

[31] Samiey, B., Cheng, C.H., and Wu, J., 2014. Organic-Inorganic Hybrid Polymers as Adsorbents for Removal of Heavy Metal Ions from Solutions: A Review, materials, 7, 673-726.

[32] Santosa, S. J., Siswanta, D., Sudiono, S., and Sehol, M., 2007. Synthesis and utilization of chitin–humic acid hybrid as sorbent for Cr(III), Surf. Sci., 601, 5148-5154.

[33] Surchi, K.M.S., 2011. Agricultural Wastes as Low Cost Adsorbents for Pb Removal: Kinetics, Equilibrium and Thermodynamics ,International Journal of Chemistry, 3(3): 103-112

[34] Tabakci, M., Ersoz, M., and Yilmaz, M., 2006. A Calix[4] arene- Containing Polysiloxane Resin for Removal of Heavy Metals and Dichromate Anion, J Macromole Sci Part A, 43, 57–69.

[35] Tadjarodi, A., Imani, M., and Kerdari, H., 2013. Adsorption kinetics, thermodynamic studies, and high performance of CdO cauliflower-like nanostructure on the removal of Congo red from aqueous solution, J. Nanostruct. Chem, 3, 51.

[36] Thajeel, A. S., 2013. Isotherm, Kinetic and Thermodynamic of Adsorption of Heavy Metal Ions onto Local Activated Carbon, Aquatic Science and Technology, 1(2): 53-77.

[37] T. J., 1997. Unit Treatment Processes in Water and Wastewater Engineering, John Wiely and Sons Ltd, England, 113-114. b) Singh, D. B., Prasad, G., Rupainwar, D., and Singh, V. N., 1988. As(III) removal from aqueous solution by adsorption, Water Air Soil Pollut, 42, 373.

[38] Tuama, A.H., and Mohammed, A.A., 2014. Removal of heavy metal ions from aqueous solutions using tobacco leaves as a sorbent, Euro. J. Appl. Eng. Sci. Res, 3(2): 19-32.

[39] Uzun, I., and Güzel, F., 2000. Adsorption of Some Heavy Metal Ions from Aqueous Solution by Activated Carbon and Comparison of Percent Adsorption Results of Activated Carbon with those of Some Other Adsorbents, Turk. J. Chem, 24, 291–297.

[40] Weinelt, F., and Schneider, H. J., 1991. Host-guest chemistry. 27. Mechanisms of macrocycle genesis. The condensation of resorcinol with aldehydes, J. Org. Chem, 56(19): 5527- 5535.

[41] W.H.O., 1996, Guidelines for drinking-water quality, 2nd ed. Vol. 2. Health criteria And other supporting information. World Health Organization, Geneva.

[42] Yurloval, L., Kryvoruchko, A., and Kornilovich, B., 2002. Removal of Ni(II) ions from wastewater by micellar-enhanced ultrafiltration, Desalination, 144, 255–260.

[43] Zewail, T.M., and El-Garf, S.A.M., 2010. Preparation of agriculture residue based adsorbents for heavy metal removal, Desal. Water Treat, 22, 363–370.

JJEES
Jordan Journal of Earth and Environmental Sciences

Volume 7, (Number 1), June, 2015
ISSN 1995-6681
Pages 11 - 17

Kinetic Study on Adsorption of Fatty HydroxamicAcids by Natural Clays

Basel M. Jafar[1], Imad Hamadneh[2], Fawwaz I. Khalili[2], Ammar H. Al-Dujaili[2]*

[1]Department of Chemistry, King Khalid University, Abha-Bisha, Saudi Arabia
[2]Department of Chemistry, Faculty of Science, University of Jordan, 11942 Amman, Jordan

Received 12 February, 2015; Accepted 17 May 2015

Abstract

Five fatty hydroxamic acids (FHAs) were synthesized by refluxing of vegetable oils, namely corn, olive, palm, soybean, and sunflower oil with hydroxylamine hydrochloride. The FHAs was synthesized by three different methods depending on the form of the fatty acids used, i.e., free fatty acid, methyl and ethyl fatty ester or raw oil. The efficiency of FHAs synthesized from methyl and ethyl ester was very high, because it gives good yield and pure product. These acids were characterized using the complex formation test of hydroxamic acid group with zinc(I), copper(II) and iron(III), elemental analysis, and Fourier transform infrared (FTIR) spectroscopy. The adsorption of these five FHAs onto bentonite (BT) and kaolinite (KT)clays was investigated using a series of batch adsorption experiments. The presentstudy primarily focuses on the adsorption kinetics to modify BT and KT clays. Four adsorption kinetic models were tested for the adsorption of FHAs onto BT and KT clay surfaces. In order to investigate the mechanism of these five fatty hydroxamic acids adsorption, characteristic constants of adsorption were determined using a pseudo-first order equation of Lagergren, a pseudo-second order equation, Elovich equation and intraparticle diffusion model.

Keywords: Vegetable oils; Fatty hydroxamic acids; Adsorption; Kinetics; Clay mineral

1. Introduction

Hydroxamic acid (HA), or (N-hydroxycarboxylic amides),has the general chemical formula R-CO-NHOH. It is regarded as a derivative of both hydroxylamine and carboxylic acids (Miller et. al., 2002). The term FHA comes when (HA) is prepared from fatty acids. A Fatty acid (FA) is a carboxylic acid with a long unbranched aliphatic chain, which is either saturated or unsaturated. FAs are usually derived from triglycerides. When they are not attached to other molecules, they are known as free fatty acids. The FA can be defined by its source (animals or plants), or by its carbon number as a short chain (fewer than six), medium (6-12), long (longer than 12), or very long (longer than 22) (Clifford and Gessuer, 1973).

In recent decades, hydroxamic acid derivatives have been widely applied as growth factors, food additives, neurotoxic drugs for anti HIV drugs, antibiotics, antimalarial drugs, antibacterial agents, cell division factor, rare earth mineral collectors and chelators (Kurzak et. al., 1992), and enzyme inhibitors (Dankwardtet. al., 2001). Hydroxamic acids complexes have been used for analytical chemistry as reagents for gravimetric and spectrometric metal determination (Agrawal and Patel, 1980; Agrawal et. al., 2000). Besides their ability to form a complex with metal ions, long-chain hydroxamic acids, by modification of the terminal OH group, are of a considerable interest as an efficient surfactant in the detergent industry(Masuyama et. al., 1987).

Several studies were carried out on the synthesis of hydroxamic acids from acids and esters with hydroxyl amine (Jahangirian et. al., 2011; Al-Mulla et. al., 2009; Holmes et. al., 2001). Many researchers synthesized fatty hydroxamic acids from palm oil using immobilized lipase as the catalyst(Dedy et. al., 2005; Vaysse et. al., 1997). Hoidy et. al. (2010) reported the synthesis of fatty hydroxamic acid using the reflux method for preparation of fatty hydroxamic acids from different oils including palm olein, palm stearin and corn oil with hydroxylamine hydrochloride

Bentonite is a clay deposit consisting essentially of smectite minerals. Smectites are unique by their extreme small crystal size and variation in the internal chemical composition, and structural characteristics (Rauf and Tahir, 2000). Bentonite is a 2:1 type of clay, which means that it is composed of units of two silica tetrahedral sheets with a central alumina octahedral sheet. All tips of tetrahedron points in the same direction and toward the center unit (Murray, 2007).

Kaolinite is a clay mineral with the chemical composition $Al_2Si_2O_5(OH)_4$, with one tetrahedral sheet linked through oxygen atoms to one octahedral sheet of aluminaoctahedral (Srivastava et. al., 2005). Kaolinite has a 1:1 layer structure, with the basic unit consisting of a tetrahedral sheet of SiO_4 and an octahedral sheet with Al^{3+} as the octahedral cation. The repeating layers of the mineral are hydrogen bonded together (Trevino and Coles, 2003).

* Corresponding author. e-mail: ah.aldujaili1946@gmail.com

The permanent negative charge in the crystal structures of some minerals (BT and KTas an examples), make them suitable for surface modification by long chain and short chain organic surfactants (Li and Bowman, 2001; Li et. al., 2002). These modifications enable those clay minerals to be used as an adsorbent for removing organic and inorganic pollutants from aqueous solution. In addition, this organomodification make clay minerals compatible with polymers to synthesis the most promising materials, i.e., clay-polymer nanocomposites (Pavlidon and Papaspyrides, 2008).

In the present study, the synthesis and characterization of fatty hydroxamic acid (FHA) derived from the reaction of hydroxylamin with five different oils, namely corn, olive, palm, soybean, and sunflower oil. The synthesized fatty hydroxamic acids were employed to modify BT and KTclays to form ten kinds of organic-modified clays, i.e., CornFHA/BT, OliveFHA/BT, PalmFHA/BT, SoybeanFHA/Bt, SunflowerFHA/BT, CornFHA/KT, OliveFHA/KT, PalmFHA/KT, SoybeanFHA/Kt, andSunflowerFHA/KT.The present paper primarily focuses on the adsorption kinetics of BT and KTclays. Four adsorption kinetic models were tested for the adsorption of FHAs onto BT and KTclay surfaces. In order to investigate the mechanism of these five fatty hydroxamic acids adsorption, characteristic constants of adsorption were determined using a pseudo-first order equation of Lagergren,a pseudo-second order equation, Elovich equation and interparticular diffusion model.

2. Materials and methods

2.1. Materials

Corn, olive, palm, soybean and sunflower vegetable oils were purchased from Universal Modern Industries Company (UMIC), Jordan. All chemicals used in this study were provided by Sigma-Aldrich Chemicals Company, where their purity is higher than 99% and used without further purification.

Samples of Jordanian BT and KT from the Azraq region in northeast of Jordan were obtained from Natural Resources Authority (NRA, Amman, Jordan). The crushed and milled samples were washed several times with deionised water with a constant stirring to remove soluble inorganic salts and any adhering materials, and then dried in a drying oven to constant weight at 110ºC. The samples were sieved and fractions of 45 μm and below were collected.

2.2. Instrumentation

FT-IR spectra were recorded using Thermo Nicolet NEXUS 670 FT-IR spectrophotometer using KBr disc. The infrared spectrum was recorded in the wave-number range 400 - 4000 cm^{-1}.

Scanning electron microscope (SEM) technique has been used to obtain information on the morphology and size of the sample by scanning electron microscopy (SEM). The morphology was studied using FEI inspect F50 scanning electron microscope operated at accelerating voltages of 2 kV with magnification of 15000 X. The particles were glued to a metallic sample holder using a carbon double-side tape and then coated with platinum to prevent the charging effect.

Ultra violet visible (UV-VIS) spectrophotometer type Cary 100 Varian spectrophotometer was used to identify the $\lambda_{max}$of FHA/Fe (III) complex and measuring the absorption intensity for all samples.

The chemical composition of BT and KT samples was performed using X-ray fluorescence (XRF) spectrometer (Philips PW 2400).

2.3. Synthesis of (FHAs)

The FHAs was prepared by three different methods depending on the form of fatty acids used, i.e., free fatty acid, methyl and ethyl fatty ester or raw oil. The FHA, prepared from methyl and ethyl ester, was found to be the best, because it gave a good yield and a pure product. The following procedure was used:The methyl and ethyl fatty ester were prepared using transesterification reaction method which was carried out by mixing methoxide/ethoxide with warmed palm oil as an example with continuous stirring for 6h (Ma and Hanna, 1999). Then, the product was separated and dissolved in hexane with hydroxylamine hydrochloride by reflux at the boiling point of hexane for 10 h, using a thermostated round bottom flask, equipped with a water cooled condenser, and a mechanical stirrer. The product was first dissolved in hot hexane, and separated from the bottom layer using a separating funnel. The hexane phase was cooled in an ice bath for 4 h to obtain FHA, then filtrated and washed by hexane three times. The products was recrystallized from hexane; finally, it was dried in vacuum desiccators over phosphorous pentoxide (Haron et. al., 1994). The reaction is shown in Scheme 1:

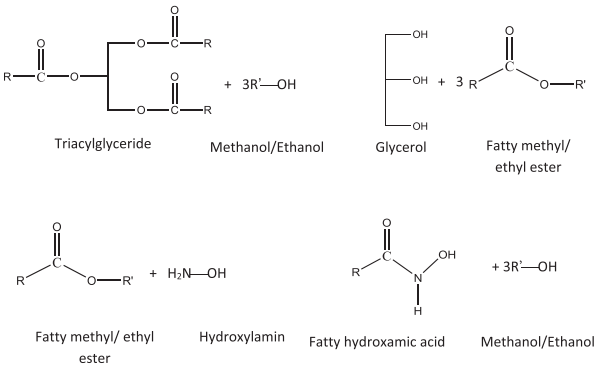

Scheme 1. The Reaction Equations of Triacylglyceride with Hydroxylamine

2.4. Adsorption of FHAs by Bentonite and Koalinite clays

Batch adsorption was carried out using Pyrex glass vessels. An accurate mass (0.5g ± 0.1 mg) of BT or KTclay measured to the nearest 0.0001g was shaken with 100 mL solutions of FHA prepared by dissolving 0.5 g of each of FHA in 100 mL of 70% ethanol at 25ºC. For adsorption, a kinetics set of experiments was carried out by taking aliquot of the solution by pipette after different times 1, 3, 6, 12, 18, 24 and 48 h. The solution was then filtered using 0.45μm micro filter. One milliliter from this solution was reacted with 10 mL of $FeCl_3$ solution in 70% ethanol to give a colored solution. All of the samples were analyzed by UV-VIS spectrophotometer at wavelength 520 nm to measure the concentration of free FHA. The calibration curve, at this wave length, was established as a function of FHA concentration. The reproducibility of the data varied in the range of 1.5%.

The FHA uptake capacity was calculated by the simple concentration difference method. The FHA uptake (mg FHA adsorbed/g adsorbent) was calculated from the mass balance equation (1) as follows:

$$q_e = \frac{(C_i - C_{eq})V}{m} \quad (1)$$

where C_i is the initial concentration (mg/L); C_{eq} is the equilibrium concentration (mg/L) of the FHA in the aqueous phase; V is the volume of solution (L) and m is the mass of the adsorbent (g).

The removal efficiency (% Removal) (%R) values were calculated as a percentage using equation (2):

$$\%R = \frac{(C_i - C_{eq})}{C_i} \times 100(2) \quad (2)$$

3. Results and Discussion

3.1. Characterization of Materials

The average molar mass of corn, olive, palm, soybean and sunflower vegetable oils was calculated by back titration technique and the calculated values were 560, 510, 435, 480 and 545 g/mol, respectively. A qualitative analysis of hydroxamic acid group on FHAs was carried out by observing the colored complex formed after methanolic solution of the FHAs reacted with iron(III), copper (II) and zinc (II) in the dilute hydrochloric acid solution. The colors of complexes of FHAs with iron(III), copper (II) and zinc (II) were green, dark red and pale yellow, respectively (Haron et. al., 1994).

The results of the elemental analysis showed that the nitrogen contentsin the FHAs synthesized from the corn, olive, palm, soybean and sunflower oil were 6.41, 5.68, 4.93, 5.39 and 6.11%, respectively.

The chemical composition of BT and KTsamples, as determined by XRF technique (wt%), are listed in Table 1. The loss on ignition (L.O.I.) values indicates the loading of mineral by the organic compounds.

Table 1. The chemical composition of bentonite and kaolinite samples (%)

Constituents	Adsorbents	
	Bentonite	Kaolinite
SiO_2	54.59	47.62
Al_2O_3	21.97	27.89
Fe_2O_3	2.09	6.11
CaO	4.17	0.49
TiO_2	0.31	0.72
Na_2O	3.42	0.84
MgO	1.01	1.01
K_2O	2.35	2.34
L.O.I.	9.56	12.10

The results of FTIR spectrum of the FHA, synthesized from palm oil as a representative example (Figure 1b), show the characteristic absorption bands of hydroxamic acid at 3426 and 3264 cm^{-1}, corresponding to N-H and OH stretching, respectively. These absorption bands are typical bands for amide (Vaysse et. al., 1997). Absorption bands at 2854 and 2917 cm^{-1}, which correspond to C-H stretching of alkyl chain, at 1641 cm^{-1} which correspond to C=O for secondary amide and at 1044 and 1113 cm^{-1} which correspond to C-N stretching, respectively.

The characterization bands of raw BT(Figure 1a) that appear at 3434-3625 cm^{-1} as a broad band is assigned to OH stretching vibrations, which may arisefrom the isomorphic substitution in the tetra and octahedral layers in bentonite (Wilson, 1994). On the other hand, the characteristic IR bands of Al and Mg bound water molecules appear at 1642 cm^{-1}. The band at 1039 is assigned to the asymmetric stretching vibration of Si-O-Si of BT. It can be seen from the spectrum of raw KT(Figure 1c) that the absorption bands of OH within the crystal structure appear at 3621-3698 cm^{-1}. The band at 1631 cm^{-1} corresponds to the OH deformation of water, because the OH stretching band at 3467 cm^{-1}suggests the presence of some interlamellar water (Gadsden, 1975). After the BT and KT were treated with FHAs, a pair of strong bands at 3434 cm^{-1} and 3625 cm^{-1} for BT and the bands at 3467 and 3654 cm^{-1} for KTwere observed which can be assigned to the symmetric and asymmetric stretching vibrations of the methylene groups (CH_2-) and their bending vibrations are between 1384 and 1470 cm^{-1}, (Figures 1d, e) which support the intercalation of FHAs molecules between the silica layers, but these stretching bands are not observed in the raw BT and KT.

The surface morphology of the raw and modified BT and KT was studied by using scanning electron microscopy (SEM). Figures 2 and 3 give a clear picture of the surface morphology of the samples. They show the porous nature of the surfaces. BT exhibits sieve like structure. In both micrographs of the modified clays it can be noted that the modifier has coated most of the pores and edges.

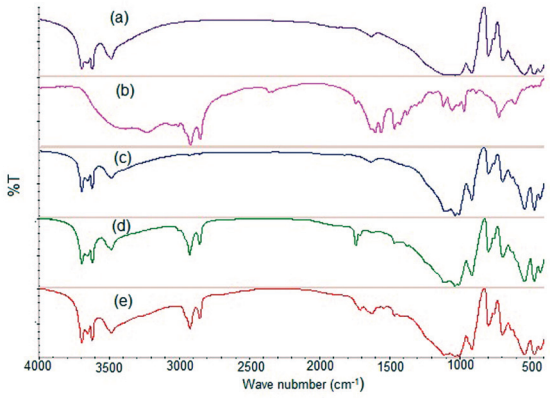

Figure 1. FTIR for (a) Unmodified BT, (b) PalmFHA, (c) Unmodified KT, (d) PalmFHA/BT, and (e) PalmFHA/KT

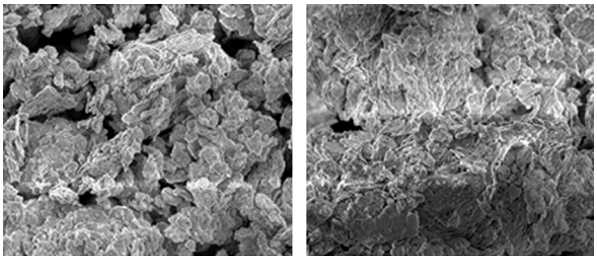

Figure 2. SEM Micrographs of (left) Unmodified BT and (right) PalmFHA/BT

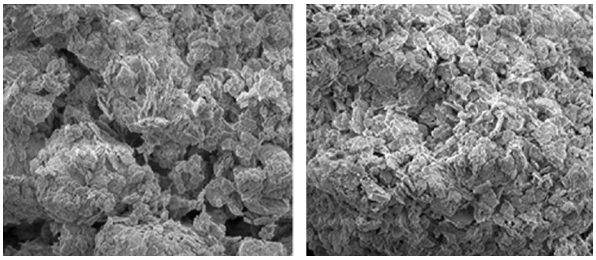

Figure 3. SEM Micrographs of (left) Unmodified KT and (right) PalmFHA/KT

3.2. Kinetic models applied to the sorption of FHAS onto bentonite and kaolinite

Figure4 shows the contact time curves for the adsorption of FHAs onto BT and KT. The adsorption equilibrium was reached after 8-10 h, depending on the FHAs type. Adsorption, first, followed a linear rising in which instantaneous extremely fast uptakes take place, and, then, a stationary state was observed. The fast initial uptake was due to the accumulation of FHAs on the surfaces of BT and KTadsorbents which is a rapid step (Al-Khalisy et. al., 2010). For all systems and in all subsequent investigations, a shaking time of 12 h was conveniently adopted followed by the standing overnight in the thermostatic bath.

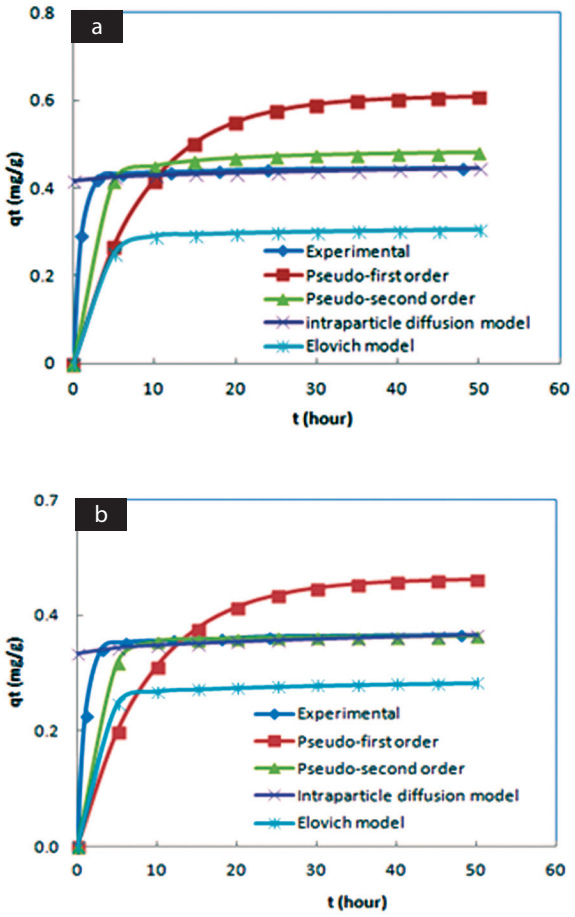

Figure 4. Different adsorption kinetic models fit for adsorption of CornFHA on BT (a) and on KT (b) at 25°C

In order to investigate the mechanism of adsorption and the potential rate of controlling steps, such as mass transport and chemical reaction processes, kinetic models were used to test the experimental data. The four adsorption kinetic models included the pseudo-first order equation, the pseudo-second order equation, Elovich equation and the intraparticle diffusion model.

3.2.1. Pseudo-First Order Rate Equation of Lagergren

The pseudo-first order equation of Lagergren (1898) is generally expressed as follows:

$$q_t = q_e(1 - e^{-k_1 t}) \quad (3)$$

where $q_{e.calcd.}$ and q_t are the amount of FHA adsorbed per unit weight (mg/g) of adsorbent at equilibrium and at any time t, respectively and k_1 the rate constant of pseudo-first order sorption (min^{-1}).

3.2.2. Pseudo-second order rate equation

If the rate of adsorption is a second order mechanism, the pseudo-second order kinetic rate equation is expressed as (Ho and McKay, 1999):

$$q_t = \frac{k_2 q_e^2 t}{1 + k_2 q_e t} \quad (4)$$

where k_2 is the rate constant of pseudo-second order sorption (g/mg min).

The constants $q_{e.calcd.}$and $k_2$values were calculated from the slopes and intercepts of t/q_t versus t plots. The value of h_i, which is the initial FHAs adsorption rate (mg/g.min) (Chion and Li, 2003), was calculated using the $k_2$rate constant obtained from pseudo-secondorderkinetic data and expressed asequation (5):

$$h_i = k_2 q_{e.calcd.}^2 \quad (5)$$

According to Tables 2 and 3, the correlation coefficients (R^2) of the pseudo second-order kinetic model for the linear plots are higher than 0.99 for all systems. These values are higher than the R^2values of the pseudo-firstorder kinetic model (maximum value 0.9265). The calculated adsorption amount ($q_{e.calcd.}$) for the pseudo second-order kinetic model is close to the experimental one ($q_{e.exp.}$) (The values were calculated from Langmuir isotherm), but $q_{e.calcd.}$ for the pseudo-first order kinetic model are generally not supported by $q_{e.exp.}$. According to the correlation coefficient constant (R^2) and the experimental adsorption amount ($q_{e.exp.}$), it could be said that the experimental data exhibit a good compliance with the pseudo- secondorder equation for FHAs removal.

3.2.3. The Elovich equation

The Elovich equation is given as follows (McKay et. al., 1999; Low, 1960):

$$q_t = \left(\frac{1}{\beta}\right)\ln(\propto.\beta) + \left(\frac{1}{\beta}\right)\ln(t) \quad (6)$$

where is the initial adsorption rate (mg/g.h) and is the desorption constant (g/mg).

The constants and can be obtained from the slope and intercept of a straight line plot of q_t versus ln t and are listed in Tables 2 and 3.

Table 2. Pseudo-First Order, Pseudo-Second Order, Elovich, and Intraparticle Diffusion Model Constants and Correlation Coefficients for FHAs Adsorption onto BT

		Adsorbents				
Kinetic model	Constants	CornFHA/BT	OliveFHA/BT	PalmFHA/BT	SoybeanFHA/BT	SunflowerFHA/BT
	$q_{e.exp.}$ (mg/g)	0.453	0.448	0.511	0.486	0.445
Pseudo-first order	$q_{e.calcd.}$ (mg/g)	0.081	0.028	0.595	0.220	0.004
	k_1 (h^{-1})	0.116	0.112	0.115	0.122	0.115
	R^2	0.9255	0.9212	0.9265	0.9122	0.9233
Pseudo-second order	$q_{e.calcd.}$ (mg/g)	0.439	0.438	0.481	0.451	0.436
	k_2 (g/mg.h)	0.308	0.263	0.239	0.241	0.254
	h_i (mg/g.h)	0.059	0.051	0.239	0.049	0.048
	R^2	0.9965	0.9968	0.9998	0.9984	0.9971
Elovich equation	(mg/g.h)	6.686	6.225	7.642	7.042	5.872
	(g/mg)	0.218	0.178	0.219	0.225	0.136
	R^2	0.7771	0.8144	0.7839	0.7631	0.8648
Intraparticle diffusion	k_{id} ($mg/g.h^{0.5}$)	0.188	0.196	0.139	0.177	0.205
	R^2	0.9184	0.9468	0.9184	0.9262	0.9184

Table 3. Pseudo-First-Order, Pseudo-Second-Order, Elovich, and Intraparticle Diffusion Model Constants and Correlation Coefficients for FHAs Adsorption onto KT

		Adsorbents				
Kinetic model	Constants	CornFHA/BT	OliveFHA/BT	PalmFHA/BT	SoybeanFHA/BT	SunflowerFHA/BT
	$q_{e.exp.}$ (mg/g)	0.476	0.46	1.061	0.501	0.444
Pseudo-first order	$q_{e.calcd.}$ (mg/g)	0.084	0.029	0.589	0.232	0.041
	k_1 (h^{-1})	0.112	0.107	0.101	0.107	0.118
	R^2	0.9213	0.9131	0.9015	0.9134	0.9217
Pseudo-second order	$q_{e.calcd.}$ (mg/g)	0.403	0.381	0.901	0.421	0.376
	k_2 (g/mg.h)	0.751	0.821	0.118	0.672	0.769
	h_i (mg/g.h)	0.122	0.119	0.145	0.119	0.108
	R^2	0.9998	0.9999	0.9998	0.9998	0.9941
Elovich equation	(mg/g.h)	6.562	10.781	10.059	11.962	5.546
	(g/mg)	0.159	0.153	0.143	0.168	0.187
	R^2	0.8806	0.8686	0.8985	0.8716	0.7854
Intraparticle diffusion	k_{id} ($mg/g.h^{0.5}$)	0.118	0.124	0.135	0.116	0.216
	R^2	0.9418	0.9403	0.9633	0.9403	0.9184

The Elovich equation was also applied to the adsorption of FHAs by BT and KT. The linearization of the equation giving the rate of reaction allows obtaining the initial adsorption rateα (mg/g.h) from the intercept of a straight line plot of q_t versus ln t. However, the experimental initial adsorption rates were substantiallyhigher than the predicted initial adsorption rates (h_i) which have no physical sense.

Elovich equation was commonly used in the kinetics of chemisorption of gases on solids (Low, 1960). This equation has been rarely applied to liquid-state adsorption. If the adsorption of FHAs onto BT and KT is predominantly chemisorption, the Elovich equation may be used to describe the kinetics of these adsorption systems. It seems that the adsorption of FHAs onto BT and KT might be physical in nature, which explains the behavior of the studied systems.

3.2.4. The intraparticle diffusion

The intraparticle diffusion model, proposed by Weber and Morris, has been widely applied to the analysis of adsorption kinetics (Wu et. al., 2009) and can be defined as shown in equation (7) (Hameed et. al., 2009; Greluk and Hubicki, 2009):

$$q_t = k_{id} t^{1/2} + C \qquad (7)$$

The intraparticle diffusion model, proposed by Weber and Morris, has been widely applied to the analysis of adsorption kinetics (Wu et. al., 2009) and can be defined as shown in equation (7) (Hameed et. al., 2009; Greluk and Hubicki, 2009):

where k_{id} (mg/g $min^{1/2}$) is the Weber and Morris intraparticle diffusion rate constant and C is a value of intercept constant of the plot that provide information about thickness of the boundary layer (mg/g). The intraparticle diffusion constant (k_{id}) was calculated from the slope of the straight line part of the plot of $q_t$versus$t^{1/2}$.

The pseudo-first-order and pseudo-second-order kinetic models could not identify the diffusion mechanism; the kinetic results were then analyzed by using the intraparticle diffusion model. According to Greluk and Hubicki (Greluk and Hubicki, 2009), the plot of uptake q_t versus the square root of time ($t^{1/2}$) should be linear if intraparticle diffusion is involved in the adsorption process and if these lines pass through the origin then intraparticle diffusion is the rate controlling step (Wu et. al., 2009; Hameed et. al., 2009; El-Sikaily et. al., 2007). When the plots do not pass through the origin, this is indicative of some degree of boundary layer control and further shows that the intraparticle diffusion is not the only rate-controlling factor, but also other kinetic models may control the rate of adsorption, all of which may be operating simultaneously (Greluk and Hubicki, 2009). As indicated by the fact that the linear plot does not pass through the origin, suggesting that the intraparticle diffusion is not the only rate-limiting step for FHAs adsorption.

The fitted parameters of adsorption kinetics for the five fatty hydroxamic acid at 25 (Tables 2 and 3) were calculated from the non-linear regressions of the integrated equations (3), (4), (6) and (7). The profiles of the fitted curves of the experimental kinetics of that fatty hydroxamic acid were displayed in Figures 4-8.

It can be deduced from the data in Tables 2 and 3 that in BT and KT modifications, the FHAs adsorption capacity, q_e is in the order:

PalmFHA>SoybeanFHA>CornFHA>OliveFHA>SunflowerFHA

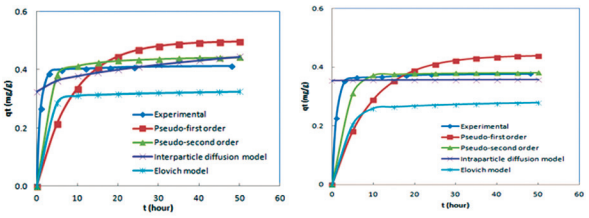

Figure 5. Different adsorption kinetic models fit for adsorption of OliveFHA on BT (left) and on KT (right) at 25°C

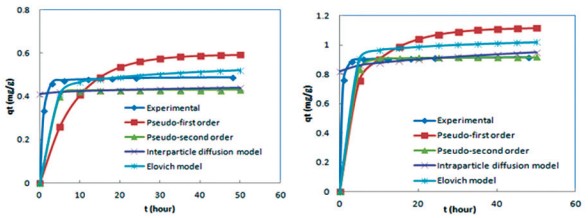

Figure 6. Different adsorption kinetic models fit for adsorption of PalmFHA on BT (left) and on KT (right) at 25°C

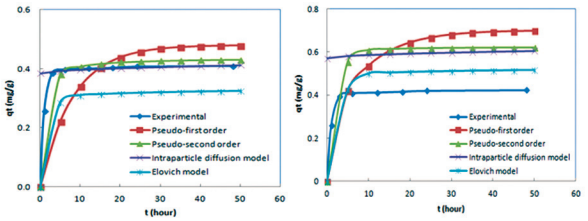

Figure 7. Different adsorption kinetic models fit for adsorption of SoybeanFHA on BT (left) and on KT (right) at 25°C

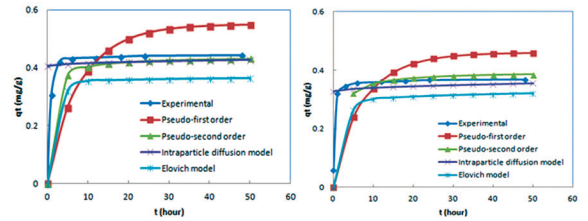

Figure 8. Different adsorption kinetic models fit for adsorption of SunflowerFHA on BT (left) and on KT (right) at 25°C

4. Conclusions

In the present study, BT and KTclays were tested as adsorbents for the removal of FHAS prepared from corn, olive, palm, soybean and sunflower vegetable oils from aqueous solution. The kinetics of adsorption of FHAs onto BT and KT was tested using four different kinetic models, namely pseudo-first order kinetic, pseudo-second order kinetic, Elovich equation and intraparticle diffusion model. All findings presented in the present study suggest that FHAssystems cannot be described by a pseudo-first order reaction and the Elovich equation. The pseudo-first order kinetic model does not give theoretical $q_{e.calcd.}$ values thatagree with the experimental $q_{e.Exp.}$ values, and the correlation coefficients R^2 values were less than 0.94. For all of the systems examined, the pseudo-second order kinetic model provided the best correlation coefficients R^2 of the experimental data (higher than 0.99) and the calculated value of adsorption capacity ($q_{e.calcd.}$) agreed well with the experimental ones ($q_{e.exp.}$), thus suggesting that the adsorption of FHAs follows the pseudo-

second order kinetic model. Intraparticle diffusion also be taken into account, but it was observed that intraparticle diffusion is not a rate-limiting step.

References

[1] Agrawal, Y. K., and Patel, S.A., 1980. Hydroxamic acids: Reagents for the solvent extraction and spectrophotometric determination of metals, Reviews in Analytical Chemistry, 4: 237-276.

[2] Agrawal, Y.K., Shrivastav, P, and Meno S.K., 2000. Solvent extraction separation of uranium (VI) with crown ether, Separation and Purification Technology, 200: 177-183.

[3] Al-Khalisy, R. S., Al-Haidary A.M.A.,and Al-Dujaili, A. H., 2010. Aqueous phase adsorption of cephalexin onto bentonite and activated carbon,Separation and Purification Technology, 45: 1286-1294.

[4] Al-Mulla, E.A.,Yunus, W.M., Nor, A.I., and Rahman, M.Z., 2009. Synthesis and characterization of N,N'-carbonyl difattyamides from palm oil, Journal of Oleo Science, 58: 467-471.

[5] Chion, M.S., and Li, H.Y., 2003. Adsorption behaviour of reactive dye in aqueous solution on chemical cross-link,ed chitosan beads,Chemosphere, 50: 95-105.

[6] Clifford, A.H., and Gessuer, G.H., 1973. The Encyclopedia of Chemistry, 3rded., Van No strand Reinhold Company, New York.

[7] Dankwardt, S.M., Martin, R.L., Chan, C.S., Van Wart, H.E., Walker, K.A.M.,Delaet, N.G., and Robinson, L.A., 2011. Amino acid derived sulfonamide hydroxamates as inhibitors of procollagenc-proteinase: Solid-phase synthesis of ornithine analogues, Bioorganic Medicinal Chemistry Letters,II: 1465-1468.

[8] Dedy, S.,Yunus, W.M.,Haron, J.,Mahiran, B., and Sidik S., 2005.Enzymatic synthesis of fatty hydroxamic acids frompalm oil, Journal of Oleo Science, 54: 33-38.

[9] El-Sikaily, A., El Nemr, A., Khaled, A.,and Abdelwehab, O., 2007.Removal of toxic chromium from wastewater using gren alga Ulva lactucaand its activated carbon, Journal of Hazardous Materials, 148: 216–228.

[10] Gadsden, J. A., 1975. Infrared Spectra of Minerals and Related Inorganic Compounds, Butterworth, London.

[11] Greluk, M., and Hubicki, Z., 2009. Sorption of SPADNS azo dye on polystyrene anion exchangers: Equilibrium and kinetic studies, Journal of Hazardous Materials, 172: 289–527.

[12] Hameed, B.H., Salman, J.M., andAhmad, A.L., 2009. Adsorption isotherm and kinetic modeling of 2, 4-D pesticide on activated carbon derived from date Stones, Journal of Hazardous Materials, 163: 121–126.

[13] Haron, M. J., Yunus, W.M., Desa, M. Z., Kassim, A., 1994. Synthesis and properties of poly(hydroxamic acid) from crosslink poly (methacrylate), Talanta, 41: 805-807.

[14] Ho, Y.S., and McKay, G., 1999. Pseudo-second order model for sorption processes, Process Biochemistry, 34: 451–465.

[15] Hoidy, W.H., Ahmad, M.B., Al-Mulla, E.A.J.,Yunus W.M.Z.W.,and Ibrahim N. B.,2010. Synthesis and Characterization of fatty Hydroxamic Acids from Triacylglycerides, Journal of Oleo Science, 59: 15-19.

[16] Holmes, J., Mast, K., Marcotte, P., Elmore, I., Li, J., Pease, L., Glaser, K., Morgan, D., Michaelides, M., and Davidsen, S., 2001. Discovery of hydroxamic acid inhibitorsof tumor necrosis factor-a converting enzyme, Bioorganic Medicinal Chemistry Letters, 11: 2907-2910.

[17] Jahangirian, H., Haron, M. J., Silong, S., and Yusof, N. A., 2011.Preparation of fatty hydroxamic acid from canola oil, Asian Journal of Chemistry,23: 3371-3374.

[18] Kurzak, B., Kozlowski, A., and Farkas F., 1992.Hydroxamic acid and amino hydroxamic acids and their complexes with metal ions, Coordination Chemistry Reviews, 114: 169-200.

[19] Lagergren, S., 1898. About the theory of so-called adsorption of soluble substances, Kungliga SvenskaVetenskapsakademiens. Handlingar 24: 1–39.

[20] Li, Z., Alessi, D., Zhang, P., and Bowman, R.S., 2002.Organo-illite as a low permeability sorbent to retard migration of anionic contaminants, Journalof Environmental Engineering, 128: 538-587.

[21] Li, Z., Bowman, R.S., 2001. Retention of inorganic oxyanions by organo-kaolinite, Water Research, 35: 3771-3776.

[22] Low, M.J.D., 1960. Kinetics of chemisorption of gases on solids, Chemical Reviews, 60: 267-312.

[23] Ma, F., Hanna, M.A., 1999.Biodiesel production: a review, BioresourceTechnology, 70: 1-15.

[24] Masuyama, A., Akiyama, K.I., Okahara, M.,1987.Surface active hydroxamic acids. I. preparation and properties of long-chain alkyl oligo (oxyethylenehydroxamic acids), Journal of the American Oil Chemists' Society, 64: 764-768.

[25] McKay, G., Ho, Y.S., and Ng, J.C.Y., 1999. Biosorption of copper from waste waters: a review, Separation and Purification Methods, 28: 87–125.

[26] Miller, J.D., Wang, X., and Li, M., 2002.Selective flotation of phosphate minerals with hydroxamate collectors, U.S. Pat., 17.

[27] Murray, H., 2007. Applied Clay Mineralogy. 1st Ed., Elsevier, Amsterdam, pp. 275-301.

[28] Pavlidon, S., and Papaspyrides C.D., 2008.A review on polymer-layered silica nanocomposites, Progress in Polymer Science, 33: 1119–98.

[29] Rauf, N., and Tahir, S., 2000. Adsorption onto Bentonite from Aqueous Solutions, Journal of Thermodynamics, 32: 651-658.

[30] Servat, F., Montet, D., Pinao, M., Galzy, P., Arnaud, A., Ledon, H., Marcou, L.,and Graillea, J., 1990. Synthesis of fatty hydroxamic acids catalyzed by the lipase of MucorMiehei, Journal of the American Oil Chemists' Society,67: 646-649.

[31] Sparks, D.L., 1986. Kinetics of reaction in pure and mixed systems,In: Soil Physical Chemistry,Edited by Sparks, D. L., CRC Press, and Boca Raton, Florida.

[32] Srivastava, P., Singh, B., and Angove, M., 2005. Competitive adsorption behavior of heavy metals on kaolinite, Chemical Journal of Colloid Interface Science, 290: 28–38.

[33] Trevino, J., and Coles, C., 2003. Kaolinite properties, structure and influence of metal retention on pH, Applied Clay Science, 23: 133–139.

[34] Vaysse, L., Dubreucq, E., Pirat, J. L., and Galzy, P., 1997. Fatty hydroxamic acid biosynthesis in aqueous medium in the presence of the lipase-acyltransferase from Candida parapsilosis, Journal of Biotechnology, 53: 41-46.

[35] Wilson, M. J., 1994. Clay Mineralogy Spectroscopic and Determinative Methods. Chapman and Hall, UK.

[36] Wu, F. C., Tseng, R. L., and Juang, R. S., 2009.Initial behavior of intraparticle diffusion model used in the description of adsorption kinetics, Chemical Engineering Journal. 153: 1-8.

JJEES
Jordan Journal of Earth and Environmental Sciences

Volume 7, (Number 1), June, 2015
ISSN 1995-6681
Pages 19 - 26

Air Quality Impact of the Upgraded Al-Samra Waste Water Treatment Plant

Abdullah Al-Mashaqbeh[1], Mahmoud Abu-Allaban[2]*, Ahmad Al-Malabah[3]

[1]Post Graduate Student, Department of Water Management and Environment, the Hashemite University, Zarqa, Jordan.
[2]Department of Water Management and Environment, the Hashemite University, Zarqa, Jordan.
[3]Department of Earth Sciences and Environment, the Hashemite University, Zarqa, Jordan.

Received 10 February, 2015; Accepted 10 April 2015

Abstract

In 2008, a new wastewater treatment plant at Al-Samra replaced the old wastewater ponds, which were designed in the sixties of the 20th century to treat the sewage influx from Amman-Zarqa areas. The upgrade has significantly improved the water quality in the Zarqa river and is believed to be a key point in restoring aquatic life in the river. It also reduced atmospheric pollution in Al-Hashemeyyah, which reduced the complaints of the neighboring residents about the odors and flies. In the present study, data for atmospheric pollution at Al-Hashemeyyah were acquired from the Ministry of Environment and investigated in order to detect the changes of air pollution levelsin the town. Data clearly show that concentrationof the atmospheric H_2S has declined significantly after 2008. AERMOD dispersion Modeling was deployed in order to quantify the contribution of Al-Samra wastewater treatment plant to ambient air pollution at Al-Hashemyyah. AERMOD results revealed that concentrations of ambient H_2S, CH_4, and NH_3in the vicinity of Al-Samra wastewater treatment facilities are well below the national and the international standards of ambient air quality. The outcomesof AERMOD also revealed that the concentrations of gasses mentioned above vanish within a short distance downwind from Al-Samra. Thus, Al-Samra wastewater treatment plant is no longer a potential source of air pollution in Al-Hashemeyyah town.

Keywords: Jordan, Air Pollution, Wastewater Treatment, Methane, Hydrogen Sulfide.

1. Introduction

Jordan has stretched water resources of only 150 m^3 per capita per year, which is at the survival level and is considered to be one of the most water scarce countries in the world. The 150 m^3 per capita per year is continuously decreasing due to rapid population growth and global warming-induced drought. This harsh situation requires Jordan to adopt a strict integrated water management plan that promotes water recycling. Therefore the local regulations allow for the direct reuse of reclaimed water to irrigate fodder and flowers. However, the reclaimed water is not to be used to irrigate vegetables or fruits unless mixed with freshwater including storm water.

Al-Samrawastewater treatment plant (ASWWTP) is the largest wastewater treatment station in Jordan. It was built in the sixties of the 20th century for the purpose of promoting water recycling and to protect ground water aquifers in Zarqa-Amman basin. Al-Samra serves a population of about 5million inhabitants living in Amman and Zarqa which are experiencing a rapid population growth due to natural, social, and political factors.Prior to the current substantial upgrade of Al-Samra, received sewage was diverted into wastewater stabilization ponds where it stayed and settled for about 48 hours before being released to Wadi Dhuleil, which empties in Zarqa river after about 10km. The quality of the released water failed the national and international corresponding standards of reclaimed wastewater, which imposed devastating impacts on the Zarqa river and King Talal dam downstream. The latter is the second largest dam in Jordan. King Talal dam stores treated sewage and storm water to be released into the Jordan valley where it is used for irrigation. Public complaints of rodents, flies, and mosquitoes were common among local communities along the route of Wadi Dhuleil and Zarqa river. Air quality was also impacted by the uncontrolled release of hydrogen sulfide (H_2S), methane (CH_4), and other odorous compounds.

In order to improve the water quality in the Zarqa river and King Talal dam, the Jordanian Ministry of Water and Irrigation decided to replace the old and overloaded Al-Samra wastewater stabilization ponds by a modernized wastewater treatment plantat a cost of $169M. The new plant treats wastewater by using the activated sludge technology. The construction of the new plant started in 2003 and ended in 2008. The new facility was officially commissioned in August 2008. The new facility treats an average flow of 267,000 cubic meters of wastewater on a daily basis. Upgrading of Al-Samra wastewater treatment plant has significantly improved the water quality in the Zarqa river (Al-Omari et, al., 2013) and is believed to be a key factor for the restoration of the aquatic life therein.

Air pollution continues to receive a great deal of interest

* Corresponding author. e-mail: abuallaban@yahoo.com

worldwide due to its negative impacts on human health and welfare. Several studies reported significant correlations between air pollution and certain diseases, including shortness of breath, sore throat, chest pain, nausea, asthma, bronchitis and lung cancer (Dockery and Pope, 1994). Extreme effects of air pollution include high blood pressure and cardiovascular problems (Pope et. al., 2002; Sanjay, 2008). Correlations between air pollution and increased morbidity and mortality rates were also reported (Laden et. al., 2000; Pope et. al., 1995).The World Health Organization states that 2.4 million people die each year from causes directly attributed to air pollution (WHO, 2007). Epidemiological studies suggest that more than 500,000 Americans die each year from cardiopulmonary diseases linked to breathing fine particle air pollution (Marsh and Bernstein, 2008). Another study showed a strong correlation between pneumonia related deaths and air pollution from motor vehicles in UK (Knox, 2008). In addition to its negative health impacts, air pollution is known to cause injuries to animals, forests and vegetation, as well as to aquatic ecosystems. Its impacts on metals, structures, leather, rubber, and fabrics include cracks, soiling, deterioration, and erosion (Boubel et. al., 1994).

Odors are the main cause of nuisance associated with wastewater treatment facilities. Inlet works, grit channels, screening and grit handling, aeration tanks, as well as sludge holding and dewatering units are the main sources of odor at the wastewater treatment facility.Hydrogen sulfide (H_2S) is the most prevalent malodorous gas associated with the domestic wastewater collection and treatment. The conditions leading to H_2S formation usually favor the production of other odorous gases, such as ammonia and mercaptants, which may have considerably higher detectable odor thresholds, and consequently H_2S may be an indicator of their presence.

In addition to odors and aerosols, wastewater treating generates methane. Wastewater is treated to remove the organic matter using biological processes in which microorganisms consume the organic matter for maintenance and growth. The anaerobe organism digests the organic component of the sewage and produces biogas, which is a mixture of methane (about 70%), carbon dioxide (about 20%), hydrogen sulfide (3%), among other gases. Most released methane at Al-Samra wastewater treatment plant is harnessed and burned to generate electricity used to operate its machineries.

The aim of the present study is to assess the impact of the newly upgraded Al-Samra wastewater treatment plant on air quality at neighboring communities.

2. Study Area

Al-Samra wastewater treatment plant (coordinates: Longitude 36° 04′ to 39º 09′ east and Latitude 32º 04′ to 32 10 north) is located approximately 50 km to the North-East of Amman within the valley of Wadi Dhuleil (Figure 1). Al-Samra falls within a semi-arid climate characterized by hot-dry summer and wet-mild winter with less than 150 mm total annual rainfall. The average annual temperature is 17.1 °C, with a minimum temperature of 2.4 °C recorded during January and a maximum temperature of 32.6 °C recorded during August. Average relative humidity ranges between 39.3% during May and 70.3% during January. Wind direction fluctuates between North-West to South-West during autumn and winter, whereas westerly wind dominates summer days (Odat, 2009).

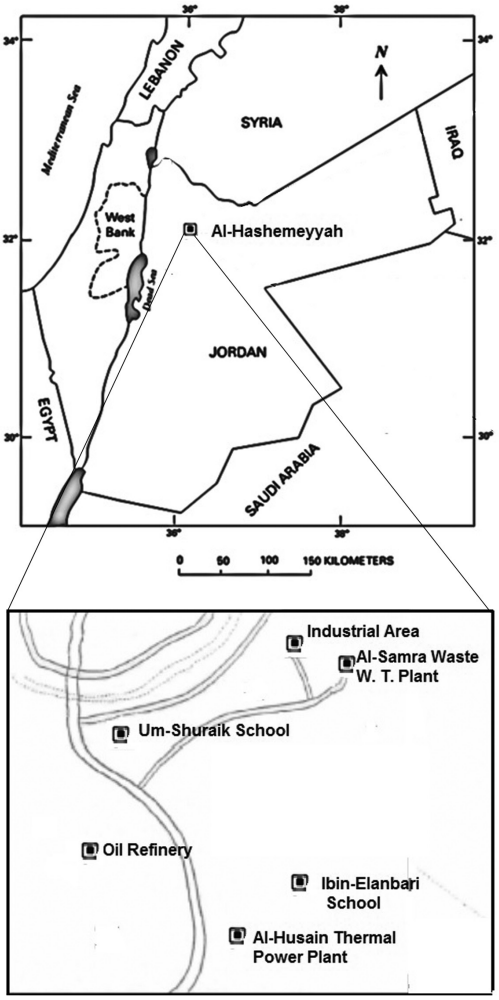

Figure 1. Location of the study area (modified after Odat, 2012)

3. Research Method

This study investigates the impact of Al-Samra water treatment plant on the air quality in the neighboring communities within Al-Hashemeyyah town. The required air quality data, through the period 2006-2010, were obtained from the Jordanian Ministry of Environment (JMOE). In addition, AERMOD (EPA, 2004) is used to estimate the concentrations of NH_3, CH_4, and H_2S in ambient air based on emissions emanated fromASWWTP.

AERMOD uses a Gaussian and a bi-Gaussian approach in its dispersion models. It generates daily, monthly as well as annual concentrations of pollutants in ambient air. The model handles a variety of pollutant sources in a wide variety of settings such as rural and urban as well as flat and complex terrain. It is an updated version of the Industrial Source Complex (ISCST3) model being proposed by the USEPA for assessing air quality impact from industrial sources in the coming years. One of the major improvements that AERMOD brings is its ability to characterize the planetary boundary layer (PBL) through both surface and mixed layer scaling (EPA, 2004).

4. Analysis of Air Quality Data

Qualification and quantification of all odorants in the vicinity of Al-Samra wastewater treatment plants is quite complex because there are many odorants that are present in very low concentrations. However, hydrogen sulfide is such an odorous compound that is often present in higher concentrations than other odorants, especially in sewer networks and in primary treatment of domestic wastewaters; therefore, it can give a general indication of the overall odor concentration. Hydrogen sulfide can be measured in very low concentrations (down to parts per billions levels).

The Ministry of Environment keeps records of measured H_2S and methane as measured in the two monitoring stations at Um-Shuraik school and Ibin-Elanbari school. Concentrations of ambient H2S for the period 2003-2010 are presented in Tables 1 and 2.

A careful reading of Table 1 leads to the conclusion that Al-Hashemyyah town is experiencing severe air pollution by H2S. In fact, a measured one-hour H2S concentration frequently exceeds the Jordanian standard of 0.03 ppm. The percentage number of exceedances at Ibin El-Anbary could be as high as 38% of the total measurements. Similarly, up to 27% of total hourly H2S measurements at Um Shuraik in 2005-2006 exceeded the Jordanian standard. The daily-averaged H2S concentration at Ibin El-Anbari and Um Shuraik also exhibited many exceedances of the 24-hr Jordanian standard of 0.01ppm. The percentage of daily exceedances could be as high as 84% and 70% at Ibin El-Anbari school and Um Shuraik, respectively.

There are several local sources that may contribute to the buildup of H2S concentration at Al-Hashemeyyah including the oil refinery and the thermal power plant in addition to Al-Samra wastewater treatment. Fortunately, the ambient concentration of H_2S decreased significantly after 2008 as compared with preceding years. This could imply that the new Al-Samra plant, which was put in service in 2008, no longer spews excessive amount of H_2S to ambient air, leaving only the oil refinery and the thermal power plant as the main polluters in the town. This important finding requires a further investigation in order to assess how much exactly Al-Samra contributes to H_2S in ambient air at Al-Hashemyyah. This is done through a dispersion modeling of H_2S, which is discussed in the next chapter.

Table 1: Summary of maximum hourly H_2S concentration in ambient air at Al-Hashemyyah town during the period 2006-2010. Maximum allowed value is 0.03 ppm not to be exceeded more than three times a year

Location	Period	Max H_2S (ppm)	Number of Exceedings	Percent of Exceedings
Ibin El-Anbari	2010	0.259	33	0.42%
	2009	0.528	839	11.30%
	2007-2008	0.068	35	0.41%
	2006-2007	0.742	2689	38.10%
	2005-2006	0.426	1771	24.30%
Um Shuraik	2010	0.206	202	2.50%
	2009	0.139	508	7.40%
	2007-2008	0.287	750	11.10%
	2006-2007	0.933	1344	17.74%
	2005-2006	0.828	1941	26.90%

Table 2: Summary of Maximum Daily Concentration Rate of H_2S at Al-Hashemyyah (2006-2010) (ppm). Maximum allowed value is 0.01 ppm not to be exceeded more than three times a year

Location	Period	Max. Daily H_2S (ppm)	Number of Exceedings	Percent of Exceedings
Ibin El-Anbari	2010	0.053	3	0.89%
	2009	0.112	122	33.70%
	2007-2008	0.011	3	0.87%
	2006-2007	0.092	240	83.92%
	2005-2006	0.074	234	77.50%
Um Shuraik	2010	0.35	27	7.69%
	2009	0. 34	68	21.10%
	2007-2008	0.057	104	38.81%
	2006-2007	0.188	144	48.81%
	2005-2006	0.308	216	69.70%

The measured H_2S data revealed that the maximum concentration occurs during the cold periods (winter time and in the evening). This shows that atmospheric stability is an important factor of pollution dispersion. Cold time periods often experience thermal inversion, which means that air temperature increases with altitude. During thermal inversion convection currents cease and air mixing will be suppressed, which in turn inhibits dilution of air pollution. This implies that air pollution increases during the thermal inversion.

Our findings go along with a previous study by Saffarini and Odat (2008) who deployed a different time series analysis of monthly air pollution at Al-Hashimeyyah, finding that air pollution data for the period 1992–2004 exhibited an overall decreasing trend in the concentrations of NO_2, CO, H_2S, NO and TSP, but with an increasing trend in PM_{10}, and Pb, whereas SO_2 did not significantly change. Odat (2009) investigated the impact of weather parameters (air temperature, wind speed, rainfall, wind direction, cloud and relative humidity) on the concentrations of air pollution at Al-Hashemeyyah and found that wind and relative humidity were the main parameters that impacted the H_2S concentration in ambient air.

4.1. Input of AERMOD Model

Odors emitted from wastewater treatment plants are becoming a significant source of environmental annoyance. Odor-related complaints from the communities surrounding the wastewater treatment plants have been constantly increasing since the past decade. This fact is typically the result of a new residential development near the plants. The main emanated odorous compounds are ammonia, methane, and sulfur containing substances such as hydrogen sulfide, methyl mercaptan, dimethyl sulfide, dimethyl disulfide, ethyl mercaptan, carbon disulfide and carbonyl sulfide. Nitrogen, containing substances such as ammonia, amines, indole and skatole, may also cause problems (Abbott, 1993; Gostelow and Parsons, 2000; Easter et. al., 2005). All of these substances are the products of anaerobic decay and, hence, wastewater which, as it is allowed to become septic, has a strong potential to become odorous. Although various odorous compounds may be present, the most significant is the hydrogen sulfide.

The main impact from the existence of H_2S in the atmosphere is the annoyance caused to humans. The detection

and perception of odors by humans is an extremely complex process. The main factors determining whether an odor causes annoyance are the concentration of the odorous compound in the air, the "odor quality," the odor appearance frequency and the odor duration (EPA, 2006).

AERMOD dispersion modeling was applied for the assessment of the odor impacts on ambient air quality. Emission rates of CH_4 and H_2S are presented in Table 3.Required surface meteorological data and upper sounding for year 2012 were obtained from Amman Airport.

Table 3: Emission rates of methane, and hydrogen sulfide

Substance	Emission Rate (g/s)
Methane (CH_4)	40.5
Hydrogen sulfide (H_2S)	2.4

4.2. AERMOD Modeling Results

4.2.1. Predicted Concentration of Hydrogen Sulfide

Predicted H_2S concentrations in ambient air are illustrated in Figures 2-4. It is clear that the highest predicted one-hour H_2S concentration is less than 8ppb, which is which is well below the Jordanian standard of 0.03 ppm (30 ppb) measured values at Um Shuraik school and Ibin El-Anbary school. 24-hr and annual H_2S concentrations in the vicinity of Al-Samra wastewater treatment plant are way below the measured values at the two monitoring sites. This is a strong piece of evidence that Al-Samra wastewater treatment plant is no longer the main source of H_2S in Al-Hashemeyyah town.

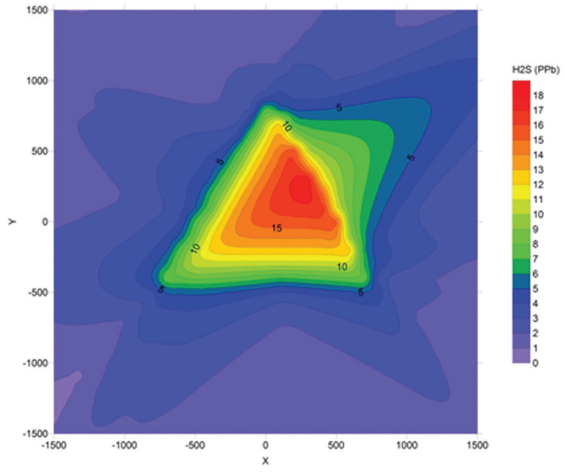

Figure 2. Contour plot for predict one-hour H_2S (ppb) in the vicinity of ASWWTP which is assumed to be at the center of the map at coordinates (0, 0)

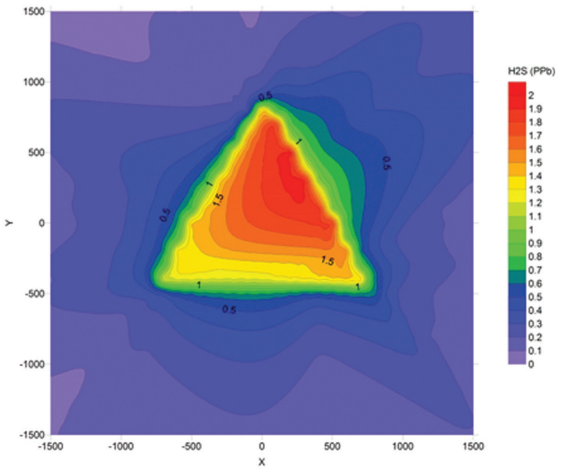

Figure 3. Contour plot for predict 24-hours H_2S (ppb) in the vicinity of ASWWTP which is assumed to be at the center of the map at coordinates (0, 0)

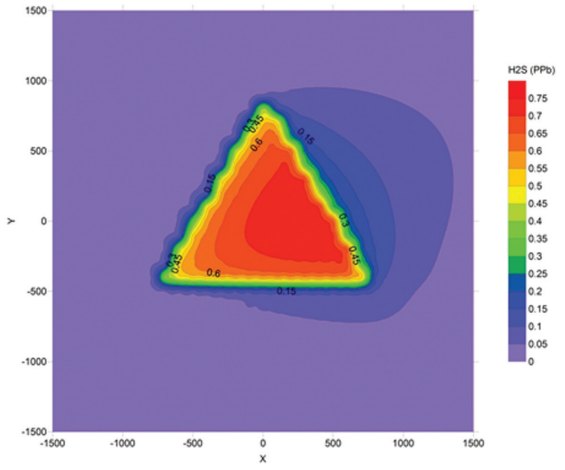

Figure 4. Contour plot for annual H_2S (ppb) in the vicinity of ASWWTP which is assumed to be at the center of the map at coordinates (0, 0)

4.2.2. Predicted Concentration of Methane

The predicted methane concentrations in ambient air are illustrated in Figures 5-7. It is clear that the highest predicted methane concentrations are about 290 ppb, 35ppb, and 13 ppb for 1-hr, 24-hrs, and annual time intervals, respectively. Because methane is a natural constituent of the air, there are no national standards that regulate its ambient concentration. In addition, most of the generated methane is harnessed locally and used to generate electricity that helps maintain a state-of-art integrated environmental management plan adopted by Al-Samra in its reformed configuration.

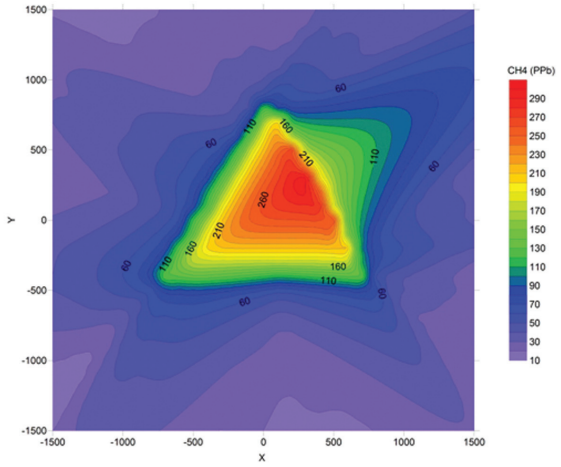

Figure 5. Contour plot for one-hour methane (ppb) in the vicinity of ASWWTP which is assumed to be at the center of the map at coordinates (0, 0)

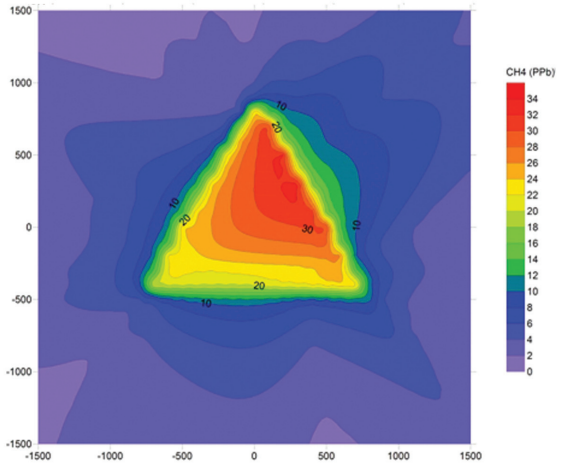

Figure 6. Contour plot for 24-hours methane (ppb) in the vicinity of ASWWTP which is assumed to be at the center of the map at coordinates (0, 0)

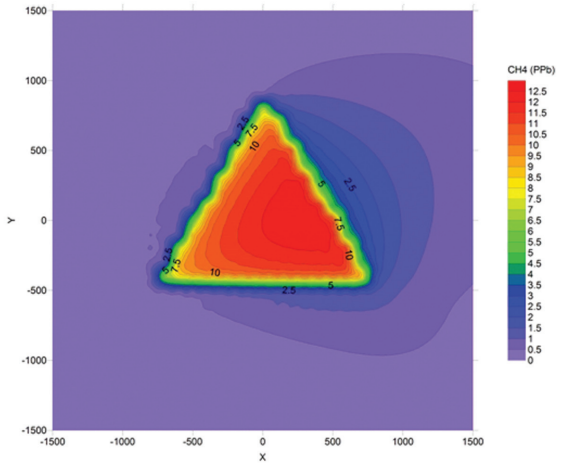

Figure 7. Contour plot for annual methane (ppb) in the vicinity of ASWWTP which is assumed to be at the center of the map at coordinates (0, 0)

4.2.3. Predicted Concentration of Ammonia

Predicted ammonia concentrations in ambient air are illustrated in Figures 8-10. It is clear that the highest predicted concentrations of ammonia are 75 ppb, 8 ppb, and 3 ppb which are well below standards suggested by the World Bank of 800 ppb, 400ppb, and 140 ppb for 1-hr, 24-hrs, and annual time intervals, respectively. Standards suggested by the World Bank are used for comparisons, because there are no Jordanian standards for ammonia in ambient air to compare our findings with.

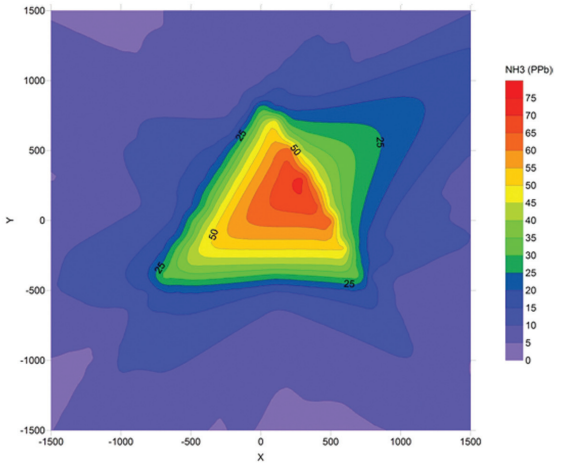

Figure 8. Contour plot for one-hour ammonia (ppb) in the vicinity of ASWWTP which is assumed to be at the center of the map at coordinates (0, 0)

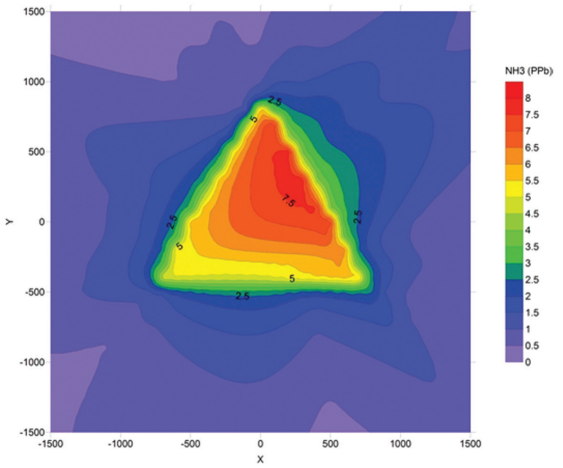

Figure 9. Contour plot for 24-hours ammonia (ppb) in the vicinity of ASWWTP which is assumed to be at the center of the map at coordinates (0, 0)

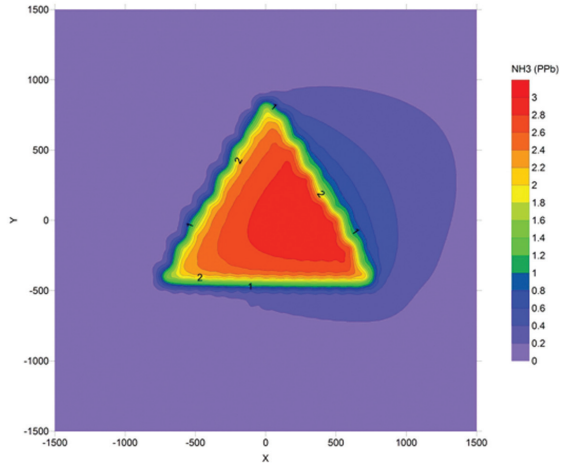

Figure 10. Contour plot for annual ammonia (ppb) in the vicinity of ASWWTP which is assumed to be at the center of the map at coordinates (0, 0)

4.3. Local Community Complains

After the construction of the new Al-Samra wastewater treatment plant, complains by local communities at Al-Hashemeyyah town significantly decreased. Currently, the main reason for annoyance is the flies invasion during the summer time. The officers at Al-Samra plant are working with local municipalities to fight flies, but still more efforts are required to prevent the flies invasion.

Another intermittent source of annoyance is the odors during moments of inversion, which are frequent during the autumn months. In late summer and early autumn, the earth surface and the adjacent air warm rapidly during the day time. During the night time, the earth surface cools rapidly but the air cools at a slower rate. Any air parcels that cool become denser and sink down leaving behind warm air molecules. These processes lead to an unusual situation where cold air is trapped below the warm air, which causes thermal inversion, the condition that suppresses dilution of H_2S, CH_4, and NH_3. Therefore, these gases are trapped close to the earth surface and travel horizontally to longer distances until reaching, and thus annoying, the neighboring communities.

The odor perception by humans is proportional to the instantaneous peak concentration of the odorant rather than to mean values (Latoset. al., 2011). AERMOD, like other dispersion models, is set for calculation of at least half-hour mean concentrations. The sensation of odor, however, depends on the momentary (peak) odor concentration and not on a mean value. Therefore, the H_2S concentrations illustrated in Figure 1 are adjusted to 5 seconds average concentration and then converted into odors unit (AU), which is equivalent to 0.47 ppb. In order to calculate the 5-second average concentration, the hourly averaged concentrations predicted by AERMOD are first converted to 3-minute average concentrations using the formula below (Duffee et. al., 1991):

$C_1 / C_s = (t_s / t_1)^n$

where C_1 and C_s are the time averaged odor concentrations in longer and shorter periods,

respectively; t_1 and t_s are the longer and shorter time averaging periods respectively; and

n is an exponential value which depends upon the stability class; it is considered to be 0.167. Note that same formula can be used to estimate the 1-minute concentration but with different values for n (usually between 0.35 and 0.65).

The 3-minute average concentration is converted to 5-second average concentrations by multiplying by a factor of 5 (OME, 1996). The findings are illustrated in Figure 11. It is now evident that the odors concentration could be as high as 800 AU inside Al-Samra plant itself, but the concentration drops exponentially to less than 50 AU at 2000m downwind from the facility.

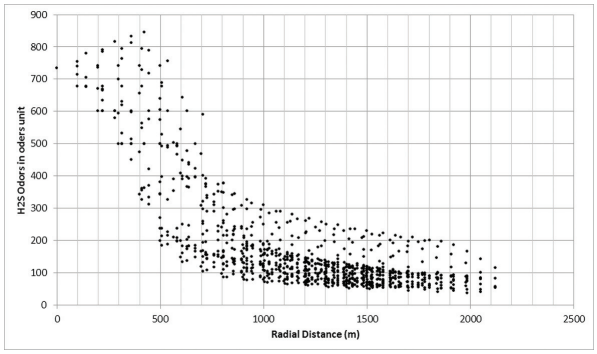

Figure 11. Spatial variation of the five-second average odors concentration in the vicinity of ASWWTP in odors unit

4. Results and Discussion

The challenge of sustainable water management in semi-arid countries like Jordan is magnified by the country's geography, hydrology, climate and trans-boundary issues. The country is divided into semi-arid, arid or hyper-arid regions with at least six rainless months per year. Rainfall variations occur from year to year, with periods of multi-year droughts or near droughts interspersed with periods of heavy rainfall.

Water scarcity has been of concern to Jordan since the fifties of the 20th century when Israel diverted Jordan River to southern regions. The rapid increase in population as a result of natural birth and refugee-waves from the neighboring states due to political instabilities and/or economic crises, coupled with extensive agricultural growth, have placed a continuous and growing demand on Jordan's limited water resources. This harsh situation persuades Jordan to adopt an integrated water management plan that promotes a sustainable use of water resources.

Among the practices that Jordan prides itself with is water recycling through the construction of several wastewater treatment stations. Sewage treatment is being accepted worldwide as an important component of integrated water management plans because it protects surface water bodies as well as groundwater aquifers and aids the agricultural sector by water of excellent quality that could be used in drip irrigation, which, in turn, increases fresh water allocations to domestic and industrial sectors.

In Jordan, there are more than 26 wastewater plants that treat about 0.5 billion cubic meter of row sewage per year. Al-Samra is the largest wastewater treatment plant nationwide; it treats about half quantity mentioned above. Al-Samra receives sewage from Amman and Zarqa cities and discharges its effluents to Wadi-Dhuleil, which is one of the tributaries of the Zarqa river. The treated water is mixed with storm water at King Talal dam and then the mixed water is released to the

Jordan Valley where it is used for irrigation.

Al-Samra wastewater treatment plant is an important component in the water management plan in Jordan. However, it used to have devastating impacts on environmental receptors in the region including the deterioration of the water quality in the Zarqa river to the extent that no aquatic life could exist in the river. Odors and sulfur compounds released during the sewage treatment was another obvious local problem. These negative impacts, in addition to Jordan's real need for every water droplet, have convinced the Ministry of Irrigation to upgrade Al-Samra wastewater treatment plant. Thereby, in 2000, the Ministry of Irrigation invited the private sector to share in building a new facility based on the Build-Operate-and Transfer (BOT) principle. In 2008, the new facility was officially opened and replaced the old plant. The new Al-Samra wastewater treatment plant produces reclaimed water with excellent properties that meet the national and the international standards.

The air quality in Al-Hashemyyah town has improved as well after upgrading ASWWTP. Staff at the Hashemite University (HU), which is located about 8km to the south-east of Al-Samra, felt the improvement of the air quality, especially during autumn. Before 2008, morning odors of urea and H_2S were very common in late summer and early autumn months. Currently, odors have almost disappeared, and HU staff experience lesser events of bad smells inside the campus.

In order to investigate the impact of upgrading the ASWWTP on air quality, the present study is undertaken. The study is divided into two phases. In the first phase, air quality data for the years 2003-2010 were investigated. The findings of this phase showed that atmospheric H_2S were often higher than the national standards of 0.03 ppm up to 2008. After 2008, atmospheric H_2S concentration decreased significantly.

In phase two, the famous AERMOD dispersion model was deployed to quantify the contribution of the upgraded Al-Samra wastewater treatment plant on atmospheric H_2S, CH_4, and NH_3. The findings of this phase revealed that Al-Samra wastewater treatment plant is no longer a potential source of the gasses mentioned above in Al-Hashemeyyah town and the surrounding areas. The concentrations of these gases in ambient air almost vanish within a short distance (2km) of the plant. However, the neighboring communities complain of H_2S odors during moments of thermal inversion due to the absence of air mixing.

5. Summary and Conclusions

The 2008 extension and upgrade of Al-Samra wastewater treatment plant led to a significant reduction of atmospheric H_2S, which used to be a main source of annoyance for the nearby communities. Thus, Al-Samra wastewater treatment plant is no longer a potential source of air pollution in Al-Hashemeyyah town, yet local residents still suffer from the high levels of air pollution, especially during the night time. This implies that there is a real need for a local emission inventory and a comprehensive source attribution study in order to determine the potential sources of air pollution and to quantify their fractional contributions to ambient air pollution.

Acknowledgment

The authors are grateful to the Jordanian Ministry of Environment for providing real data for ambient H_2S concentration in Al-Hashemyyah area.

This study is part of the master thesis of the first author.

References

[1] Al-Omari, A.S., Al-Houri, Z. M., Al-Weshah, R. A. (2013) Impact of the As Samra wastewater treatment plant upgrade on the water quality (COD, electrical conductivity, TP, TN) of the Zarqa River. Water Science & Technology, 67(7):1455-64. DOI: 10.2166/wst.2013.686

[2] Abbott J. (1993)Enclosed wastewater treatment plants-health and safety considerations. Foundation for Water Research Report FR/W 0001.

[3] Boubel, R.W., Fox, D.L., Turner, D.B., and Stern, A.C. (1994) Effects on Materials and Structures. Fundamentals of Air Pollution, 3rd ed. Academic Press, New York.

[4] Dockery, D.W., Pope , C.A. (1994) Acute respiratory effects of particulate air pollution. Annual Revision Public Health 15, 107–132.

[5] Duffee, R.A., O'Brien, M.A., Ostojic, N., 1991, OdorModeling: Why and How, Transactions -Air & Waste Management Association, Pittsburgh, Pennsylvania, 1991. In recent Developments and Current Practices in Odour Regulations, Control and Technology.Edited by D.R. Derenzo and A. Gnyp.

[6] Environmental Protection Agency (EPA, 2004) AERMOD, Description of Model Formulation. EPA-454/R-03-004) at the environmental protection agency main site www.epa.gov/scram001/7thconf/aermod/aermod_mfd.pdf

[7] Easter, C., Quigley, C.,Burrowes, P., Witherspoon, J., Apgar, D. (2005) Odor and air emissions control using biotechnology for both collection and wastewater treatment systems. Chemical Engineering Journal, 113: 93-104

[8] EPA 2006. Assessment and Management of Odor from Stationary Sources in NSW", NSW Environment Protection Authority, Sydney.

[9] Gostelow P. and Parsons S. A. (2000) Sewage treatment works odor measurement. Water Science and Technology, 41(6): 33–40.

[10] Knox, G. (2008) Atmospheric pollutants and mortalities in English local authority areas. J. Epidemiol Community Health, 62:442-447 doi:10.1136/jech.2007.065862.

[11] Laden, F., Neas, L.M., Dockery, D.W., Schwartz1, J. (2000) Association of Fine Particulate Matter from Different Sources with Daily Mortality in Six U.S. Cities. Environ Health Perspect, 108:941–947. http://ehpnet1.niehs.nih.gov/docs/2000/108p941-947laden/abstract.html

[12] Latos, M. , P. Karageorgos, N. Kalogerakis, M. Lazaridis (2011) Dispersion of odorous compounds emitted from wastewater treatment plants. Journal of Water Air and Soil Pollution, 215(1):667-677. DOI: 10.1007/s11270-010-0508-8

[13] Marsh, C. and Bernstein, M. (2008) Newly detected air pollutant mimics damaging effects of cigarette smoke. American Chemical Society. http://www.eurekalert.org/pub_releases/2008-08/acs-nda072308.php.

[14] Odat, S. (2009): Diurnal and Seasonal Variation of Air Pollution at Al-Hashimeya Town, Jordan. JJEES 2(1): 1 -6.

[15] Odat, S. (2012): Data Analysis of Air pollution and meteorological effects in Al-HashimeyaTown, Zarqa- Jordan. Elixir Pollution 52: 11231-11237.

[16] Ontario Ministry of Environment (OME), 1996, Odor Impacts - An Overview.Science and Technology Branch, Environmental Engineering Services, STB Technical Bulletin No. EES-1, February 1996.

[17] Pope, C.A., Thun, M.J., Namboodira, M., Dockery, D.W., Evans, J.S., Speizer, F.E., Health Jr., C.W., (1995) Particulate air pollution as a predictor of mortality in a prospective study of US adults. American Journal of Respiratory Critical Care Medicine, 151: 669–674.

[18] Pope, C.A., Burnett, R.T., Thun, M.J., Calle, E.E., Krewski, D., Ito, K., and Thurston, G.D. (2002) Lung Cancer, Cardiopulmonary Mortality, and Long-term Exposure to Fine Particulate Air Pollution. Journal of American Medical Association, 287(9): 1132-1141.

[19] Saffarini, G. and Odat, S. (2008): Time Series Analysis of air pollution in Al-Hashimeya Town Zarqa, Jordan. JJEES, 1(2): 63- 72

[20] Sanjay, R.(2008) Exposure to Bad Air Raises Blood Pressure. Science Daily, Ohio State University. http://www.sciencedaily.com/releases/2008/07/080728114026.htm

[21] World Health Organization (2007) Estimated deaths & DALYs attributable to selectedenvironmental risk factors, by WHO Member State. Department of Public Health &Environment, January 2007.

JJEES
Jordan Journal of Earth and Environmental Sciences

Volume 7, (Number 1), June, 2015
ISSN 1995-6681
Pages 27 - 35

Rainfall Fluctuation for Exploring Desertification and Climate Change: New Aridity Classification

Mohammed A. Salahat*[1], Mohammed I. Al-Qinna[1]

[1]Department of Land Management and Environment, Faculty of Land Management and Environment, The Hashemite University, Zarqa, Jordan

Received 26 January, 2015; Accepted 17 May 2015

Abstract

The research community in Jordan is basically relying on universal defined aridity classifications, which do not consider the local conditions of Jordan and climate change effects on Jordan. The present study aims at producing a customized aridity classification that better fits the conditions of Jordan. Monthly rainfall data for the period between 1961-2012, for 22 weather stations covering the whole country, were obtained from Jordanian Meteorological Department (JMD). A ten-year moving average was calculated and used for conducting a historical trend analysis and generating aridity spatial maps. Monthly, annual, and ten years moving average aridity trends were tested using Tukey test, Mann-Kendall rank, and a simple linear regression. According to the historical trend analysis, rainfall across the country is significantly (< 0.0001) spatially and temporally distributed, where 90% of the country falls within arid to semi-arid classes. Climate change impacts in Jordan resulted in a shorter rainy season with lower amounts of precipitation and the number of rainfall events. The overall annual rainfall tended to decrease significantly (P<0.05) by time with an average reduction rate of 1.1 mm per year. Although the overall trend for most of the rainfall stations was decreasing, individual annual rainfalls analysis indicated the possibilities of extreme events to occur at some locations. The overall trend showed that more frequent drought seasons are expected. According to the new generated aridity classification maps, the country is suffering from a severe shifting to lower rainfall means. The southern and the northern-eastern parts shifted from strongly arid (100-150 mm) into hyper arid class (< 100). Moreover, west-middle part also shifted to moderately arid class (150 – 200 mm). On the other hand, the most obvious shift occurred at the semiarid classes especially the slightly and moderately subclasses. Currently, the wettest two classes (sub-humid and slightly semi-arid) are not present in the map and shifting towards a strongly semi-arid class.

Keywords: Aridity, desertification, climate change, rainfall variability, Jordan

1. Introduction

Dry lands form about one third of the world lands with insufficient rainfall that supports only sparse vegetation and a limited population of people and animals. They are generally threatened by land degradation mainly linked to the low amounts of mean annual precipitation, such as desertification, loss of biota, drought, etc. Aridity, in general, is thrived by climate change since it usually results in lower precipitation amounts with increasing the opportunity of extreme events. Aridity is very important in water resources management issues, where it has a basic role in determining spatial location of water deficit and extreme shortage of water supply.

Defining aridity is crucial to understand the motivators for many aspects of land degradation, and there are many aridity indices used by research community (Middleton and Thomas, 1997; Noin and Clarke, 1998), with many techniques to derive them. Most classifications rely on some combination of the number of days of rainfall, the total amount of annual rainfall, evapotranspiration, temperature, humidity, or other factors.

It is hard to distinguish between aridity and drought since they have almost the same effects. The conceptual difference between them is equivalent to that between climate and weather. In the case of aridity, the lack of rainfall depends on the local climate and represents a permanent or seasonal condition. While drought is a transitory phenomenon related to the meteorological variability and, as such, it can strike everywhere and at any time with levels of intensity and persistence which cannot be determined a priori (Cook et. al., 2004). Aridity and drought, however, represent two sides of the same coin; along with the long-term trends triggered by climate change there has been a tight recurrence of drought episodes that had affected areas previously not prone to such phenomena, as well as other areas suffering from water shortage (Salvati et. al., 2013).

In the Mediterranean region the rainfall seasonality strengthens the effects and impacts of climate change (Salvati, 2009; Toreti et. al., 2010). Trends in climate aridity and the increasing frequency in drought events can lead to desertification (UNCCD, 2010). That said, it is necessary to investigate intensity, spatial distribution, and temporal evolution of water shortage caused by aridity.

Jordan, located in an arid region, suffers highly from

* Corresponding author. e-mail: mdsalahat@hu.edu.jo

water deficit. Globally, Jordan is ranked among the first three countries with water scarcity. Jordan water resources are very scarce and mainly rely on rainfall. Therefore, any reduction in annual rainfall will in turn affect the water status and hence all sectors that use water, i.e., agriculture and industry. Change in intensity of precipitation has been used as an indicator for anticipated climate change. There is evidence that a climate change is changing the behavior of precipitation, especially, the extremes (MoE, 2009; Trenberth, 2011). The spatial distribution of rainfall has also been observed to change. Generally, throughout the subtropics dry areas becoming drier and wet areas becoming wetter especially in the mid to high latitudes (Trenberth, 2011).

In Jordan, most studies on precipitation were focused on trends in mean daily, monthly and annual rainfall (Al-Qudah and Smadi, 2011). The reduction in the total rainfall and the number of rainy days was reported in Jordan (Smadi and Zghoul, 2006). Despite the crucial importance of trends in maximum and intensity of precipitation to indicate climate change, still they are not fully understood yet (Al-Qudah and Smadi, 2011). In general, the results of most previous research were not able to statistically find a significant trend (Freiwan and Kadioglu, 2008; Ghanem, 2011).

The research community in Jordan is basically relying on the universal defined aridity classification, which does not consider the local conditions of Jordan and the way it is affected by climate change. Therefore, the present work aims to produce a new customized aridity classification that fits the conditions of Jordan. The proposed new classification will emphasize more on regions with low rainfall, and will generate a spatial map that shows temporal rainfall changes, thus, providing a powerful tool for researchers to understand climate change effects and investigate food security issues, etc.

2. Materials and Methods

2.1. Study Area

Jordan is located about 80 km to the east of the Mediterranean Sea with a predominant Mediterranean climate; hot and dry summers and wet and cool winters. Jordan is also characterized by a unique topographic nature, where the western part represents the world lowest valley that lies north-south between two mountain ranges with a length of about 400 km and a width varies from 10 km in the north to 30 km in the south and elevation between 170-400 m below Mean Sea Level (MSL). The Jordan River passes through this valley from north to south down to the Dead Sea. Just to the east of the Jordan Valley the north-south mountain range reaches about 1150 m above MSL in the northern parts and about 1500 m above mean sea level in the southern parts of Jordan. To the east of this mountain range, a semi desert plateau extends to cover approximately 80% of the total area of the country.

According to the geographic and topographic characteristics, Jordan is divided into three main climatic regions (FAO, 2012): the Ghor Region (lowlands), Highlands, and the Badia and Desert region (Figure 1).

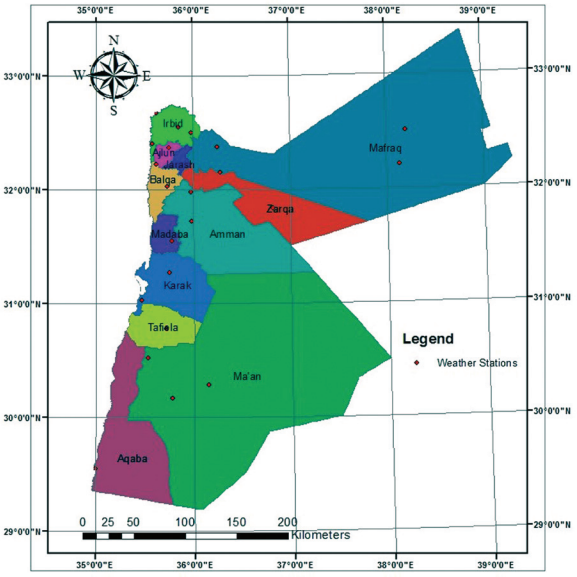

Figure 1. Study area and the location of weather stations

The Ghor (Lowlands) is part of the Great Rift Valley with a length of about 400 km extending from north to south. The Ghor consists of three parts: the Northern Jordan Valley, the Dead Sea (The lowest elevation on earth) and Wadi Araba. The elevation of the Ghor ranges from 197 m below MSL in the north to more than 400 m below MSL at the Dead Sea. The width of the Ghor is approximately 15 km in the north expanding gradually to about 30 km in the south. The area of the Ghor east of River Jordan and Dead Sea is about 3000 km^2.

The Highlands and Marginal Scarpment Region extends north-south to the east of the Ghor. The mountainous region extends from the Yarmouk River in the north to Ras El-Naqab in the south; the mountain ranges are dissected at several locations by valleys such as Zerqa River, WadiMujib and Wadi El-Hasa. The elevation of the peaks of these mountains varies from 1150m above MSL in the north (RasMuneef) to about 1365m above MSL in the south (Al-Shoubak), some peaks exceeds 1500m above MSL (El-Qurain). The total area of the mountains regions is about 7900 km^2. The marginal steppes region stretches from north to southeast of the mountainous region, from the Syrian borders in the north to Ras Al-Naqab in the south. It has an area of 9000 km^2 that represents most potential rangeland of Jordan.

The Badia and desert region extends north-south from the foot of the highlands eastward. The total area of the Badia and the desert is about 70000 km^2, with an elevation of about 600-750 above MSL, the annual rainfall of the Badia ranges from 50 to 100 mm. The south-east of the region is true desert with annual rainfall less than 35 mm; the total area of the Jordanian Desert is 30000 km^2.

2.2. Rainfall Stations Data

Monthly rainfall data for the periods of (1961-2012) for 22 weather stations were obtained from Jordanian Meteorological Department (JMD) distributed across the countryto represent all the topographic and climatic regions and to cover larger

parts of the country (Figure 1). The annual rainfall magnitudes for each station were calculated.The robustness of local data time series is one of the major constrains and limitations for assessing the climate variables and indices future projections, thus a ten-year Moving Average (MA) was calculated for each station point. Both the individual rainfall and the ten years MA data were used for conducting historic trend analyses and spatial mapping for aridity.

2.3. Aridity Index

There are many techniques to derive an aridity index. Most of the available classifications (e.g., Intergovernmental Panel on Climate Change (IPCC 2007), UNESCO (1979), Thornthwaite, 1948) rely on some combination of the number of days of rainfall, the total amount of annual rainfall, evapotranspiration, temperature, humidity, or other factors. In the present study, using only mean annual rainfall was selected to derive and customize the aridity index due to its reliability, simplicity, and small amount of data needed (only rainfall). Based on the IPCC, 2007 index, areas with less than 250 mm mean annual rainfall is considered arid, areas between 250 and 500 mm are semi-arid, while areas with annual precipitation higher than 500 mm are considered sub-humid and humid. Accordingly, Jordan is mostly arid and semi-arid, therefore the investigation was focused on the low rainfall areas dividing them into subclasses that fit Jordan's conditions using Geographic Information Systems (GIS) spatial analyst platform. Initially, spatial maps were generated using GIS version 10.3 software based on different ranges of rainfall, then the selection of the approved classification was made after visually studying the generated spatial maps and selecting the map with least impurities and that has a reasonable number of subclasses.

2.4.Variability Testing and Trends Analyses

Aridity trends and changes were tested through testing monthly, annual, and ten years Moving Average (MA) rainfall variability using the comparison between means Tukey HSD (Honestly Significant Difference) platform within JMP (2012) statistical software. Tukey HSD test is an exact alpha-level test (usually P = 0.05, where the confidence is 95%) that is based on Least Significant Difference (LSD) similar to t-test; however, it is conservative since it tackle the differences in the sample sizes (Hayter, 1984; Tukey, 1991).

The annual and ten years MA trends of monotonic increase or decrease between the beginning and the end of an available time series was detected using two methods: (1) the linear regression trends (Pearson Product-Moment Correlation), and (2) nonparametric "Mann-Kendall rank trend test" (Bartlett and Kendall, 1946). The trend analysis was made on both year and month basis to assess monotonic changes dominancy over the historic period.

The Pearson product-moment correlation coefficient (r) was calculated using the Multivariate Platform within JMP (2012) statistical software. It measures the strength of the linear relationship between two variables (Equation 1). If there is an exact linear relationship between two variables, the correlation is 1 or -1, depending on whether the variables are positively or negatively related. If there is no linear relationship, the correlation tends toward zero:

$$R = \frac{\sum_{i=1}^{n}(x_i - \bar{x}_i)(y_i - \bar{y}_i)}{\sqrt{\sum_{i=1}^{n}(x_i - \bar{x}_i)^2}\sqrt{\sum_{i=1}^{n}(y_i - \bar{y}_i)^2}} \quad (1)$$

The Mann-Kendal Test (τ_b) was performed using Non-Parametric test Platform within JMP (2012) statistical software, where observations are ranked in order according to the value of the first variable. The observations are then re-ranked according to the values of the second variable. The number of interchanges of the first variable is used to compute Kendall's τ_b coefficients. The Kendall's τ_b coefficients range from -1 to +1 and are based on the number of concordant and discordant pairs. A pair of rows for two variables is concordant if they agree in which variable is greater. Otherwise, they are discordant or tied. The Kendall's was computed using Equation (2):

$$\tau_b = \frac{\sum_{i<j}^{n} \mathrm{sgn}(x_i - x_j)x_i \mathrm{sgn}(y_i - y_j)}{\sqrt{\left(\frac{n(n-1)}{2} - \sum\frac{(t_i)(t_i-1)}{2}\right)\left(\left(\frac{n(n-1)}{2} - \sum\frac{(u_i)(u_i-1)}{2}\right)\right)}} \quad (2)$$

where, sgn (z) is equal to 1 if z > 0, 0 if z = 0, and -1 if z < 0.The t_i (the u_i) are the number of tied x (respectively y) values in the ith group of tied x (respectively y) values, n is the number of observations, and Kendall's τ_b ranges from -1 to 1. If a weight variable is specified, it is ignored.

2.5. Spatial Modeling

The individual and 10-year MA rainfalls were spatially analyzed using ordinary interpolation within ArcGIS software (ESRI® version 10.1). ArcGIS Geostatistical Analyst tool was used to interpolate the spatial behavior of rainfall distributions following four stages of analysis: (1) histogram analysis and standardization, (2) autocorrelation using Moran I tests, (3) characterization and selection of best empirical fit to represent the actual spatial variations using semivariogram modeling, and (4) interpolation of rainfalls at unknown locations using kriging techniques.

The semi-variance clouds in all directions were computed using Equation 3 (Selker et. al., 1999), and the best empirical variogram model was selected based upon the lowest root mean square error (RMSE) (Goovaerts, 1997):

$$\gamma(h) = \frac{1}{2N(h)}\sum_{i=1}^{N(h)}\left[(Z(x) - Z(x+h)\right]^2 \quad (3)$$

where, g(h) is the semi-variance, z(x) is the value of initial potential at site x, z(x+h) is the value of potential at site (h) distance from (x), and N is the number of sample pairs.

The Ordinary Kriging (OK) technique was used to assess the spatial extent of rainfall quantities. The OK method assumes a constant unknown mean, where the value at the unsampled point can be predicted by a linear weighing of the variation between the surrounding points derived from

variogram analyses (Equations (4a) and (4b)):

$$Z(X_0) = \mu + \varepsilon(X_0) \quad (4a)$$

$$Z(X_0) = \sum \lambda_i \ \gamma(x_i), \quad \sum \lambda_i = 1 \quad (4b)$$

where, μ is an unknown constant and $e(X_0)$ is the error associated with an unknown location X_0, $Z(X_0)$ is the estimated value of Z at X_o, and λ_i is the weight that gives the best possible estimation from the surrounding points.

3. Results and Discussion

3.1.Characterization of Current Climatic Conditions

According to the historic meteorological data, rainfall across the country is significantly (< 0.0001) spatially and temporally distributed. Table 1indicates that the major part of the country (90%) is arid to semi-arid, characterized by very low annual precipitation that averages less than 220mm. The annual total precipitation amounts varied sharply from one climatic region to another from a minimum average of 28 mm at the southern Badia region to a maximum average of 573 mm at the upper northern highlands region of RasMuneef. Along the Ghor region, the highest point was at the north where it may reach 280 at Deir-Alla and decreased towards the south till 71 mm at Ghor Safi. In mountains, the average annual precipitation exceeded 573 mm in RasMuneef and 542 mm at Salt mountains, decreasing gradually southward to 333 mm in ErRabbah, and 270mm in Shoubak.

In the steppes region, the amount of rainfall was about 100-200 mm. It was 153 mm in Mafraq and 139 mm in Wadi Dhulail. In the Badia, it was about 75-110 mm in the north decreasing to about 60 mm in the south (57 mm in Azraq south and 97 mm in Qatraneh, 80 mm in Rawaished, and 41mm in Ma'an). In the Jordanian Desert (south east of Jordan) the annual rainfall was less than 30 mm in Al-Jafr till reaching Aqaba with 30 mm annual precipitation.

Sometimes, unstable summer rainfall events might occur due to heat convection from land to atmosphere, uplifting and condensation at mountains, but their quantities are almost negligible.

Table 1. Individual annual mean and mean of 10 years moving average (MA) comparison using Tukey HSD test per station

Station	Available data	Count of years	Individual annual mean		Mean of 10 years MA	
			Mean	Tukey HSD* Rank	Mean	Tukey HSD* Rank
RasMuneef	1960-2012	52	573.0	a	576.5	a
Salt	1961-2012	51	541.9	a	547.5	b
Irbid	1960-2012	52	469.2	b	472.5	c
Baqura	1967-2012	45	382.8	c	390.8	d
ErRabbah	1960-2012	52	333.0	cd	340.8	e
Wadi El-rayyan	1960-2012	52	295.6	de	301.1	f
DeirAlla	1960-2012	52	281.3	def	288.1	fg
Shoubak	1960-2012	52	270.2	def	276.9	gh
Amman Airport	1960-2012	52	260.2	ef	263.0	h
Alhasan/Tafileh	1971-2012	41	229.7	efg	224.4	i
Ramtha	1976-2012	36	220.8	fgh	224.0	i
Q.A.I.Airport	1960-2012	52	166.1	ghi	165.3	j
Mafraq	1960-2012	52	153.0	hij	157.0	jk
WadiDhulall	1968-2012	44	139.2	ijk	140.9	k
Qatraneh	1960-2012	52	97.0	jkl	97.2	l
Rwaished	1960-2012	52	79.6	klm	81.5	lm
Ghor Safi	1974-2012	38	71.4	klm	74.3	m
Safawi	1960-2012	52	71.1	klm	72.0	m
Azraq South	1981-2012	31	57.3	lm	60.2	mn
Ma›an	1960-2012	52	40.8	lm	42.0	no
Al Jafer	1960-2012	52	30.4	m	31.4	o
Aqaba	1960-2012	52	28.2	m	29.4	o

* Levels not connected by same letter are significantly different according toTukey HSD test at 95% confidence level.

The rainy season extends from around October to May of the next year and about 80% of the seasonal rainfall occurs through the months of December to March (Table 2). Maximum rainfall events generally occurred in January, however, it might sometimes occur earlier in November or delayed till late January or February. According to Figure 2, it is observable that the climate change impacted the rainy season considerably through shortening the season, reducing the quantity of rainfall, lowering the number of rainfall events, and shifting the time of occurring. The temporal change indicated that the maximum rainfall started to be more observable in February and, thus, a shift existed with shortening or narrowing the rainy month's extents at both ends (i.e., October-November and April-May rainfalls were becoming rare).

Table 2. Average over years of rainfall quantities for each month for the different stations

Station	Jan	Feb	Mar	Apr	May	Jun	Jul	Aug	Sep	Oct	Nov	Dec
Q.A.I.Airport	41.0	36.4	28.1	9.3	2.0	0.1	0.0	0.0	0.1	3.7	14.6	32.0
Al Jafer	5.9	3.7	4.3	3.3	1.2	0.0	0.0	0.0	0.1	3.9	3.3	4.4
Alhasan/Tafileh	57.6	46.7	40.8	15.6	1.7	0.0	0.0	0.0	0.0	3.7	16.3	45.2
Amman Airport	62.3	59.0	43.3	12.7	2.7	0.1	0.0	0.0	0.1	7.2	23.9	48.6
Aqaba	5.5	4.4	3.4	2.9	0.9	0.0	0.0	0.0	0.0	2.2	2.9	6.0
Azraq South	12.8	9.8	9.1	4.1	1.3	0.0	0.0	0.0	0.3	2.8	6.2	9.8
Baqura	92.1	75.6	54.3	20.4	5.4	0.2	0.0	0.0	0.8	14.1	44.9	80.3
DeirAlla	66.2	55.7	42.7	14.9	3.1	0.1	0.0	0.0	0.5	10.2	33.9	54.2
ErRabbah	85.0	74.3	54.3	19.6	3.9	0.0	0.0	0.0	0.1	6.2	28.5	61.7
Ghor Safi	13.7	16.5	11.7	5.1	1.2	0.0	0.0	0.0	0.2	3.1	5.7	14.0
Irbid	104.9	104.4	81.4	24.7	5.7	1.0	0.0	0.0	0.6	14.0	45.6	85.7
Ma'an	8.5	7.2	5.8	3.1	1.5	0.0	0.1	0.0	0.2	4.9	3.8	5.6
Mafraq	34.9	31.5	25.2	7.4	2.1	0.1	0.0	0.0	0.3	6.4	17.8	27.2
Qatraneh	24.7	20.3	16.5	6.5	1.5	0.0	0.0	0.0	0.0	4.1	7.6	18.0
Ramtha	47.9	51.1	37.8	10.4	3.2	0.7	0.0	0.0	0.2	7.8	24.9	39.1
RasMuneef	129.1	127.9	93.1	30.0	7.6	1.0	0.1	0.0	0.6	17.4	64.1	115.0
Rwaished	13.5	14.3	10.0	10.9	3.7	0.2	0.0	0.0	0.3	7.0	9.4	10.8
Safawi	13.7	14.2	9.2	5.4	1.9	0.0	0.0	0.0	0.1	5.1	9.0	11.7
Salt	136.0	124.7	90.3	26.4	3.5	0.1	0.0	0.0	0.2	12.4	50.6	105.6
Shoubak	69.6	55.9	46.4	16.9	4.0	0.1	0.0	0.0	0.2	5.5	19.5	51.3
WadiDhulall	34.6	29.0	21.9	6.9	2.2	0.1	0.0	0.0	0.1	4.7	15.6	24.2
Wadi El-rayyan	70.1	58.8	42.2	13.8	4.4	0.1	0.0	0.1	0.7	14.0	35.5	60.7
Average	**51.8 a**	**46.9 b**	**35.4 d**	**12.4 f**	**3.0 gh**	**0.1 h**	**0.0 h**	**0.0 h**	**0.3 h**	**7.4 g**	**22.2 e**	**41.7 c**

3.2.Rainfall Variability and Trend Analysis

The Mann-Kendall trend and the linear trends of the time series at overall scale and station scale are presented in Table 3. Mann-Kendall results indicatedthat the rainfall at country scale was statistically significant at either 5 percent or the 1 percent confidence levels. The resulted trends are strong evidence of climate change in Jordan during the last 50 years. According to the historic climatic linear analyses, the overall annual precipitation regardless the station tended to decrease significantly ($P<0.05$) by time with a reduction rate of 1.0 to 1.1 mm per year for individual annual and 10-years MA, respectively.

According to the trend analysis for annual and 10-year MA rainfall at station level, a climatic change was obviously apparent and its impact was noticed as indicated by their high significant Kendall and linear regression trends (Table 3). However, very few stations showed a significant increase in precipitation, such as Ras Muneef and Wadi El-Rayyan. Precipitation tended to decrease in number of rainy days, which may be attributed to an increase in the daily rainfall intensity and, thus, an increase in the chance of recording extreme precipitation events. On the other hand, many other stations experienced an increasing number of rainy days associated with decreasing annual precipitation amounts, leading to a decrease in daily rainfall intensity such as Wadi Dhuleil, Irbid and Al-Rabba (Figure 3).

Although the overall trend for most the rainfall stations is decreasing as indicated by the MA; however, individual annual rainfalls showed the variations in wet and drought seasons and, thus, possibilities of extreme events. Figure 4 shows an example of one of the stations where very wet seasons occurred in 1967, 1974, 1980, and 1992, while drought seasons were more frequent and observable at all stations during 1963, 1970, 1973, 1976-1979, 1984, 1986, 1999, 2000, 2004, and 2008.

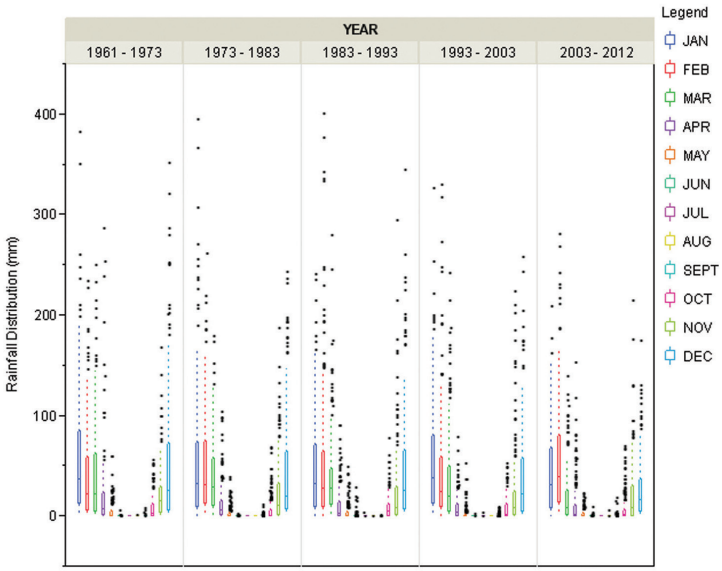

Figure 2. Temporal change in rainfall distribution around the year

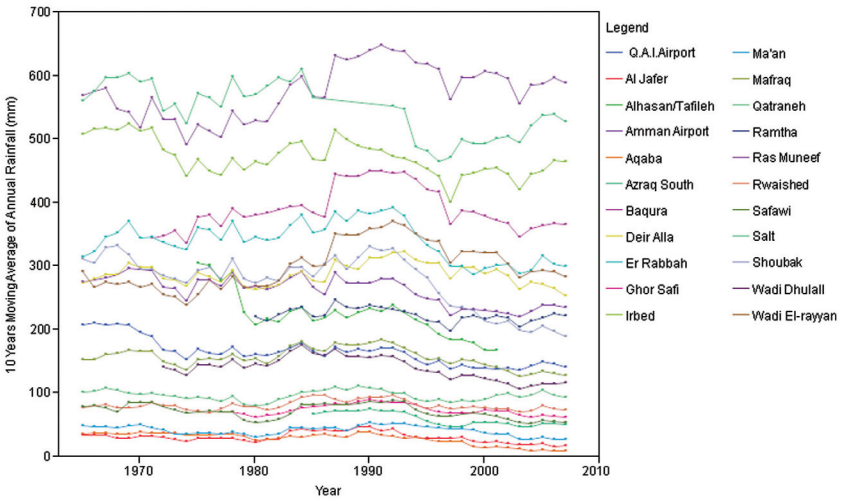

Figure 3. 10 years moving average annual rainfall distribution per station

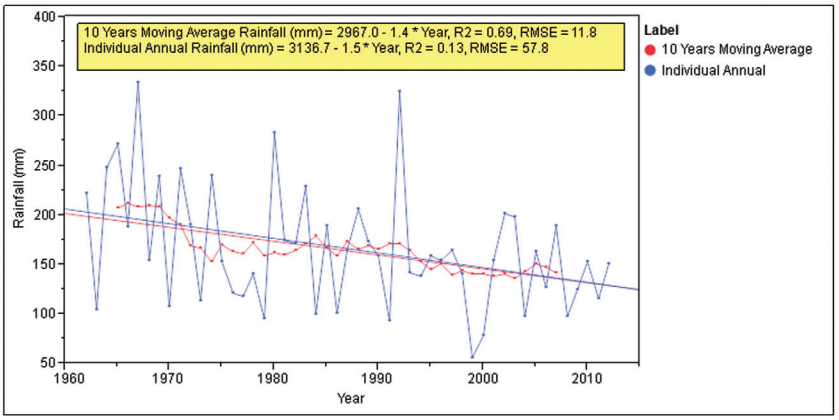

Figure 4. Example for moving average and individual annual rainfalls for Q.A.I. Airport station

Table 3. Mann-Kendall and Pearson trend statistics of individual annual and 10-years moving average (MA) rainfall by station

No.	Station name	Individual annual			10 years MA			10 years MA rainfall trend			
		Kendall τ	Prob>|τ|	R	Kendall τ	Prob>|τ|	r	Trend Equation	R^2	RMSE	Prob> F
1	Q.A.I.Airport	-0.2376	0.0139*	-0.3680	-0.6035	<.0001**	-0.8771	= 2967.0 - 1.41 * Year	0.6960	11.85	<.0001**
2	Al Jafer	-0.1911	0.0503	-0.2233	-0.2935	0.0055**	-0.3958	= 435.1 - 0.20 * Year	0.1009	7.71	0.0379*
3	Alhasan/Tafileh	-0.2034	0.0857	-0.4115	-0.5556	<.0001**	-0.8747	= 7521.3 - 3.67 * Year	0.6519	21.71	<0.0001**
4	Amman Airport	-0.1576	0.1026	-0.2055	-0.5127	<.0001**	-0.8217	= 3010.4 - 1.38 * Year	0.5887	14.70	<0.0001**
5	Aqaba	-0.3392	0.0004**	-0.4348	-0.6700	<.0001**	-0.8796	= 1282.6 - 0.63 * Year	0.7016	5.23	<0.0001**
6	Azraq South	-0.2000	0.1140	-0.2719	-0.5494	0.0002**	-0.9023	= 2617.7 - 1.28 * Year	0.7010	5.81	<0.0001**
7	Baqura	-0.0081	0.9376	0.0119	0.0601	0.6009	0.1447	= -384.7 + 0.39 * Year	0.0153	34.30	0.4652
8	DeirAlla	-0.0510	0.5975	-0.0754	0.0122	0.9084	0.0468	= 1832.0 + 0.05 * Year	0.0016	17.04	0.8017
9	ErRabbah	-0.0510	0.5975	-0.1219	-0.1849	0.0805	-0.4810	= 2380.4 - 1.03 * Year	0.1733	28.50	0.0055**
10	Ghor Safi	-0.1964	0.0827	-0.2281	-0.1908	0.1387	-0.4200	= 624.7 - 0.28 * Year	0.0787	8.47	0.1331
11	Irbid	-0.1341	0.1649	-0.1501	-0.4219	<.0001**	-0.6942	= 3288.8 - 1.42 * Year	0.3901	22.53	<.0001**
12	Ma'an	-0.1859	0.0542	-0.2155	-0.2447	0.0207*	-0.4282	= 460.3 - 0.21 * Year	0.1294	6.94	0.0178*
13	Mafraq	-0.0886	0.3587	-0.1231	-0.2182	0.0392*	-0.4024	= 1027.1 - 0.44 * Year	0.1219	14.94	0.0217*
14	Qatraneh	-0.0259	0.7887	-0.1279	-0.1185	0.2628	-0.2143	= 256.3 - 0.08 * Year	0.0157	8.07	0.4241
No.	Station name	Individual annual			10 years MA			10 years MA rainfall trend			
		Kendall τ	Prob>|τ|	R	Kendall τ	Prob>|τ|	r	Trend Equation	R^2	RMSE	Prob> F
15	Ramtha	0.0032	0.9783	-0.0459	-0.2698	0.0439*	-0.5002	= 1255.6 - 0.52 * Year	0.1592	9.97	0.0354*
16	RasMuneef	0.0149	0.8774	0.0720	0.3178	0.0027**	0.6382	= -3206.1 + 1.90 * Year	0.3277	34.67	<0.0001**
17	Rwaished	-0.0086	0.9288	-0.0810	-0.0831	0.4325	-0.0313	= 122.8 - 0.02 * Year	0.0012	7.77	0.8286
18	Safawi	-0.1937	0.0448*	-0.2821	-0.3245	0.0022**	-0.5429	= 905.7 - 0.42 * Year	0.2173	10.12	0.0016**
19	Salt	-0.0828	0.4225	-0.1797	-0.4084	0.0004**	-0.7783	= 5056.1 - 2.27 * Year	0.5215	29.78	<0.0001**
20	Shoubak	-0.2675	0.0056**	-0.3678	-0.4640	<.0001**	-0.7908	= 5163.2 - 2.46 * Year	0.5286	29.53	<0.0001**
21	WadiDhulall	-0.1534	0.1425	-0.2394	-0.4159	0.0004**	-0.6721	= 2177.1 - 1.02 * Year	0.3516	14.86	<0.0001**
22	Wadi El-rayyan	0.0298	0.7576	0.0813	0.3577	0.0007**	0.5873	= -2708.5 + 1.52 * Year	0.2823	30.70	0.0002**
Overall mean		-0.0584	0.0052**	-0.0891	-0.0537	0.0195*	-0.1055	= 2289.7 - 1.04 * Year	0.0057	165.47	0.0261*

* sign indicates significant trends at the 5 percent confidence level, and
** sign indicates significant trends at the 1 percent confidence level

The trend statistical analysis of precipitation on a monthly basis indicated that the reduction is highly significant during the whole rainy season except for February where the rainfall tended to increase by a rate of 0.25 mm per year (Table 4). On the other hand, summer rainfall events tended to increase insignificantlyduring the dry seasons of June, July August, and September.

 - Volume 7, (Number 1), (ISSN 1995-6681)

Table 4. Historical trend analysis for average monthly rainfall

Month	Linear Model	Mann-Kendall τ	Prob>|τ|	R^2	RMSE	Prob> F
Jan	= 560.45 - 0.26 * Year	-0.0194	0.3504	0.0045	55.69	0.0303*
Feb	= -442.9 + 0.25 * Year	0.0498	0.0167*	0.0042	55.16	0.0352*
Mar	= 813.8 - 0.39* Year	-0.1175	<0.0001**	0.0187	41.22	<0.0001**
Apr	= 430.8 - 0.21* Year	-0.1260	<0.0001**	0.0167	23.51	<0.0001**
May	= 80.5 - 0.04 * Year	-0.0065	0.7726	0.0069	6.79	0.0072**
Jun	= -5.7 + 0.003 * Year	0.0057	0.8193	0.0008	1.48	0.3468
Jul	= -0.3 + 0.0002 * Year	0.0180	0.4772	0.0002	0.17	0.6692
Aug	= -0.7 + 0.0004 * Year	0.0083	0.7430	0.0008	0.18	0.3458
Sep	= -13.4 + 0.007 * Year	0.1158	<0.0001**	0.0063	1.25	0.0096**
Oct	= 48.9 - 0.02* Year	-0.0247	0.2544	0.0007	11.87	0.4080
Nov	= 115.7 - 0.05 * Year	-0.0678	0.0013**	0.0004	33.51	0.5090
Dec	= 1028.7 - 0.50 * Year	-0.0660	0.0015**	0.0187	52.44	<0.0001**

* sign indicates significant trends at the 5 percent confidence level, and
** sign indicates significant trends at the 1 percent confidence level

3.3. Spatial Modeling and Aridity

According to the spatial analysis for the 10 years MA annual rainfalls, the semi-variogram suggested anisotropic rainfall behavior with an orientation of 24 degrees. In general, the aridity of the country was spatially and temporally obvious and increased over time. Several aridity classifications were investigated and the most appropriate was chosen and applied as in (Table 4). The western northern part of the country and across all the years received the highest rainfall (> 400 mm), while the eastern and southern parts were the most arid (<100 mm) (Figure 5). The country is suffering from shifting to lower rainfall means. A strongly arid class existed at the southern and the northern-eastern parts from year 1960 till 2000 disappeared and turned into hyper arid class. Moreover, west- middle part are slightly arid class that used to receive 200 to 250 mm, currently it shifted to be under moderately arid class with range of 150-200 mm. before year 2000.

On the other hand, it is obvious that the climate change impact was more effective on the semi-arid classes, especially the slightly and moderately subclasses. Currently, the two wet classes have disappeared from the map and have shifted towards strongly semi-arid.

The results of moving average clearly showed that the period 1970 to 1980 was the most wet period, and the rainfall amount exceeded 500 mm was during this period only (Fig. 5).

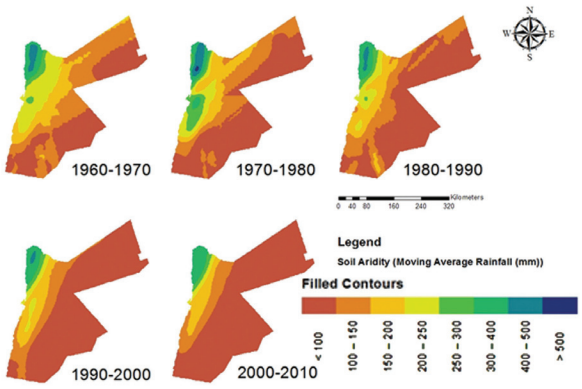

Figure 5. Spatial and temporal distribution of MA annual rainfall across the country with adopted aridity classification

Table 5. Recommended aridity subclasses customized to Jordan conditions

Class	1 Hyper arid	2 Strongly Arid	3 Moderately Arid	4 Slightly Arid	5 Strongly Semi arid	6 Moderately Semi arid	7 Slightly Semi arid	8 Subhumid
Mean annual rainfall (mm)	< 100	100 – 150	150 - 200	200 - 250	250 - 300	300 - 400	400 - 500	>500

4. Conclusions

The use of spatial and temporal statistics of rainfall was helpful in identifying the extent of aridity classes in Jordan. In the present study, the rainfall index was enough to illustrate and visualize the extent of aridity change across the country. Statistical trend analyses of monthly, annual, and ten years moving average rainfall using Tukey HSD, Mann-Kendall rank, and Pearson Correlation Coefficient of Linear Regression for 22 weather stations indicated clear evidence on the severity of global warming and, thus, the desertification impact. The rainfall variability over the past 50 years was highly significant that is temporally and spatially variable.

The climate change had considerablyimpacted the rainy season through shortening the season, reducing the quantity of rainfall, lowering the number of the rainfall events, and the shifting time of occurring. Temporal analyses revealed a shift

in the maximum rainfall to be more observable at February with narrowing the rainy month's magnitudes at both ends. The rainfall linear trend analysis suggested a significant decrease ($P<0.05$) by about 1.1 mm per year and, thus, acerbating the pressurized demand on water for various sectors. On the other hand, very few stations showed a significant increase in precipitation, such as RasMuneef and Wadi El-Rayyan that could be used for further strategic planning as surface water catchments.

In terms of sever events, the monthly and annual individual trend analyses indicated an increase in the possibility of both wet and drought seasons where the drought phenomenon is more observable across the country. Although the wet season's temporal and spatial magnitudes are still unpredictable, their existence is evident and increasing over time and, thus, should be taken seriously in the future strategic planning under the theme of flood risk assessments.

Although the major part of the country (90%) is arid to semi-arid and characterized by a very low annual precipitation that averages less than 220mm, the aridity of the country is increasing over time. The adopted aridity classification was able to visualize the existing shifts occurred over the past 50 years using the temporal and spatial modeling tools within GIS.The shift was clearer at the semi-arid classes, especially the slightly and moderately subclasses that changed towards a strongly semi-arid class. In addition, strongly arid classes within southern and the northern-eastern parts of the country are changing into a hyper arid class. Moreover, a slightly arid class at west-middle parts was shifted to a moderately arid class.

The results of the present study vitally and critically urge the need for National Adaptive Management Action Plans (NAMA) in all related sectors especially water and agriculture. Future scenarios for natural resources management at a local scale should incorporate projects that demonstrate the actual aridity status and change with the adopted new classification.

References

[1] Al-Qudah, K. A. and A. A. Smadi. 2011. Trends in Maximum Daily Rainfall in Marginal Desert Environment: Signs of Climate Change American Journal of Environmental Sciences. 7 (4): 331-337.

[2] Bartlett, M.S. and D.G. Kendall. 1946. The Statistical Analysis of Variances-Heterogeneity and the Logarithmic Transformation.JRSS Suppl. 8, 128-138.

[3] Cook E. R., C. A. Woodhouse, C. M. Eakin, D. H. Meko, and D. W. Stahle. 2004. Long-term aridity changes in the western United States, Science, vol. 306, no. 5698, pp. 1015–1018.

[4] ESRI. 2014. ArcGIS Software Version 10.1 Redlands, California, USA: ESRI Inc.

[5] FAO, 2012. Assessment of the risks from climate change and water scarcity on food productivity in Jordan.

[6] FreiwanMuwaffaq and MikdatKadioglu. 2008. Spatial and temporal analysis of climatological data in Jordan. Int. J. Climatol. 28: 521–535 DOI: 10.1002/joc.1562.

[7] Ghanem, A.A., 2011. Climatology of the areal precipitation in Amman/Jordan. Int. J. Climatol., 31: 1328-1333. DOI: 10.1002/joc.2160.

[8] Goovaerts P. 1997. Geostatistics for natural resources evaluation. Oxford University Press, New York.

[9] Hayter, A.J. 1984. A proof of the conjecture that the Tukey-Kramer multiple comparisons procedure is conservative. Annals of Mathematical Statistics, 12 61-75.

[10] [IPCC] Intergovernmental Panel on Climate Change. 2007. Climate change 2007: Impacts, adaptation and vulnerability. In M. L. Parry, O. F. Canziani, J. P. Palutikof, P. J. van der Linden, & C. E. Hanson (Eds.), Contribution of working group II to the fourth assessment, report of the intergovernmental panel on climate change. Cambridge, UK: Cambridge University.

[11] JMP. 2012. Statistics and Graphics Guide, Cary, NC, USA:SAS Institute Incorporation.

[12] Middleton, N., and Thomas, D. 1997. World atlas of desertification. London: UNEP/Arnold.

[13] [MoE] Ministry of environment. 2009. Second National Communication to the United Nations Framework Convention on Climate Change (UNFCCC)unfccc.int/resource/docs/natc/jornc2.pdf.

[14] Noin, D., and Clarke, H. 1998. Population and environment in arid regions of the world. In J. Clarke, & D. Noin (Eds.), Population and environment in arid regions (pp. 1–18). Paris: UNESCO/Partenon Publishing Group.

[15] Salvati L., Marco Zitti, Rosanna Di Bartolomei, and Luigi Perini. 2013. Climate Aridity under Changing Conditions and Implications for the Agricultural Sector: Italy as a Case Study Geography Journal, doi: 10.1155/2013/923173.

[16] Salvati L.2009.Are Mediterranean coastal regions more exposed to land degradation in recent years?. Journal of Coastal Research,Coastal Education & Research Foundation, vol. 56, pp. 262–266.

[17] Selker JS, Keller CK, McCord JT. 1999. Vadose zone processes. Lewis Publishers/CRC Press LLC, Florida.

[18] Thornthwaite, C. W. 1948. An approach toward a rational classification of climate. Geographical Review, 38(1), 55–94.

[19] Toreti, F. Desiato, G. Fioravanti, and W. Perconti. 2010. Seasonal temperatures over Italy and their relationship with lowfrequency atmospheric circulation patterns. Climatic Change, vol. 99, no. 1-2, pp. 211–227.

[20] Trenberth, K.E., 2011. Changes in precipitation with climate change. Clim. Res., 47: 123-138. DOI: 10.3354/cr00953.

[21] Tukey, J. 1991. The Philosophy of Multiple Comparisons,Statistical Science, 6, 100-116.

[22] [UNCCD] United Nations Convention on Combating Desertification. 2010. Water scarcity and desertification, UNCCD climatic factsheet series No. 2, http://www.unccd.int/documents/Desertificationandwater.pdf.

[23] [UNESCO] United Nations Educational, Scientific and Cultural Organization. 1979. Map of theworld distribution of arid regions: Map at scale 1:25,000,000 with explanatory note. MAB Technical Notes 7, UNESCO, Paris.

JJEES

Volume 7, (Number 1), June, 2015
ISSN 1995-6681
Pages 37 - 48

Jordan Journal of Earth and Environmental Sciences

Structural and Stress Analysis of the Area between Al-Akeider and Mughayer As-Sirhan, Northwestern Badia- Jordan

Abdullah Diabat*

Institute of Earth and Environmental Sciences, Al al-Bayt University, Mafraq, Jordan

Received 29 September, 2014; Accepted 24 May 2015

Abstract

Major tectonic elements of Jordan have been investigated in many studies, in which attention was mainly given to the Dead Sea Transform fault and the associated deformation. However, on a finer scale, our lack of knowledge about the geologic structures as well as the stress regimes of different parts of Jordan is an impediment to understanding the tectonic activities in detail. In this regard, the present study presents the first structural results obtained from fault-slip data, extensional fractures and conjugate shear fractures of the Paleocene- Eocene rock units in northwestern Badia.In aggregate, 142 fault-slip data and 579 fractures were analyzed. Results show that two stress regimes have been distinguished in the study area. The first stress regime is strike-slip which is characterized by σ_1SHmax oriented NNW-SSE and the second stress regime is extensional (normal faulting) in which σ_1 is vertical, σ_2(SHmax) and σ_3(Shmin) is swinging mainly around NE-SW. At least four stress states associated with these regimes were distinguished. The first stress state is characterized by NNW- SSE σ1corresponding to the main compression direction in the study area and resulting in the formation of the folds and the related N-S sinistral and WNW-ESEdextral fault sets. The other three states are of extension direction (σ_3); the first is oriented NNE-SSW, and the second is oriented ENE-WSW. These two trends correspond to the main extension defined during the Neogene. The third extension direction is WNW- ESE to E-W which is related to a very late extensional event in Miocene to Pleistocene.

Keywords: Paleostress, Fractures, Tertiary, Northwestern Badia, Jordan.

1. Introduction

Locally derived stress tensors with similar orientations of principal stress axes, together with the values of stress ratio (Sassi and Faure, 1996), distributed over a large region,are considered to represent a regional paleostress solution (Tripathy and Saha, 2013). In deducing lithospheric stresses and their temporal and spatial variation, if any, brittle structures of the earth upper crust are important resources (Angelier, 1989, and 1994). In this regard, structures such as fractures, in general, and faults are used as kinematic indicators to extract useful information about tectonic activities and evolution.

Fracture is, more general, a type of brittle deformation pervasively found in the crust. Depending on their origination and activation mechanism, different fracture modes are identified, such as joints or shear fractures. Pollard and Aydin (1988) defined joints as fractures with evidence of opening mode displacement (i.e., extensional fractures). Others have defined joints as a surface along which there is no appreciable displacement (Price, 1966; Hancock, 1985). Also, shear fractures (e.g., extensional and conjugate) are frequently exposed in association with relatively lower order (major) faults or independently, which can be used in recognizing relative stress regimes.

Faults are one of the most studied fracture types and their relation with their running forces was investigated at various levels and aspects (Jensen et. al., 2011). The term fault is specifically used to refer to shear fractures, that is, a relatively narrow discontinuity with observable displacement at a given scale (Jensen et. al., 2011). It is accepted that a fault is induced when deviatoric tectonic stresses produce a shear stress that exceeds the shear strength on a particular plane in the rock mass (Kersten, 1990). Consequently, produced kinematic indicators reveal some characteristics of resolved shear stress on a given plane.

Many studies were carried out about the Dead Sea Transform (DST) fault and other related structures to understand the deformation of the region (Fig. 1). In this regard, the regional tectonics of the continental part of the Arabian plate, including Jordan,were studied through macro-structures by many authors (e.g., Quennell, 1958; Burdon, 1959; Bender, 1968, 1974; Mikbel and Zacher, 1981; Quennell, 1983; Mikbel, 1986; Atallah, 1992). Few analyses, however, focused on the regional tectonics based on meso-structures in Jordan (e.g., Salameh and Zacher, 1982; Diabat 1999, 2002, 2009, 2013; Zain Eldeen et. al., 2002; Diabat et. al., 2003, 2004).

Although many details of the tectonic structures of Jordan are now well recognized, these are mainly about the DST fault itself. Other areas in Jordan, except for the DST fault, have received little attention of tectonic and/ or structural studies.

* Corresponding author. e-mail: adiabat@ aabu.edu.jo

The area the present study is focused on is one of these poorly investigated areas in Jordan. It represents the northeastern end of the Ibbin-Housha fold belt located few to tens kilometers east of the DSTfault, with very obvious brittle structures (e.g., faults, joints, fractures) that deserve to be studied.

The purpose of the present study is to increase our knowledge about the various structures, and to get a better resolution of the paleostresses of the study area on which no such studies are available. This is achieved by analyzing different structural elements, e.g., folds, fractures (joints), and faults in the study area. The field work was carried out with the objectives of determining: (1) structural (e.g., spatial and kinematic) characteristics of fracture sets and (2) determining stress states, where ever possible.

2. Tectonic setting

The study area lies within the east Jordanian Plateau according to Bender (1974). It is located a few kilometers from two major faults; the first is the Jordan Valley Fault(JVF), a sinistral strike-slip fault of the northern segment of the DST fault, and the second is the Sirhan Fault (SF), with extensional characteristics (Fig. 1). The study area is located to the northeastern extremity of Ibbin-Housha fold belt (Figs. 1 and 2). This fold belt is part of the three fold belts in northern Jordan; Halawa-Husn fold belt, Ibbin-Housha fold belt and Balaama-Mafraq fold belt which are located east of (JVF) (Fig. 1). The major trend of these folds is NE to ENE and formed by the compressive stresses related to the northward movement of the Arabian plate and the DSTfault (Atallah and Mikbel, 1992).

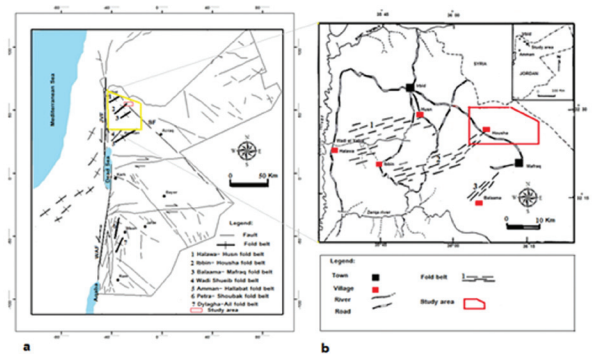

Figure 1. a) Structural pattern of Jordan (compiled from Diabat and Masri, 2005; Atallah and Mikbel, 1992), showing the major structures in Jordan, JVF is Jordan Valley fault, WAF is Wadi Araba fault, SF is Sirhan fault; b) Fold belts in north Jordan (modified after Atallah and Mikbel, 1992).

The DST fault is the most prominent structure in Jordan that resulted from the northward faster movement of the Arabian plate relative to that of the African plate, probably in relation to the Red Sea opening (Quennel, 1958; Garfunkel, 1981). Northward motion of the Arabian plate (Miocene to recent) released opening of the Red Sea and the Gulf of Aden and controls much of the structural pattern of Jordan.This left-lateral transform boundary extends a thousand kilometers from the Gulf of Aqaba in the south to south of Turkey in the north (Freund et. al., 1970). In Jordan, the DST fault composed of the Wadi Araba fault (WAF) in the south and the (JVF) in the north (Fig. 1).

3. Stratigraphy

The outcropping rocks in the study area are Upper Cretaceous to Tertiary (Bender, 1974; Powell, 1989) (Fig. 2).

The following represents a brief description of the exposed rocks in the study area; Amman Silicified Limestone Formation (ASL) (Santonian-Campanian) is widespread in Jordan, whereas it crops out only in the southeastern part of the study area. This Formation is of a varying thickness in different locations of Jordan. ASL Formation is distinguished by hard, massive chert beds which form a steep cliff above the pale weathering chalks of Umm Ghudran Formation in central and north Jordan (Powell, 1989). The top of Amman Formation (ASL) is usually distinguished by the first appearance of thick phosphorite beds of Al Hasa Phosphorite Formation (AHP). AHP Formation (late Campanian-early Maastrichtian) consists of a heterogeneous lithology of medium-thick beds of phosphorite, which are intercalated with thin-medium-bedded chert, marl, chalky marl, microcrystalline limestone and oyster-coquina grainstones (Powell, 1989).

The Muwaqqar Chalk- Marl Formation (MCM) (Maastrichtian to Paleocene) is exposed in parts of the study area (Fig. 2). The exposed part is a few meters thick and mainly consists of soft pale yellow, light grey, yellowish to reddish and brown green, occasionally whitish cream chalky marl and marly limestone with calcite in extensional joints. This formation is overlain by Umm RijamChert- Limestone Formation (URC) (Eocene), which is widespread and well exposed at the road cuts of the study area. The exposed part of the formation is a few meters thick and consists of limestone, chalky limestone and chert (Fig. 2).

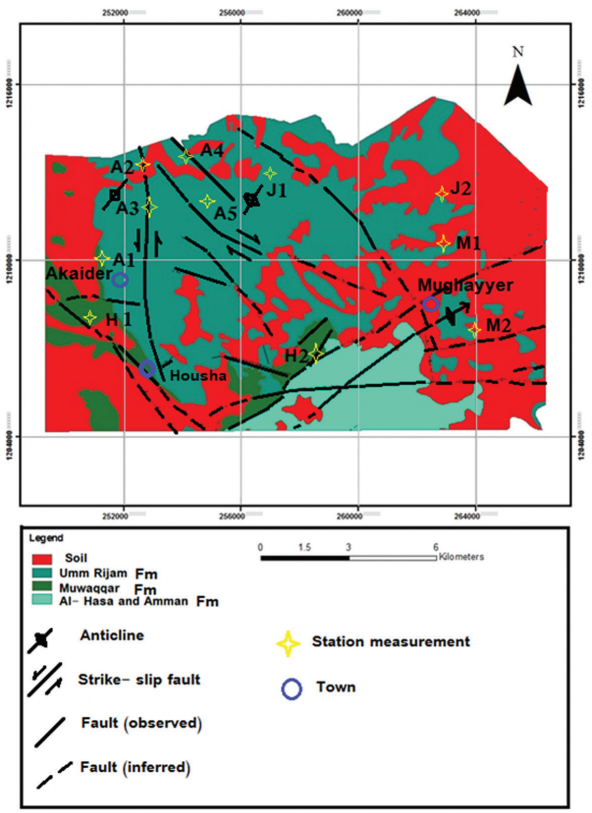

Figure 2. Geological map of the study area with located measurement stations; A1, A2, A3, A4, A5, H1, H2, J1, J2, M1 and M2.

4. Data and method

4.1. Data

Meso-scale brittle structures and statistical analysis methods (Price and Cosgrove, 1990; Hancock, 1991; Twiss and Moores, 1992) were used to infer the fracturing patterns and states of stress controlling the tectonic evolution of the study area.

Determination of paleostress was done using two basic types of brittle structures: (1) faults with slip lines slickensides; (2) fracture planes without slip lines (Angelier 1994; Dunne and Hancock, 1994; Delvaux and Sperner, 2003).

These two types of data were collected from eleven stations along road cuts and abandoned quarries in the study area (Fig. 2). The attitude of fault planes and the associated slickenlines (142 in number), together with the sense of slip, were measured in six stations (i.e., A3, A4, H1, J2, M1 and M2) (Fig. 2 and Table 1). Many exposures were examined, however, only those have been considered as site that have suitable number of faults (at least 7) with associated unquestionable slip sense, as well as significance fractures. Slickenlines and mineral steps were kinematic indicators to determine the sense of slip on the measured faults.

Brittle structures, other than the commonly used slickensides, can also be used as stress indicators (Dunne and Hancock, 1994).The relationship between fractures and principal stress directions implied by the Coulomb fracture criterion suggests that we can use fractures to estimate the directions of the principal stresses (Price and Cosgrove, 1990; Hancock, 1991; Twiss and Moores, 1992). As this takes place, it is essential to reliably identify the conjugate shear fracture sets that formed or were reactivated at the same time (Lunina et. al., 2005).

Therefore, shear and extensional fractures were measured in the study area particularly, in areas where fault-slip data or marker displacement are not available.The fracture planes (579 in total), which have a significance in the structural analysis, were measured in eight stations (i.e., A1, A2, A3, A4, A5, H1, H2 and J1) and represented as rose diagrams. According to the Coulomb' criteria extensionalfractures form parallel to σ_1, and normal to σ_3, and shear fractures form parallel to σ_2 as a conjugate set, c. 30 degrees either side of σ_1 (Belayneh, 2004).

The conjugate shear fracture systems can be separated from other sets of fractures as follows: the conjugate fracture sets are determined by using criteria such as intersection of the fractures, mutually, opposite sense of displacement, constancy of the angle between them under a general change of their orientation, analogous distribution and connection with regional structures (Twiss and Moores, 1992). The used method is primarily based on the fundamentals of rock mechanics, which suggest that two possible orientations of conjugate shear fractures can develop under the influence of a homogeneous stress field.

Table 1: Stress tensor results in the study area. n: number of data used in the subset; nt: total number of measured data; σ_1, σ_2 and σ_3: are the principal stress axes; R: stress ratio; R': stress regime index; QRw is the world stress map quality rank and QRt is the tensor quality rank ranging from A: very good, E: very poor; SHmax: horizontal maximum compressional axes; regime (SS: strike- slip regime and NF: normal regime); and misfit angle using function F5.

Station / Tensor	n/nt	σ_1	σ_2	σ_3	R	Misfit	F5	'R	QRw	QRt	SHmax / Shmin	Regime
A3	11/15	16/155	65/284	18/059	0.69	2.8	0.5	1.31	C	C	151	SS
A4a	16/24	01/147	89/312	00/057	0.5	3.6	1.3	1.5	C	C	147	SS
A4b	7/7	70/109	01/201	20/291	0.43	2	1.2	0.43	D	E	021	NF
H1a	17/23	18/147	68/288	13/052	0.65	11.8	5.4	1.35	C	D	144	SS
H1b	10/16	87/188	02/328	02/058	0.22	2	0.3	0.22	C	D	148	NF
J2	13/15	55/186	27/324	20/065	0.88	9.4	8.6	0.88	C	C	144	NF
M1	8/13	73/292	00/201	17/111	0.23	1	0.3	0.23	D	E	020	NF
M2a	17/25	15/136	73/340	07/228	0.64	6.8	2.9	1.36	C	C	137	SS
M2b	10/14	87/200	00/105	03/015	0.04	1.2	0.1	0.04	C	D	105	NF

Accordingly, the principal stress axes can be inferred as: (1) the line of intersection of the conjugate faults is the intermediate stress axis (σ_2); (2) the compressional stress axis (σ_1) bisects the acute angle between the fault planes; and (3) the tensional stress axis (σ_3) bisects the obtuse angle (Price and Cosgrove, 1990; Hancock, 1991; Twiss and Moores, 1992; Lunina et. al., 2005) (Fig. 3a, b). Therefore, the direction of σ_1 was deduced from the conjugate shear fractures in which bisector of the acute angle is parallel to σ_1, and from the extensional fractures that form parallel to σ_1 (Fig.3c).

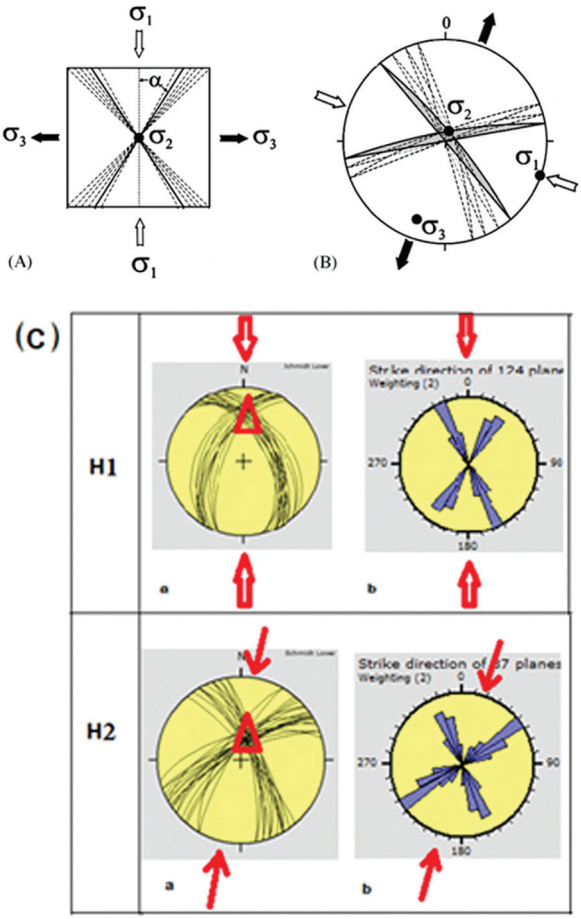

Figure 3. The concept of statistical analysis for the determination of the conjugate fracture systems and reconstruction of the principal stress directions:(A) scheme of the scattering development, α, angle of shear (after Lunina et. al., 2005); (B) diagram of the principal stress directions (σ1, σ2 and σ3 are the maximum, intermediate and minimum compressive stress axes, respectively (after Lunina et. al., 2005)) obtained from a set of conjugate fractures ; (C) examples from the study area in stations H1 and H2 (equal-area lower hemisphere projection (left), and rose diagrams (right); red arrows indicate σ1, triangle represents σ2.

4.2. Method (stress inversion)

Most of the inversion methods of obtaining stress tensor from fault-slip data are based on Wallace (1951) and Bott (1959) hypotheses that assume slip occurs parallel to the direction of the maximum shear stress on fault plane.

The fault-slip data are inverted to obtain the parameters of the reduced stress tensor. These parameters are the principal stress axes σ_1, σ_2 andσ_3, where $\sigma_1 > \sigma_2 > \sigma_3$ and the ratio of principal stress differences $R = \sigma_2 - \sigma_3 / \sigma_1 - \sigma_3$, which defines the shape of the stress ellipsoid (Delvaux et. al., 1997).

According to Delvaux et. al. (1997), the stress regime is a function of the orientation of the principal stress axes and the shape of the stress ellipsoid (R): extensional when σ_1 is vertical, strike-slip when σ_2 is vertical, and compressional when σ_3 is vertical. Therefore, they introduced the stress regime index R'. The relations between R and R' are:

R' = R when σ_1 is vertical (extensional stress regime)

R' = 2- R when σ_2 is vertical (strike-slip regime)

R' = 2+ R when σ_3 is vertical (compressional regime)

R'.defines the stress regime on a continuous scale from 0 (radial extension) to 3 (radial compression), in detail from 0 to 1 for normal faulting regime (σ_1 sub- vertical), from 1 to 2 for strike-slip regime (σ_2 sub- vertical), and from 2 to 3 for thrust faulting regimes (σ_3 sub- vertical).

The data were processed interactively by the Win TENSOR program; first using the "Right Dihedron method" a graphical method for determining the possible orientations of σ_1 and σ_3 (Angelier and Mechler, 1977). The initial result is used as a starting point for the iterative grid-search "Rotational Optimization" procedure using the misfit function F5 in the Win TENSOR program package (described as f3 in Delvaux and Sperner, 2003; Delvaux, 2012) (Fig. 4).

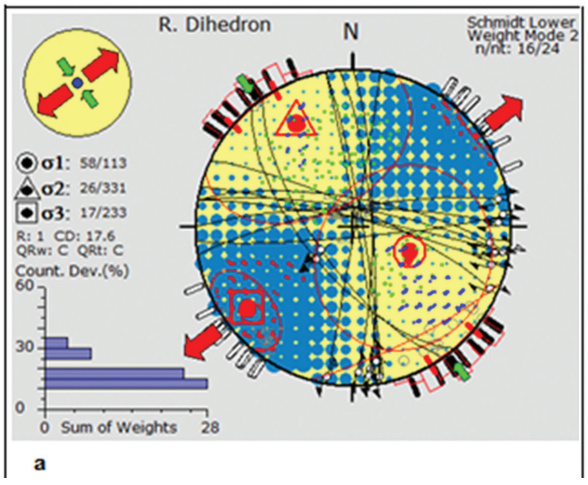

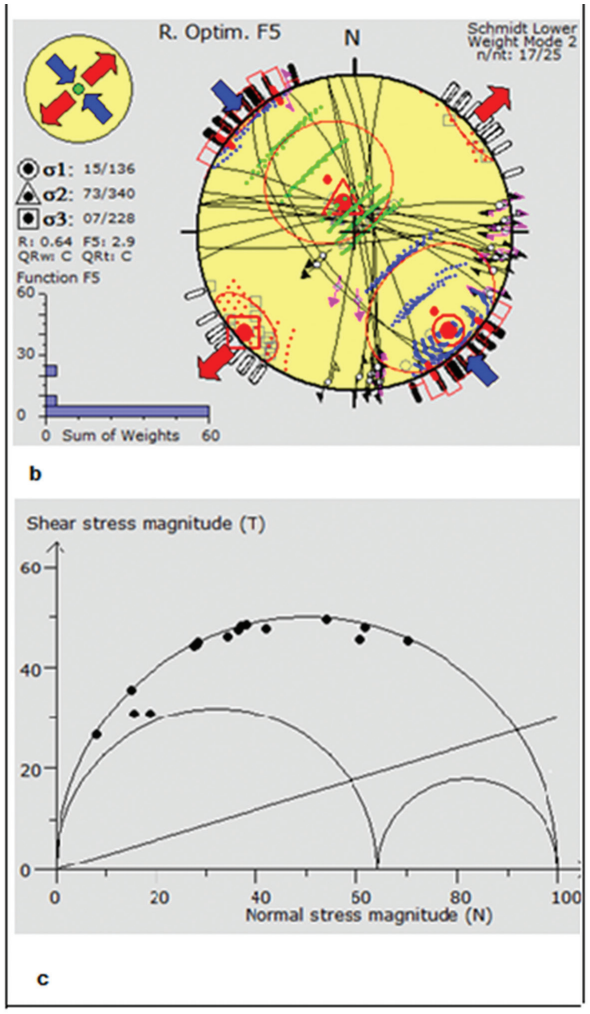

Figure 4. Example of tensor solutions in the study area: a) Right Dihedron method, green arrows for maximum principal compression, red arrows for minimum principal compression, the histogram gives the counting deviation angles; b)Rotational Optimization, blue arrows for maximum principal compression, red arrows for minimum principal compression, the histogram gives the distribution of measured data against the function F5. For best fit F5 approaches 0 for all measurements (for more details see Table 1); c) Mohr diagram illustrates the stress regime and the area of fault activation (the failure curve is based on Byerlee, 1978 initial friction angle 16.7).

5. Results

5.1. Folds

The Ibbin-Housha fold belt that is described by Atallah and Mikbel (1992) (Fig. 1) is a well-developed fold belt, consisting of anticlines and synclines with sub-parallel axes trending mainly ENE- WSW to NE- SW(Fig. 2) .

In the study area, the NE extremity of the Ibbin-Housha fold belt to the northeast of Housha is marked by a single anticline that plunges to the NE (Fig. 2). This anticline was investigated locally in the present study (M2). Its ENE-WSW oriented axis (Fig. 5) indicates NNW-SSE directed local compression. Because the anticline was formed in Umm Rijam Formation (Eocene), the related stress is attributed to Post-Eocene tectonic regimes.

The anticline is cross cut by several E-W high-angle normal faults (Figs. 6c and d). In addition, oblique and horizontal slickenlines were observed on some fracture planes along this anticline (Fig. 6e). In the northwestern part of the study area, two anticlines with sub-parallel axes trending NE-SW were also delineated in the present study (Fig. 2).

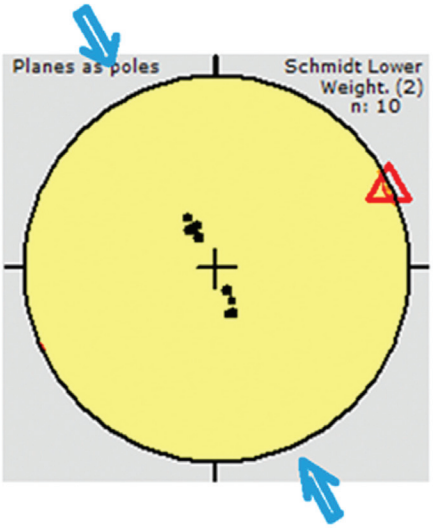

Figure 5. Example of ENE slightly plunging anticline in station M2; solid black dots are the poles to bedding and the triangle is the hinge orientation, the blue arrows indicate the direction of compression .

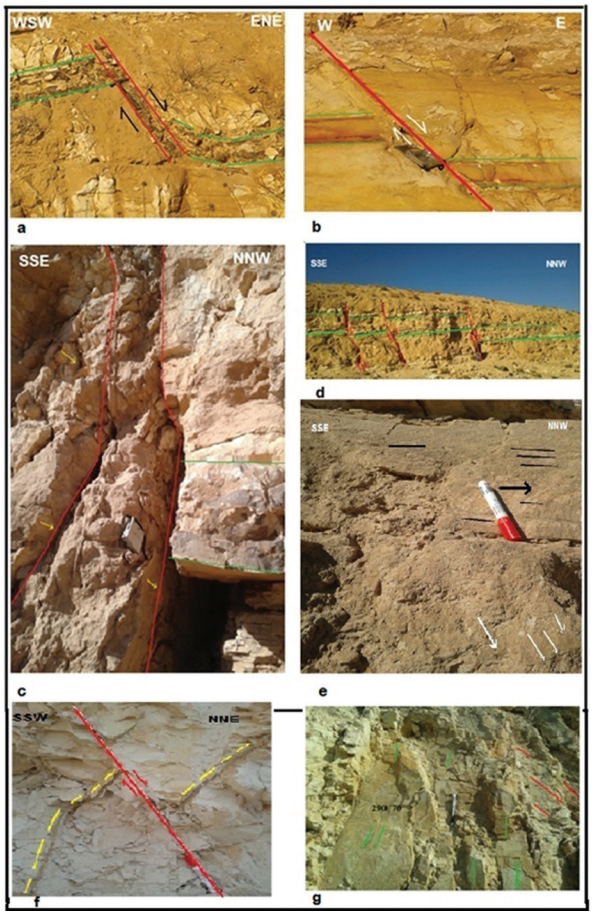

Figure 6. Field examples of normal and oblique- slip faults. a: normal fault zone filled chert (silicification) in station- A4. b: low- angle-normal fault in station- A5. c: oblique- slip fault (yellow arrows indicate slickensides show normal- sinistral slip) cut fold limb in station-M2. d: vertical to high- angle normal faults cut fold limb at station- M2. e: superposition of oblique and horizontal slickensides in station- M2. f: normal fault crosscut vein in station- H1. g: vertical and oblique slickenlines in station- A4.

 - Volume 7, (Number 1), (ISSN 1995-6681)

5.2. Syndepositional structures

Syndepositional structures were observed in Paleocene rocks of Muwaqqar Formation of station-A1 (Fig. 7), in which the throw of the NE-SW oriented low-angle normal fault of marker 1 at the bottom is greater than those of the other markers (Fig.7). In addition, beds, at the top of the fault, appear to be offset less or not at all than beds 1, 2 and 3. Bed 4 may not be disrupted by the fault; however, it is possible that the fault continues toward the top-left of the photo (Fig.7).

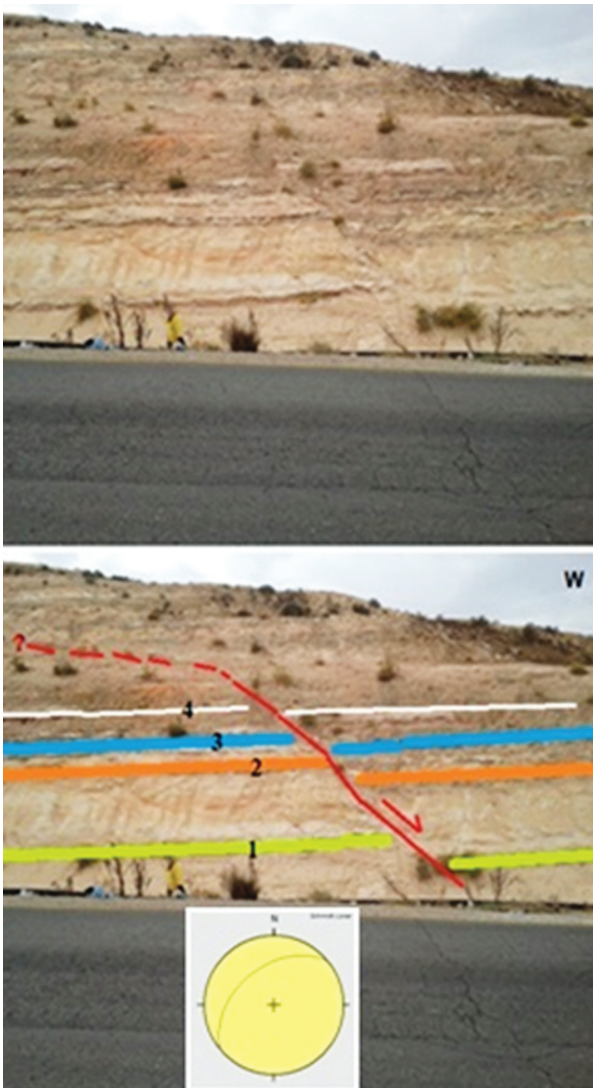

Figure 7. A syndepositional fault in Paleocene rocks of station- A1; stereographic projection lower hemisphere of low angle normal fault, the fault strikes NE- SW and dips toward NW, the fault shows decreasing throw upwards (marker 1 has greater throw than other markers 2, 3, and 4).The fault movement occurred during the Paleocene under NW- SE extension.

5.3. Fault- slip data

The mapped faults in the study area are trending NW-SE, N-S, NE-SW and E-W (Fig. 2). Two major strike-slip faults are seen at the western half of the study area. The first fault extends from Housha in the south to the northern border of the study area in N-S direction. It shows oblique slickensides of normal and sinistral components of slip on its surface that appears along road cut (Fig. 8a). The second fault extends from Mughayer in the southeast in a general NW-SE trend toward station-A2 in northwestern part of the study area; this fault is of dextral-slip (Fig. 2). These two faults could be conjugate, resulting from NNW-SSE compressional stresses.

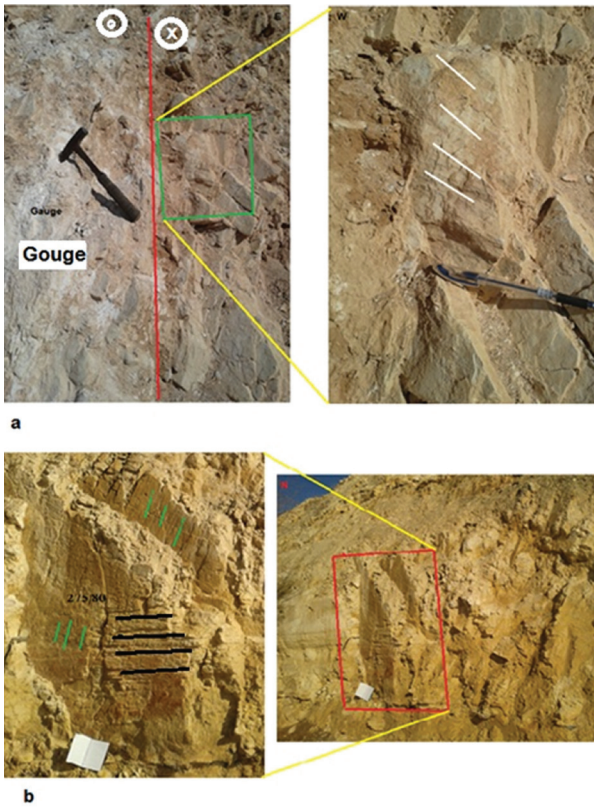

Figure 8. Field examples of fault kinematic indicators. a: Sinistral strike- slip fault (red line), inset photo shows slickenlines on bedding planes of normal- sinistral slip (station- A3). b: superposition of normal slip and strike- slip slickenlines on a fault plane (station- A4).

The number of the measured fault-slip data in the field is 142, but that of those used in defining stress states is 109, that is, the 33 measurements were omitted because they are incompatible with slip deviations and show unreasonable results. This may be due to the measurement error in the field or to local block rotation around fault blocks.Most prominent measured meso-scale faults in the study area are of strike-slip and normal displacement (Fig. 8). All fault slip data were measured in Umm Rijam Formation (Eocene) except for those of station-H1, measured in Muwaqqar Formation (Paleocene).

The results of stress inversion applied on the measured data from different stations (Fig. 9 and Table 1) are as follows:

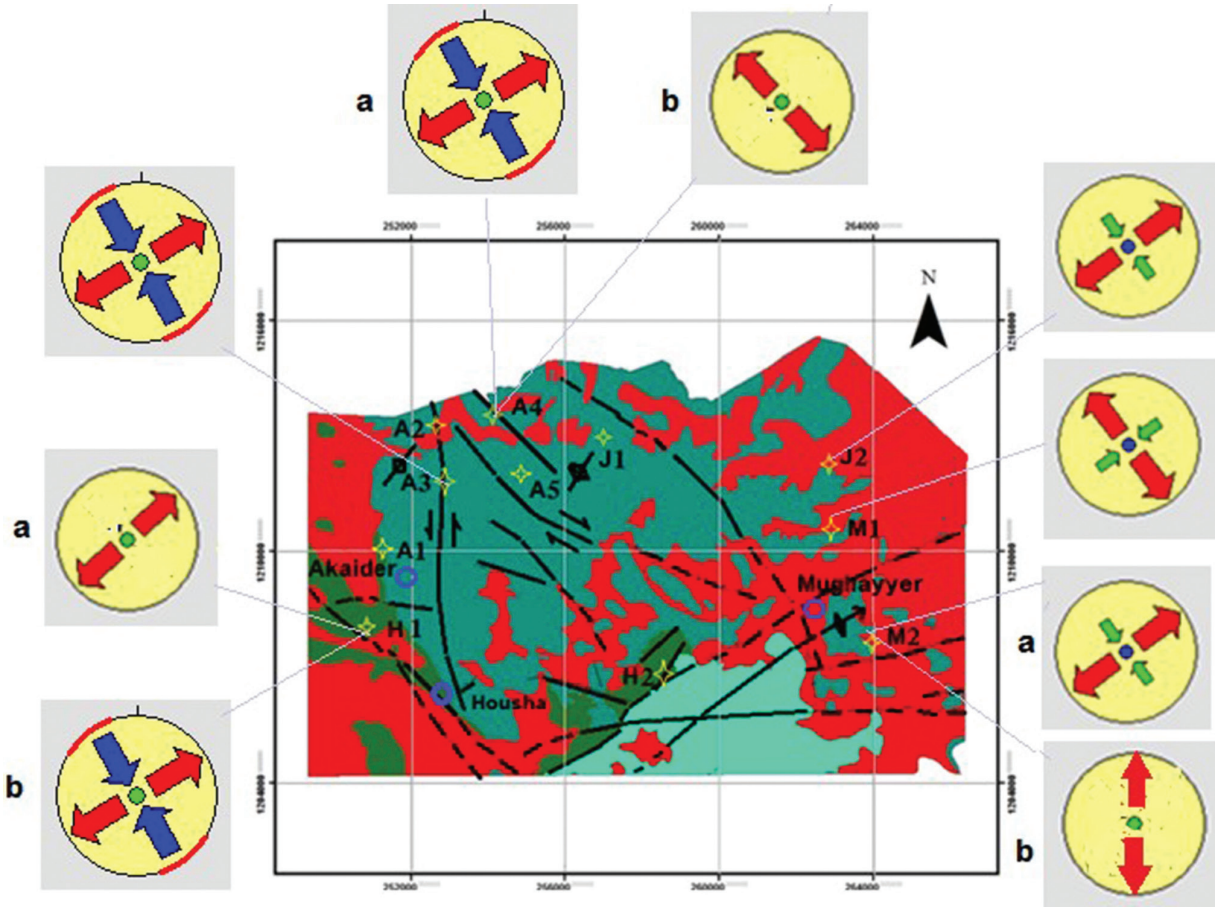

Figure 9. Tensor solutions in the study area. Blue, red and green arrows show the maximum, minimum and intermediate principal compression, respectively.

5.3.1. Station A3

Eleven fault-slip data were measured in a road cut located in the northwestern part of the study area along an N-S sinistral strike-slip fault (Fig. 9 and Table 1). The stress tensor is characterized byσ_1:16/ 155, σ_2: 65/ 284, σ_3:18/ 059 and R= 0.69.The determined stress tensor belongs to strike-slip regime and indicates NNW-SSE directed compression and ENE-WSW directed extension. It is responsible for the activation of the measured conjugate N-S sinistral and WNW-ESE dextral strike-slip faults.

5.3.2. Station A4

Twenty-three measurements were measured in a cliff outcrop located in the northern most part of the study area (Fig.9 and Table 1). Two stress tensors were obtained from the whole fault population; the first stress tensor (A4-a) is characterized by σ_1 01/ 147, σ_2 89/312, and σ_3 00/057 with R= 0.5. It belongs to strike-slip regime and indicates NNW-SSE oriented compression and ENE-WSW extension direction. It is responsible for the activation of measured conjugate N-S sinistral and WNW-ESE dextral strike-slip faults. The second stress tensor (A4-b) is characterized by σ_1 70/ 109, σ_2 01/ 201, and σ_3 20/ 291 with R= 0.43. It belongs to extensional regime and indicates WNW-ESE extension direction. This tensor produced the NNE-SSW normal faults.

5.3.3. Station H1

Twenty-seven fault-slip data were measured in a quarry of Muwaqqar Formation (Paleocene) located in the western part of the study area along an N-S sinistral fault (Fig.9 and Table 1). Two stress tensors were obtained from the whole fault population; the first stress tensor (H1-a) is characterized by σ_1 18/147, σ_2 68/288, and σ_3 13/052 with R= 0.65. It belongs to strike-slip regime and indicates NNW-SSE directed compression and ENE-WSW directed extension. It is responsible for the activation of measured N-S sinistral strike-slip faults. The second stress tensor (H1-b) is characterized by σ_1 87/ 188, σ_2 02/ 328, and σ_3 02/ 058 with R= 0.22. It belongs to the extensional regime and indicates ENE-WSW extension direction. This tensor produced the NNW-SSE normal faults.

5.3.4. Station J2

Thirteen fault-slip data were measured in a road cut located in northeastern part of the study area (Fig.9 and Table 1). The determined stress tensor is characterized by σ_1 55/ 186, σ_2 27/ 324, and σ_3 20/ 065 with R= 0.88. It belongs to extensional regime and indicates ENE-WSW extension direction. This tensor is responsible for the activation of measured NNW-SSE normal faults.

5.3.5. Station M1

Eight fault-slip data were measured in a quarry located in the east central part of the study area (Fig. 9 and Table 1). The stress inversion analysis reveals a stress tensor that is characterized by $\sigma_{1:}$ 73/ 292, $\sigma_{2:}$ 00/ 201, and $\sigma_{3:}$ 17/ 111 with R= 0.23. It belongs to the extensional regime and indicates ESE-WNW oriented extension. This tensor is responsible for the activation of the measured NNE to N-S trending normal faults.

5.3.6. Station M2

Twenty-seven fault-slip data were measured in a quarry located in the southeastern part of the study area in an anticline outcrop (Fig. 9 and Table 1). Two stress tensors were obtained from the whole fault population; the first stress tensor (M2-a) is characterized by $\sigma_{1:}$ 15/ 136, $\sigma_{2:}$ 73/ 340, and $\sigma_{3:}$ 07/ 228 with R= 0.64. It belongs to strike-slip regime and indicates NW-SE oriented compression and NE-SW oriented extension. It is responsible for the activation of the conjugate N-S sinistral and WNW-ESE dextral strike-slip faults. The second stress tensor (M2-b) is characterized by $\sigma_{1:}$ 87/ 200, $\sigma_{2:}$ 00/ 105, and $\sigma_{3:}$ 03/ 015 with R= 0.04. It belongs to the extensional regime and indicates a general N-S to NNE-SSW oriented extension. This tensor is of local extensional direction produced the E-W normal faults that affects the stratigraphic horizons of the bedding planes of the anticline in this station, in which the downthrows along these faults reach up to 90 cm (Fig. 6d).

5. 4. Fractures

According to the information obtained from the investigation of fractures, shown in rose diagrams in Figure (10), it is obvious that different fracture sets were produced in the study area. These fractures can be categorized with respect to their failure mechanism or structural setting as follows:

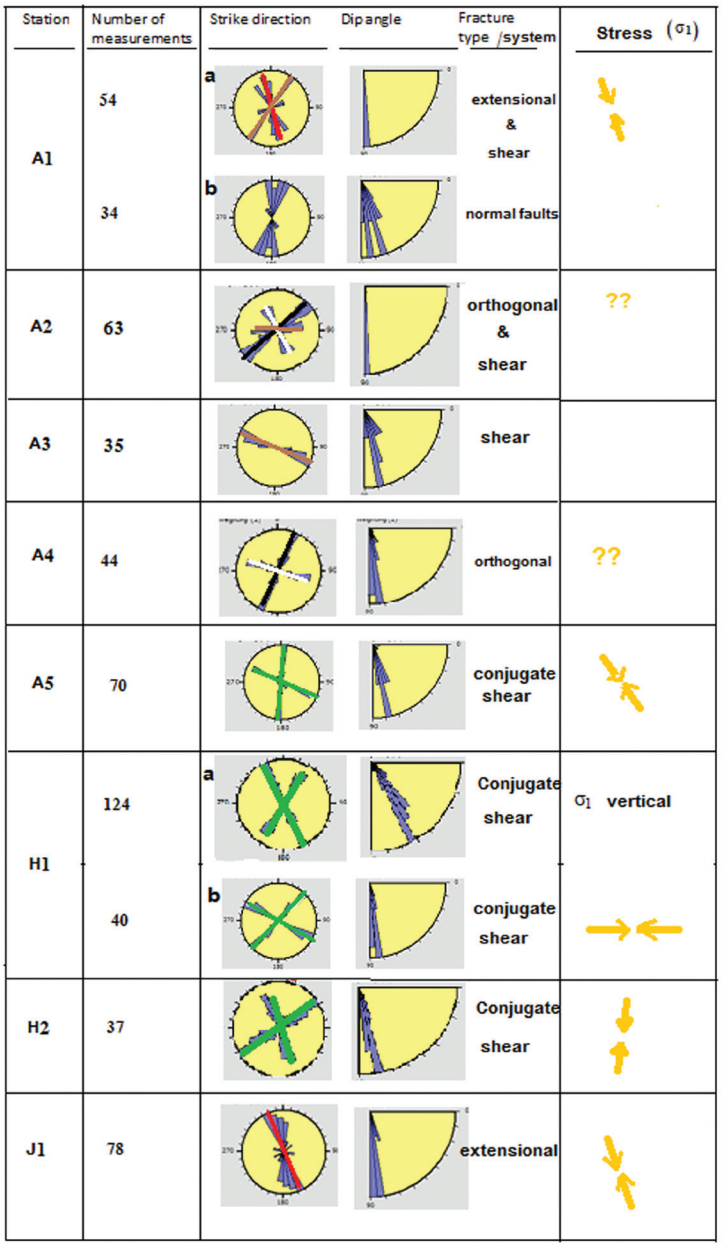

Figure 10. Results of 579 fracture data and the deduced σ_1 direction in different stations of the study area. The red, brown, green, and black-and-white lines delineate the strike of extensional, shear, conjugated shear, and orthogonal fractures, respectively.

1- Extensional fractures are observed in stations A1 and J1 and their NNW-SSE strikes indicate the direction of σ1 (Figs.10, A1-a and J1,11a). All fractures have a dip angle greater than 80 degrees.
2- Conjugate shear fractures are dominant in stations A5, H1 and H2 and have strikes in various directions, e.g., N-S, NE-SW, NW-SE, NNW-SSE, NNE-SSW and ESE-WNW (Figs. 10, 11 c-e). However, σ1 deduced from these fractures is different in the stations; therefore, it varies as NNW-SSE in A5, NNE-SSW in H2, and ENE-WSW in H1-b (Fig. 11 c). All fractures related to these directions have a dip angle greater than 70 degrees. In H1, also, there are quite large numbers of conjugate shear fractures that indicate vertical σ1 (Figs. 10, H1-a, 11 d). These fractures have dip angles less than 70 degree.
3- Shear fractures are observed in stations A1, A2 and A3 (e.g., Fig. 11 f).
4- Orthogonal fractures are measured in stations A2 and A4 (Fig. 11 b).

In the case of the last two categories, insufficient kinematic and temporal restrictions posed an impediment to deducing stress direction.

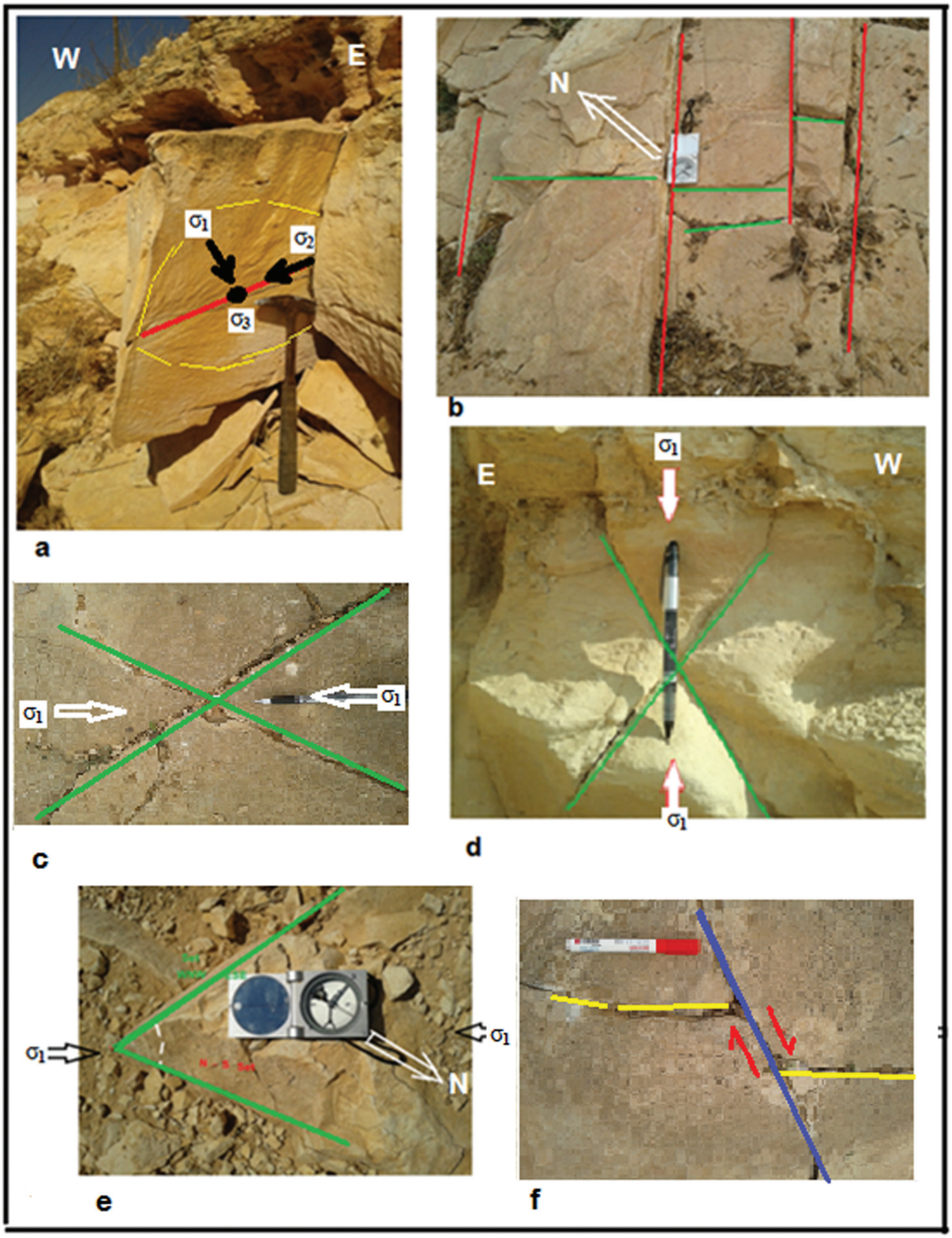

Figure 11. Field examples of some kinematic indicators. a: plumose sub- vertical tension fracture in station- A5 shows the directions of the principal stresses. b: orthogonal joint system (master joints in red color and cross joints in green color) in station A2. c, d and e: conjugate shear fractures in which the acute bisector is parallel to σ_1 (c, d in H1; e in A2) f: right-lateral displacement affects bedding surface in station- A2.

  - Volume 7, (Number 1), (ISSN 1995-6681)

6. Interpretation of results

The results of stress inversion on fault-slip data collected in six sites reveal the existence of strike-slip and extensional regimes. In this regard, the obtained results show that σ1 (SHmax) and σ3 (Shmin) are generally sub-horizontal and σ2 is sub-vertical in four stress tensors (e.g., A3, A4-a, H1-a, and M2-a), and their R' value range between 1.31- 1.50. Therefore, they belong to a major strike-slip regime in which σ1 swings around NNW-SSE (N137°E - N151°E) (Table 1 and Figs. 9, 12). On the other hand, in five stress tensors (A4-b, H1-b, J2, M1 and M2-b) σ1is vertical and σ2 (SHmax) and σ3 (Shmin) are (sub) horizontal (Table 1 and Figs. 9, 12), and their R' values vary between 0.04- 0.88. Although these parameters indicate an extensional regime, the direction of maximum extension (σ3) differs as 1- NNE-SSW (N 015°E - N111°E) in A4-b and M2-b, 2- ENE-WSW in H1-b and J2, and 3- WNW-ESE in M1. The first two stress states are consistent with the Neogene main extension determined by previous works (e.g., Diabat et. al., 2004; Hardy et. al., 2010). The third stress state probably is related to late extensional activities in Miocene to Pleistocene, as a similar stress state is recognized by Hardy et. al., (2010) in Galilee area (north Palestine).

According to field observations (e.g., in A4, H1 and M2) many fault planes show at least two phases of superimposed movements. Kinematic indicators (Figs. 6 and 8) show that the movements with normal sense are overprinted on those with strike-slip sense. This implies that the extensional stress regime is younger than the strike-slip regime in the study area.

According to the direction of σ1 resulted from extensional and conjugate shear fractures, in some stations (A1-a, A5 and J1) the direction is NNW-SSE. This trend is in a good accordance with the NNW-SSE compression direction resulted from fault slip analysis.

In general, the direction of maximum compression (NNW-SSE),resulting from the analysis of both fault-slip data and extensional as well as conjugate shear fractures, is in agreement with NNW-SSE direction resulted from fold measurements of the present study – also the general trend of folds in a larger scale in Jordan. In addition, it is compatible with the results of other works in the region and along DST fault in which the relative stresses are considered active since the Middle Miocene (e.g., Eyal and Reches, 1983; Badawy and Horváth, 1999; Hardy et. al., 2010) .

Since the chronostratigraphy in the study area was based on the relative vertical positions of lithologic units, similar lithology, in sites in which data are collected, does not allow a temporal constraining of recognized stress states more precisely. Detailed dating of lithologic units in the study area, in the future, may help to put more strict restriction, in terms of temporal variation of defined stress states.

On the whole, in the present study, through the analysis of fault-slip data in Badia, Northwestern of Jordan, two main stress regimes are recognized: 1- a strike slip regime with NNW-SSE direction of σ1. This regime is responsible for the activation of WNW-ESE to E-W dextral and N-S sinistral faults; 2- an extensional regime (normal fault setting) with three different direction of σ3, i.e., NNE-SSW, ENE-WSW and WNW-ESE. The existence of these regimes is supported by other geologic evidence such as syn-depositional normal faults, extensional and conjugate shear fractures. Superposition of movements with a normal sense on those with strike-slip sense suggest young (Neogene) extensional activities in the area; however, these extensional activities are probably local, considering the domination of strike-slip stress regime in larger scale.

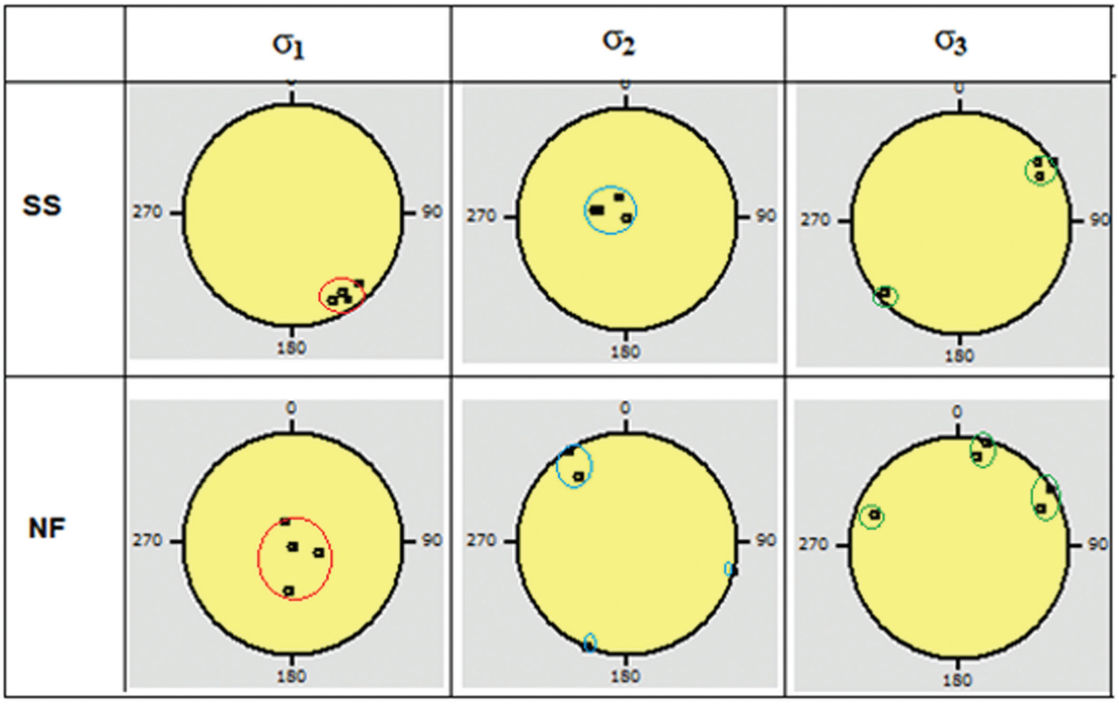

Figure 12. Stress regimes in the study area; SS is strike- slip regime, NF is extensional or normal - slip regime: clusters are the orientation of the principal stress axes; red circle for σ_1, blue for σ_2 andgreen for σ_3.

Acknowledgement

The author is very grateful to Al al-Bayt University as this research was accomplished during the sabbatical year granted. The author also thanks two anonymous reviewers for their constructive comments, which substantially improved the quality of the manuscript.

References

[1] Angelier, J., 1989. From orientation to magnitudes in palaeostress determinations using fault slip data. J. Struct. Geol., 11: 37-50.

[2] Angelier, J., 1994. Fault- slip analysis and paleostressreconstuction. In: Continental Deformation (ed. Hancock, P.L.), 1 edn., pp. 53- 100. Pergamon Press, U.K., Bristol.

[3] Angelier, J., and Mechler, P., 1977. Surunemethodgraphique de recherché des contraintes principales egalemant utilizable en tectonique et en seismology: la methode de diederesdroits. Bull. Soc. Geol. Fr. 7:1309-1318.

[4] Atallah, M., 1992. On the structural pattern of the Dead Sea Transform and its related structures in Jordan. Abhath Al-Yarmouk (Pure Sciences and Engineering) 1, 127-143.

[5] Atallah, M., Mikbel, Sh., 1992. Structural analysis of the folds between Wadi el- Yabis and the basalt Plateau, northern Jordan. Dirasat (pure and applied sciences) 19, 43- 58.

[6] Badawy, A., Horvath, F., 1999. Recent stress field of the Sinai subplate region. Tectonophysics 304, 385- 403.

[7] Belayneh, M., 2004.Paleostress orientation inferred from surface morphology of joints on the southern margin of Bristol Cannel Basin, UK. In: Cosgrove, J.W.& Engelder, T. (eds) The initiation, propagation, and Arrest of joints and other fractures. Geological Society, London, Special Publications 231, 241-255.

[8] Bell, F. G., 1993. Engineering Geology. Black Well Publications London. 359P.

[9] Bender, F., 1968. Geology of Jordan. Borntraeger, Berlin. 196p.

[10] Bender, F., 1974. Geology of Jordan; Berlin, Gebruder Borntraeger.

[11] Bott, M. H. P., 1959. The mechanics of oblique- slip faulting, Geological Magazine 96, 109- 117.

[12] Burdon, D. J., 1959. Handbook of the Geology of Jordan: to accompany and explain the three sheets of 1: 250,000 Geological Map, East of the Rift.

[13] Byerlee, J.D, 1978: Friction of rocks. Pure and Applied Geophysics. 116: 615-626.

[14] Delvaux, D., 2012. Release of program Win- Tensor 4.0 for tectonic stress inversion: statistical expression of stress parameters. EGU General Assembly, Vienna, 2012. Geophysical Research Abstracts, Vol. 14, EGU 2012- 5899. Program available at http: // users.skynet.be/ damien. delvaux/ Tensor/ tensor- index.html.

[15] Delvaux, D., Sperner, B., 2003. Stress tensor inversion from fault kinematic indicators and focal mechanism data: the TENSOR program. Geological Society of London, Special Publications 212, 75- 100.

[16] Delvaux, D., Moeys, R., Stapel, G., Petit, C., Levi, K., Miroshnich, K., Ruzhich, V., Sankov, V., 1997. Paleostress reconstructions and geodynamics of the Baikal region, Central Asia, Part 2. Cenozoic rifting. Tectonophysics, 282, 1- 38.

[17] Diabat, A., 1999. Paleostress and strain analysis of the Cretaceous Rocks in the Eastern Margin of the Dead Sea Transform, Jordan. Ph.D. thesis, Baghdad University.

[18] Diabat, A., 2002. Strain analysis of the Cretaceous rocks in the Eastern margin of the Dead Sea Transform, Jordan. Dirasat 29, 159-172.

[19] Diabat, A. (2009). Structural and stress analysis based on fault-slip data in the Amman area, Jordan. Journal of African Earth Sciences 54, 155-162.

[20] Diabat, A., 2013. Fracture systems of granites and Quaternary deposits of the area east of Aqaba: indicators of reactivation and neotectonic activity. Arabian Journal of Geosciences, vol. 6, No. 3: 679- 695.

[21] Diabat, A., Salih, M., and Atallah, M., 2003. Magnitudes of the paleostresses at the Eastern Rim of the Dead Sea Transform Fault, Jordan. Dirasat, 30, 1-18.

[22] Diabat, A., Atallah, M., Salih, M., 2004.Paleostress analysis of the Cretaceous rocks in the eastern margin of the Dead Sea transform. Journal of African Earth Sciences 38, 449-460.

[23] Diabat, A., and Masri, A., 2005. Orientation of the principal stresses along Zerqa- Ma,in Fault. Mu,ta Lil-Buhuth wad-Dirasat. 20: 57- 71.

[24] Dunne, W.M., Hancock, P.L., 1994. Paleostress analysis of small- scale brittle structures. In: Hancock, P.L. (Ed.) Continental Deformation. Pergamon, Oxford, 101- 120.

[25] Eyal, Y., 1996. Stress field fluctuations along the Dead-Sea Rift since the middle Miocene. Tectonics 15: 157-170.

[26] Eyal, y., and Reches, Z., 1983. Tectonic analysis of the Dead Sea Rift region since the late Cretaceous based on mesostructures. Tectonics, 2: 167-185.

[27] Eyal, M., Eyal, Y., Bartov, Y., Steinitz, G., 1981. Tectonic development of the western margin of the Gulf of Elat(Aqaba) rift. Tectonophysics 80, 39-66.

[28] Eyal, Y., Gross, M.R., Engelder, T., Becker, A., 2001. Joint development during fluctuation of the regional stress field in southern Israel. Journal of Structural Geology, 23: 279-296.

[29] Freund, R., Garfunkel, Z., Zak, I., Goldberg, M., Weissbrod, T., Derin, B., 1970. The shear along the Dead Sea rift. Philosophical Transaction of the Royal Society of London 267, 107- 130.

[30] Garfunkel, Z.,1981. Internal structure of the Dead Sea leaky transform (rift) in relation to plate kinematics. Tectonophysics 80, 81- 108.

[31] Goodman, R. E. 1980. Introduction to rock mechanics. John Wily and sons. 478 P.

[32] Hancock, P.L., 1991. Determining contemporary stress directions from neotectonic joint systems. In: Whitmarsh, R.B., Bott, M.H.P., Fairhead, J.D., Kusnir, N.J., (Eds.), Tectonic Stress in the Lithosphere. Phil. Trans. Royal. Soc. London A 337, 29–40.

[33] Hardy, C., Homberg, C., Eyal, Y., Barrier, E., Muller, c., 2010. Tectonic evolution of the southern Levant Margin since the Mesozoic. Tectonophysics 494, 211-225.

[34] Jensen, E., Cembrano, J., Faulkner, D., Veloso, E., Arancibia, G., 2011. Development of a self- similar strike- slip duplex system in the Atacama Fault system, Chile. Journal of Structural Geology, 33, 1611- 1626.

[35] Kersten, R. W. O., 1990.The Stress Distribution Required for Fault and Joint Development. Proceedings of the International Conference of Mechanics of Jointed and Faulted Rock, Vienna, Austria, H. P. Rossmanith (ed.), Blakema, Rotterdam, 251 P.

[36] Leeder, M.R., Gawthorpe, R.L., 1987. Sedimentary models for extensional tilt-block/half graben basins. In: Coward, M.P., Dewey, J.F., Hancock, P.L. (Eds.), The Geological Society Special Publication 28, 139–152.

[37] Lunina, O. V., Mart, Y., Gladkov, A. S., 2005.Fracturing patterns, stress fields and earthquakes in the Southern Dead Sea rift. Journal of Geodynamics 40 , 216–234.

[38] Mikbel, Sh., 1986. Some relevant tectonical and geotechnical considerations of south Amman area/ Jordan.. Dirasat 7, 215-225.

[39] Mikbel, Sh., Zacher, W., 1981. The WadiShueib structure in Jordan. NeuesJaharbuchfuerGeologie und Paleontologie Monatshefte 9, 571-576.

[40] Pollard, D.D. and Aydin, A., 1988: progress in understanding jointing during the past centur. Geological Society of America Bulletin, 100, 1981-1204.

[41] Powell, J. H., 1989. Stratigraphy and sedimentation of the phanerozoic rocks in central and south Jordan. Geological mapping division, natural resources authority, Jordan.Bulletin 11, 130p.

[42] Price, N.J., Cosgrove, J.W., 1990. Analysis of Geological Structures. Cambridge University Press.
[43] Price, N.J., 1966, Fault and joint devlopment in brittle and semi-brittle rocks. Pergamon press, Oxford, 176 pp.
[44] Quennell, A., 1958.Thestructure and evolution of the Dead Sea rift.Quaternary Journal of the Geological Society, 64: 1- 24.
[45] Quennell, A.M., 1983. Evolution of the Dead Sea Rift. A review, First Jordanian Geologic Conference 460-482.
[46] Salameh, E., Zacher, W., 1982. Horizontal stylolites in Jordan. Neues JaharbuchfuerGeologie und Paleontologie Monatsheftee 8, 504- 512.
[47] Sassi, W., Faure, J. L., 1996. Role of faults and layer interfaces on the spatial variations of stress regime in basins: inferences from numerical modeling. In: Cloetingh, S., Ben-Avraham, Z., Sassi, W., Horvath, F.(Eds.), Dynamics of Basin Formation and strike- slip Tectonics, Tectonophysics, 266, 101- 119.
[48] Tripathy, V., Saha, D., 2013. Plate margin paleostress variations and intercontinental deformations in the evolution of the Cuddapah basin through Proterozoic. Precambrian Research, 235, 107- 130.
[49] Twiss, R.J., Moores, E.M., 1992. Structural Geology. W.N. Freeman and Company Press, New York.
[50] Wallace, R. E., 1951. Geometry of shearing stress and relation to faulting. Journal of Geology 59, 118-130.
[51] Zain Eldeen, U., Delvaux, D., Jacobs, P., 2002.Tectonic evolution in the Wadi Araba Segment of the Dead Sea Rift, Southwest Jordan. EGU Stephan Mueller Special Publication Series 2, 63- 81.

JJEES

Volume 7, (Number 1), June, 2015
ISSN 1995-6681
Pages 49 - 63

Jordan Journal of Earth and Environmental Sciences

Concentrations, Human and Ecological Risks of Metals in Soils in the Vicinity of Asphalt Plants in Delta States, Nigeria

Chukwujindu M. A. Iwegbue,[1*]
Stephen A. Osakwe,[1] Cyril I. Elokozie[1] and Godwin E. Nwajei[1]

[1]*Department of Chemistry, Delta State University, P.M.B. 1, Abraka, Nigeria.*

Received 14 February, 2014; Accepted 31 March 2015

Abstract

The concentrations of metals, cadmium (Cd), lead (Pb), chromium (Cr), nickel (Ni), copper (Cu), cobalt (Co), iron (Fe), manganese (Mn) and zinc (Zn) were measured in soil profiles in the vicinity of asphalt plants in Delta State, Nigeria by atomic absorption spectrometry after acid digestion. The concentrations of the metals in all depths and distances from the asphalt plants ranged from 0.07 to 0.58 mg kg^{-1} for Cd; 37.1 to 177 mg kg^{-1} for Cr; 2.0 to 31.1 mg kg^{-1} for Cu; 2.0 to 11.1 mg kg^{-1} for Co; 20 to 143 mg kg^{-1} for Ni. The concentrations of metals in these sites were below the Department of Petroleum Resources' maximum allowed values of metals in soils, except for Ni and Cr. The estimated contamination/pollution index indicates that the examined sites fall into slight to severe pollution ranges with a significant contribution from Cr and Ni. The total ecological risk (RI) values of metals in these soil profiles were <150 which suggested low ecological risks for these soils. However, the total cancer risk of metals in these soil profiles exceeded the target value of ($1/10^6$) one in a million chance of developing cancer.

Keywords: Heavy metals; Soil contamination; Asphalt plants; Nigeria.

1. Introduction

Anthropogenic emissions, arising from agricultural development, industrialization and urbanization, have become the major sources of soil contamination by metals. The soil acts as a geochemical reservoir and a natural medium for the transportation and the redistribution of contaminants in the biomass, terrestrial and aquatic environments (Behaddya and Hadjel, 2014). Metals are of environmental and human health concerns because (i) they exhibit a wide range of toxicity and chronic health effects such as cancer, reproductive, developmental and neurological disorders, cardiovascular, kidney and renal problems, lung damage, contact dermatitis, and brittle hair and hair loss. Many are suspected endocrine disruptors and respiratory toxin; (ii) they are resistant to degradation under natural terrestrial surface conditions; and (iii) they are discharged into the environment through a range of natural and anthropogenic processes (Lieben et. al., 2012). Metals may accumulate rapidly in soils but they may be removed from soils through leaching, plant uptake, erosion or deflation very slowly, requiring times of centuries or even millennia. Such persistent contaminants in soil make soil pollution much more serious than air or water pollution. Soil contamination affects every other components of the environment including food chain, namely plants, grazing animals and, ultimately, man (Itana, 1998).

Road construction is one of the strategic priorities of economic, social and political development in every country. In Nigeria, the need for road construction and rehabilitation is urgent because of the bad quality of roads and the increasing traffic density. The number of asphalt plants established is increasing as the need for the construction of these roads increases year by year. These asphalt plants continuously emit particles into the atmosphere; such emissions may contaminate air, soil and surface water as well as groundwater. Particulate matters have devastating effects on plants when directly absorbed through the leaves. Absorption of dust through the leave stomata lead to destruction of the chlorophyll and retardation of plant growth (Maina et. al., 2009).

Studies on the impact of various industrial discharges on the metal concentrations of soils in Nigeria have been documented, e.g., battery (Onianwa and Fakayode, 2000) fertilizer (Aina and Srhida, 2004), oil and gas (Iwegbue et. al., 2006) and cement industries (Maina et. al., 2009). However, relatively little or no information is currently available on the concentrations and distribution of metal in soils close to the asphalt plants in Nigeria, although Iwegbue (2013) provided information on the chemical fractionation and mobility patterns of metals in these soil profiles. The objective of the present study was to determine the concentrations of metals, Cd, Pb, Zn, Ni, Cr, Mn, Fe, Cu and Co, in soils in the vicinity of asphalt plants with a view of providing information on the extent of contamination, human and ecological risks associated with discharges from these plants.

* Corresponding author. e-mail: maxipriestley@yahoo.com

2. Materials and Methods

Soil samples were collected from five asphalt plants at different locations in Delta State (Fig. 1). At each site, soil samples were collected at immediate vicinity of asphalt plants) and at 500 m distance from the plant in the windward direction. At each distance, at least 10 random samples were collected at different depths (0-15, 15-30 and 30-60 cm), using a 150 m stainless steel auger. Samples collected at a given depth and distance were mixed together to form composite samples. The soil samples were air dried and sieved to pass through 2 mm mesh sieve. The soil pH was determined in soil water suspension (1:2.5 soil: water ratio) by using glass electrode (Abollino et. al., 2002). The electrical conductivity of the soil was determined on the filtrate obtained from filtering the suspension used for pH determination by using conductivity meter. Total organic carbon was determined by the wet dichromate method as described by Radojevic and Bashkin (1999).

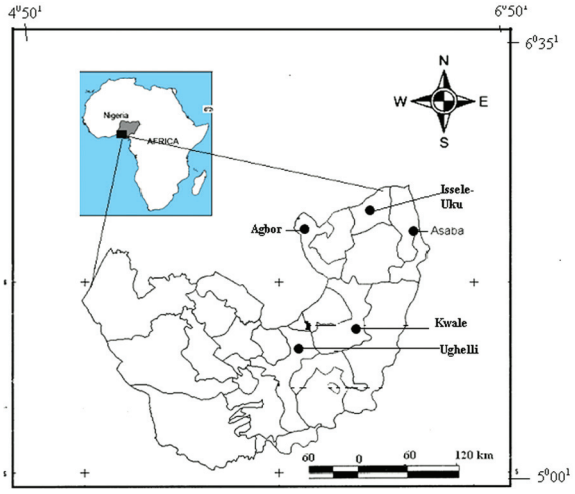

Figure 1. Map of Delta State showing the Study Areas.

A 1.0 gram sample of the soil sample was placed in a digestion tube, followed by the addition of 15 mL of aqua regia (3:1 HCl: HNO_3) and was then swirled to wet the sample and allowed to stand overnight. The following day, the tube was heated in a heating block of 50 ^oC for 30 min. and raise to temperature of 120 ^oC for 2 h. The digest was cooled to room temperature, the cover of the digestion tube was rinsed with 0.25 mol/L HNO_3 into the digest and filtered through Whatman No1 filter and made up to 25 mL with 0.25 mol/L HNO_3 (Radojevic and Bashkin, 1999). The sample solutions were analysed for Cd, Pb, Ni, Cr, Cu, Co, Fe, Mn and Zn by using atomic absorption spectrometry (Buck Model 205) equipped with D_2 background correction devices.

Reagent blank of the digestion process was analysed with each batch of 10 samples. The acids used for digestion were of analytical grades. Calibration standards for atomic absorption analysis were prepared by diluting a commercial Merck standard solutions of the metals (1000 mg/L) with 0.25 M HNO_3 to closely matching the matrix of diluted digest. Each sample was analysed in triplicates and the coefficient of variations between the triplicates analyses were less than 8% in all for metals. The quality control was assured by the use of blanks and spike recovery method. The average bland reading was used to correct all instrument readings. The procedure was validated by introducing known standards of the studied metals at three concentration levels into fresh portions of the sample and repeating all analysis steps from digestion to atomic absorption analysis. The spike recoveries for the various metals were within 100% $\pm$ 10%.

Contamination/pollution index (C/PI): This provides adequate information about the significance of the measured concentrations of metals on the intrinsic soil features and how the values obtained are related to the maximum allowable limits for the metals (Iwegbue et. al., 2010). The contamination/pollution index was computed as a ratio of metal concentration measured by chemical analysis to reference value. The contamination/pollution index was derived by employing the contamination/pollution index as defined by Lacutusu (2000):

$$C/PI = \frac{\text{Concentration of metal in soil}}{\text{Reference value}} \quad (1)$$

The reference value in this case is the Department of Petroleum Resources of Nigeria maximum allowable levels of metals in soil (DPR 2002) (Table 1). The conversion formula used for the C/P index varies from one country to another based on the chosen criteria. C/P index value greater than unity (1) defines the pollution range and when the value is less than unity defines the contamination range. The presence of one metal can significantly affect the impact that another has on organisms. This effect can be synergistic, additive or antagonistic, this reason, the multiple pollution index (MPI) is derived by the addition of the C/PI values for individual metals greater than 1. The computed C/P index and multiple pollution index (MPI) values were interpreted according to the scheme provided in below. The categorization of degree of contamination/pollution based on this index is as follows; <0.1 = very slight contamination; 0.10-0.25 = slight contamination; 0.26-0.5=Moderate contamination; 0.51-0.75 = Severe contamination; 0.76-1.00 = very severe contamination; 1.1-2.0 = slight pollution. 2.1-4.0 = moderate pollution; 4.1-8.0 = severe pollution; 8.1-16.0 = very severe pollution; >16.0 = excessive pollution.

Table 1: Some international environmental guidelines for metals in soils (mg kg^{-1})

Metal	Assessment Criteria						
	DTV	AEIL	EC	CEQC	DPR	Crustal abundance value	Shale[a]
Cd	0.8	3	3.0	0.5	0.8	0.11	0.3
Cr	100	400	-	20	100	100	90
Cu	36	100	140	30	36	50	45
Ni	35	60	75	20	35	80	68
Pb	85	600	300	25	85	14	20
Zn	140	100	300	60	140	75	95
Co	20		-		20	20	19
Mn						950	850
Fe						4.1*	4.7*

*value in (%)
[a]Wedephl and Turekien, 1961

Quantification of Enrichment Factor (EF): The enrichment factor was computed using the expression:

$$EF = \frac{\frac{C_n\ (Samle)}{C_n\ (reference)}}{\frac{B_n\ (test\ elements)}{B_n\ (reference)}} \quad (2)$$

where

Cn (Sample) = concentration of the test element in the sample

Cn_{ref} = Concentration of the reference element in the sample

Bn test element = background concentration of the test element in crustal rock

Bn_{ref} = background concentration of the reference element in crustal rock (Reimann and De Caritat, 2000).

In this case, iron was chosen as the reference element because it is the most abundant element in the earth crust. The crustal abundance values for the respective metals (Turiekian and Wedepohl, 1961) are used for the estimation of the enrichment factors (Table1). Five contamination categories are recognized on the basis of the enrichment factor (Sutherland, 2000; Loska and Wiechula, 2003). EF<2 =deficiency to minimal enrichment. EF=2-5 = Moderate enrichment. EF=5-20 = significant enrichment. EF=20-40 =Very high enrichment. EF>40 =extremely high enrichment.

Geoaccumulation index (Igeo): The index of geoaccumulation is useful for comparing the current and pre-industrial concentrations of metals in bottom sediments (Muller, 1969). It has also been applied in the assessment of the extent of soil contamination. The geoaccumulation index is given by the equation:

$$Igeo = \text{Log } 2\ \frac{C_n}{1.5B_n} \quad (3)$$

where Cn is the measured concentration of the element and Bn is the background concentration. In this case, the background concentration is the crustal abundance values of the respective metals (Table 1) (Turiekian and Wedepohl, 1961). Factor 1.5 is applied because of the possible variations in the background values due to lithological variations (Rogan et. al., 2010). The Muller index has seven classes depending on its value: <0 or 0 no pollution, values from 0 to 1, not polluted to moderately polluted (class 1); 1-2, moderately polluted (class 2); 2-3, moderately polluted to polluted (class 3); 3-4, polluted to strongly polluted (class 4); 4-5, strongly polluted (class 5); 5-6, strongly polluted to very polluted (class 6); and >6, very polluted (class 7).

Statistical Analysis: Two-way analysis of variance (ANOVA) and student's t test were used to determine whether the concentrations of metals varied significantly between sampling sites, depths and distance, with values less than 0.05 ($p<0.05$) considered statistically significant. The relationship between the metals was established by means of principal component analysis. The statistical calculations were performed with SPSS 20.1 version (SPSS Inc, Chicago IL, USA).

2.1. Ecological risk assessment

The index of evaluating ecological risks of metals was originally introduced by Hakanson (1980). This index has been used for ecological risk assessment of metals in sediments, soil and dusts (Saeedi et. al., 2012). The potential ecological risk index is given by the equation:

$$RI = \Sigma\ Er \quad (4)$$

$$\text{where } Er = Tr \times CF \quad (5)$$

$$CF = Cs / Cn \quad (6)$$

where CF= contamination factor which a ratio of metal concentration in the sample (Cs) and that of the background (Cn). Also, the background concentrations used are the crustal abundance values of the respective metals (Turiekian and Wedepohl, 1961).

Er and RI are the ecological risks of each metal and that of multiple metals, respectively.

Tr is the toxic response factor for the given element. The toxic response factors for Cd, Cu, Pb, Cr and Zn were 30, 5, 5, 2 and 1, respectively (Hakanson, 1980). The Er and RI have been classified into five and four categories depending on their values, respectively. Er value <40 denotes low potential ecological risk; ≥40<80 moderate potential ecological risk; ≥80<160 considerable potential ecological risk; ≥160<320 high potential ecological risk and ≥320 very high potential ecological risk. RI value <150 indicates low ecological risk; ≥150<300 moderate ecological risk; ≥300<600 high ecological risk and ≥600 very high ecological risk (Hakanson, 1980).

2.2. Human exposure and health risk assessment

Humans can be exposed to metals in soil through three pathways which include direct ingestion of soil, inhalation of particulates emitted from soil and dermal absorption of metals through soil adhered to exposed skin (Shi et. al., 2014; Lai et. al., 2010). The non-carcinogenic and carcinogenic risk of these exposure pathways were considered in this study. The non-carcinogenic hazard risk (HI) for children and adults was calculated using equations (7)-(12) adapted from USDOE (2011) and USEPA (2001; 2011):

$$CDI_{ing\text{-}nc} = \frac{C \times IngR \times EF \times ED}{BW \times AT_{nc}} \times 10^{-6} \quad (7)$$

$$CDI_{inh\text{-}nc} = \frac{C \times EF \times ET \times ED}{PEF \times 24 \times AT_{nc}} \quad (8)$$

$$CDI_{derma\text{-}nc} = \frac{C \times SA \times AF \times ABSd \times EF \times ED}{BW \times AT_{nc}} \times 10^{-6} \quad (9)$$

$$\text{Hazard Quotient (HQ)} = \frac{CDI_{nc}}{RfD} \quad (10)$$

$$\text{Hazard index (HI)} = \sum HQ = HQ_{ing} + HQ_{inh} + \text{HQ dermal} \quad (11)$$

$$\text{Hazard index (HI)} = \frac{CDI_{ing}\ -nc}{RfD_{ing}} + \frac{CDI_{inh}\ -nc}{RfC_{inh}} + \frac{CDI_{dermal}\ -nc}{RdDermal} \quad (12)$$

The carcinogenic risk was calculated for the life time exposure, estimated as the incremental probability of an individual developing cancer over a lifetime as a result of total exposure to the potential carcinogens (Cd, Cr, Ni and Pb). The carcinogenic hazard risk (Total Risk) for children and adult was calculated using equation (13)-(20) adapted from USDOE (2011):

$$CDI_{ing\text{-}ca} = \frac{C \times IngRadj \times EF}{ATca} \times 10^{-6} \quad (13)$$

$$IngR_{adj} = \frac{ED_{child} \times IngR_{child}}{BW_{child}} + \frac{(ED_{adult} - ED_{child})}{BW_{adult}} \times IngR_{adult} \quad (14)$$

$$CDI_{inh}\text{–ca} = \frac{\text{C x EF x ET x ED}}{} \times 10^{3} \quad (15)$$

$$CDI_{dermal}\text{–ca} = \frac{\text{C x ABSd x EF x DFSadj}}{} \times 10^{-6} \quad (16)$$

$$DFS_{adj} = \frac{ED_{child} \times SA\ child \times AF\ child}{BW_{child}} + \frac{(ED_{adult} - ED_{child}) \times SAadult \times AF\ adult}{BW_{adult}} \quad (17)$$

$$Risk = CDI_{ca} \times CSF \quad (18)$$

$$Total\ Risk = Risk_{ing} + Risk_{inh} + Risk_{dermal} \quad (19)$$

$$Total\ Risk = CDI_{ing}\text{–ca} \times CSF_{ing} + CD_{inh}\text{-ca} \times IUR + \frac{CDI_{dermal} \times CSF_{ing}}{ABS_{GI}} \quad (20)$$

where CDI_{ing}, CDI_{inh}, CDI_{dermal} are the chronic daily intake or dose contacted through ingestion, inhalation and dermal contact with soil, respectively. RfD is the reference dose, RfD_{ing} (chronic oral reference dose), RfC_{inh} (chronic inhalation reference concentration), RfD_{dermal} (chronic dermal reference dose = RfD_{ing} x ABS_{GI}) through the three exposure pathway, respectively. CSF_{ing} is chronic oral slope factor via ingestion, IUR is the chronic inhalation unit risk, CSF_{dermal} is chronic dermal slope factor = CSF_{ing}/ABS_{GI} and C is the concentration of metals in soil. The definitions of the symbols and values for Nigerian-specific variables are displayed in Table 2 while the toxicological parameters of the investigated metals used for health risk assessment are displayed in Table 3.

Table 2: Values of variables for estimation of human health risk assessment

Parameters	Unit	Definition	Values		References
			Child	Adult	
C	µg/g	Metals concentration in soil			
ABS_d	-	Dermal absorption factor	0.03	0.001	USEPA, 2011
AF	mg/cm^2	Soil to skin adherences factor	0.2	0.07	USEPA, 2011
BW	Kg	Average body weight	15	60	
ED	Year	Exposure duration	6	24	USEPA, 2001
EF	d/yr	Exposure frequency	313	313	Man et. al. (2013)
ET	h/d	Exposure time	8	8	USEPA, 1987
IngR	mg/d	Soil ingestion rate for receptor	200	100	USEPA, 2001
SA	cm^2/event	Skin surface area	2800	5700	USEPA, 2001
ATnc	D	Averaging time for non-carcinogenic	ED x 365		USEPA, 1997
ATca	d	Averaging time for carcinogenic	LT x 365		USEPA, 1997
DFS_{adj}	mg/yr/kg/d	Soil dermal contact for-age-adjusted	110		Equation (14)
$IngR_{adj}$	mg/yr/kg/d	Soil ingestion rate-age adjusted	344		Equation (11)
LT	Year	Lifetime	48.9		
PEF	m^3/kg	Soil to air particulate emission factor	1.36×10^9		USDOE, 2011

Table 3: Toxicological parameters of the investigated metals used for health risk assessment

Element	CSF_{ing} (mg/kg/d)	IUR (µg/m^3)	RfD_{ing}	RfC_{inh}	ABS_{GI}
Cd		1.8×10^{-3}	1.0×10^{-3}	1.0×10^{-5}	0.025
Cr	5.0×10^{-3}	1.2×10^{-2}	3.0×10^{-3}	1.0×10^{-4}	0.013
Ni		2.6×10^{-4}	2.0×10^{-2}	9.0×10^{-5}	0.04
Fe			7.0×10^{-1}		1
Zn			3.0×10^{-1}	$4.0 \times 10^{-3*}$	1
Co			3.5×10^{-3}	6.0×10^{-6}	1
Pb	8.5×10^{-3}	1.2×10^{-5}	1.4×10^{-1}	$2.0 \times 10^{-4*}$	1
Mn			4.0×10^{-1}	5.0×10^{-5}	1
Cu				1.4×10^{-3}	1
Reference	USDOE, 2011	USDOE, 2011	USDOE, 2011	USDOE, 2011	USEPA, 2011

*MOEE, 2008

The qualitative description of human health risk assessment followed that HQ value above 1 suggests the level of concern. That is, HQ ≤ 1 suggested unlikely adverse health effects whereas HQ > 1 suggested the probability of adverse health effects (Luo et. al., 2012a). In general, the total cancer risk lower than 10^{-6} (a probability of 1 chance in 1,000,000 of an individual developing cancer) are considered to be negligible and cancer risks above 10^{-4} are considered unacceptable by most international regulatory agencies (US EPA, 1989; Guney et. al., 2010; Luo et. al., 2012a). The value 10^{-6} is also considered the carcinogenic target risk (US EPA, 2011; Luo et. al., 2012a).

3. Results and Discussion

The results of some physicochemical characteristics and concentrations of metals in soils within the asphalt plants and at 500 m distance from the plants are displayed in Table 4. The soil pH ranged from 6.5 to 8.2. The soil pH decreased with increasing depth. The soil pH, cation exchange capacity and organic matter are some of the factors that control the availability, retention and mobility of metals. The electrical conductivity of the examined soil samples ranged from 21.6 to 246.1 µScm^{-1} for all sites and depths. The conductivity of the examined soils corresponds to the values reported for some

soil types in southern Nigeria (Iwegbue et. al., 2006; Iwegbue et. al., 2009). Total organic carbon and soil conductivity decreased with increasing depth of the soil profile. The total organic carbon (TOC) values ranged from 0.3 to 0.9%. The total organic carbon contents of the topsoil for the different sites showed no significant difference ($p>0.05$).

Table 4: Physicochemical characteristics and total metal concentrations (mg kg^{-1}) in soils within the plants and 500 m distance from the Asphalt plant

		Within the Asphalt plant					500 m distance from the Asphalt plant				
Parameter	**Depth (cm)**	**I**	**II**	**III**	**IV**	**V**	**I**	**II**	**III**	**IV**	**V**
pH	0-15	8.2	6.8	7.9	8.2	7.9	7.8	7.5	7.4	7.6	7.1
	15-30	6.9	8.2	6.5	7.6	6.5	6.9	6.7	6.5	7.8	6.4
	30-60	7.1	7.8	6.5	6.7	6.9	7.4	6.9	7.3	6.4	6.8
Conductivity (µS cm^{-1})	0-15	246	211	232	197	212	124	196	129	99.7	97.7
	15-30	134.7	139	143	142	135	86.5	78.3	76.7	10	78.3
	30-60	117	59.0	21.6	112	66.0	55.7	51.5	52.0	49.3	61.7
TOC (%)	0-15	0.9	0.9	0.9	0.8	0.8	0.6	0.6	0.6	0.6	0.5
	15-30	0.5	0.3	0.7	0.5	0.4	0.3	0.4	0.4	0.4	0.6
	30-60	0.5	0.5	0.6	0.3	0.3	0.2	0.2	0.2	0.3	0.3
Cd	0-15	0.3	0.4	0.3	0.3	0.3	0.2	0.2	0.1	0.2	0.1
	15-30	0.2	0.3	0.1	0.1	0.2	0.1	0.1	0.1	0.1	0.1
	30-60	0.1	0.1	0.1	0.1	0.1	0.1	0.1	0.1	0.1	0.1
Pb	0-15	3.5	4.1	3.0	3.1	3.0	2.0	2.8	1.7	1.5	1.4
	15-30	1.0	2.0	2.1	1.5	1.6	1.2	1.0	1.0	1.0	1.6
	30-60	0.9	1.1	1.0	1.0	1.0	1.0	0.9	0.9	0.7	0.6
Ni	0-15	115	119	12	143	138	65.0	131	96.1	76.9	69.8
	15-30	87.9	107	106	120	113	42.1	126	72.1	37.3	74.7
	30-60	63.0	91.3	59.1	97.6	93.8	38.0	103	105	21.1	20.1
Cr	0-15	156	150	165	176	166	96.8	88.4	107	89.8	102
	15-30	12.4	189	147	149	150	61.1	60.1	55.7	56.3	87.6
	30-60	9.0	12.0	9.1	121	126	50.2	49.5	50.1	37.1	41.7
Cu	0-15	28.8	31.1	26.1	10.1	12.3	19.1	28.1	9.0	6.0	12.0
	15-30	12.4	10.7	21.0	6.2	8.0	7.3	12.4	11.1	4.1	5.7
	30-60	9.7	9.0	10.4	2.0	4.7	4.3	9.9	10.0	2.0	1.9
Co	0-15	8.6	10.1	10.1	11.1	9.8	6.4	6.6	7.4	6.8	7.0
	15-30	4.2	9.8	8.6	6.2	1.8	4.0	4.1	3.1	4.1	6.0
	30-60	2.2	4.0	2.0	4.0	2.0	2.0	2.0	2.0	2.2	2.0
Fe	0-15	257	257	231	224	243	188	123	129	170	151
	15-30	98.4	101	113	108	116	89.7	67.3	90.7	86.3	89.0
	30-60	78.4	86.1	81.7	77.9	81.5	68.1	59.0	58.0	62.9	71.3
Mn	0-15	183	278	165	151	194	162	151	74.1	70.4	91.5
	15-30	71.6	74.0	76.3	69.9	85.0	87.0	56.2	69.7	62.6	63.4
	30-60	56.1	61.1	60.7	54.1	61.4	47.0	43.1	42.3	48.0	55.0
Zn	0-15	101.8	32.0	100.0	50.2	60.7	92.9	89.9	46.9	41.3	42.2
	15-30	65.1	80.8	79.5	43.1	41.3	56.8	61.0	56.1	27.0	39.9
	30-60	52.1	60.1	58.9	32.1	36.1	48.8	49.7	50.1	21.2	1.0

The concentrations of metals in the investigated soils decreased with respect to the depths and the distance from the asphalt plants. The concentrations of metals observed in soil profiles within the asphalt plants were higher than the concentrations of metals observed in soils collected at 500 m distance from asphalt plants. The differences observed in the concentrations of metals at these sites were significant ($p<0.05$), except for Cd. The concentrations of metals in the studied soils were compared with crustal abundance values, national and international guidelines for metals in soil (Table 1). The concentrations of the examined metals were below their respective crustal abundance values except for Cd, Cr and Ni.

The concentrations of Cd ranged from 0.1- 0.4 mg kg^{-1} and from 0.1 - 0.2 mg kg^{-1} within the plant areas and 500m away from the asphalt plant, respectively. The maximum allowable concentration of Cd in soil is 0.8 mg kg^{-1} (DPR, 2002). The concentrations of Cd observed in these soil profiles were below the maximum allowable concentration. Dudka et. al. (1996) reported Cd levels in arable soil in industrial area of Upper Silesia, South Poland to be 3.2 $mgkg^{-1}$ while Umoren and Onianwa (2005) reported concentrations in the range of 1.7-23 mg kg^{-1} Cd in soils around urban industrial area in south western, Nigeria. Similarly, Inuwa et. al. (2007) found

Cd levels of 0.10-0.70 mg kg^{-1} in soils of major industrial areas of north-western Nigeria. The concentrations of Cd found in these soil profiles are comparable to the levels of Cd in soils reported by Inuwa et. al. (2007).

The concentrations of Pb in these soil profiles ranged from 0.9 - 4.1 mg kg^{-1} and from 0.6 - 2.8 mg kg^{-1} within the asphalt plants and 500 m distance from the plants, respectively. The highest concentration of Pb was observed in site II. The maximum allowable concentration of Pb in soil in Nigeria is 85 mg kg^{-1} (DPR, 2002). The concentrations of Pb found in these soil profiles were lower than the maximum allowable concentrations. The concentrations of Pb observed in these sites were lower than the concentrations of Pb observed in soils around some industrial sites in Nigeria (Iwegbue et. al., 2006; Iwegbue et. al., 2009 b; Maina et. al., 2009) and India (Krishna and Govil, 2008).

The concentrations of Ni in these soil profiles varied from 59.1-143 mg kg^{-1} within the plants premises, and from 20.1-131 mg kg^{-1} at 500 m distance from the asphalt plants. The concentrations of Ni in the soil profile of site IV were higher than that of the other sites. The concentrations of Ni in these soil profiles exceeded the Department of Petroleum Resources of Nigeria permissible limit of 36 mg kg^{-1} (DPR, 2002) except for the soils collected from the 30 – 60 cm depth of sites IV and V at 500 m distance from the asphalt plants. Asphalt is a residue from petroleum refining process which is known to contain substantial amounts of Ni. Similar levels of Ni were reported in surface soils of industrial zones in south-western Nigeria (Umoren and Onianwa, 2005). The concentrations of Ni observed in these sites were higher than the concentrations of Ni found in soils in the vicinity of gas plant (Iwegbue et. al., 2006) and crude oil contaminated sites in the Niger Delta (Iwegbue et. al., 2009).

The concentrations of Cr in these soil profiles ranged from 9.0 - 189 mg kg^{-1} within the plants and from 37.0-107 mg kg^{-1} at 500 m distance from the plants. Higher concentrations of Cr were found in the soil profiles of sites IV and V compared to the other sites investigated. The Department of Petroleum Resources maximum allowable level of Cr in soil is 100 mg kg^{-1}. The concentrations of Cr in the top and sub soil samples collected within the asphalt plants were above the maximum allowable levels of Cr in soil, while at 500 m distance, only the topsoil of site V had higher concentration of Cr than the limit. Inuwa et. al. (2007) reported Cr concentration in the range of 21.1-85.4 mg kg^{-1} in surface soil around industrial areas in the northern part of Nigeria. The concentrations of Cr observed in these soils were higher than the concentrations of Cr in soils around some industries in Nigeria (Inuwa et. al., 2007; Iwegbue et. al., 2007) but were comparable to the concentrations of Cr in soils of urban industrial zones in south western Nigeria (Umoren and Onianwa, 2005).

The concentrations of Cu in these soil profiles ranged from 2.0-31.0 mg kg^{-1} within the asphalt plants and from 1.9-28.0 mg kg^{-1} at 500 m distance from the asphalt plants. Lower concentrations of copper were observed in the subsoil compared to the concentrations of Cu observed in the topsoil. The concentrations of Cu found in these sites were lower than the Department of Petroleum Resources of Nigeria permissible limit of 36 mg kg^{-1} Cu in soil. The concentrations of Cu found in these sites were lower than the DPR target value. The concentrations of Cu we found in our sites were higher than concentrations of Cu observed in soils in the vicinity of crude oil processing facilities in Nigeria (Iwegbue et. al., 2006; Iwegbue et. al., 2009). Much higher Cu levels (68.8 to 103.3 mg kg^{-1}) were reported in soils in the vicinity of cement factory in Nigeria (Maina et. al., 2009) and in soils near copper smelter in Poland (Kabala and Singh, 2001). Copper is complexed by organic ligands especially by the carboxylic and phenolic groups. As the solubility of the organic matter increases with increasing pH, the dissociation of Cu – organic matter complexes can result in the leaching of copper to ground water (Bhattacharya et. al., 2002). The solubility of Cu and Zn is governed by pH and redox conditions and at pH range of 5.4-6.5, Cu and Zn are distinctly more soluble under oxidising conditions than reducing conditions (Bhattacharya et. al., 2002). In the present study, only the subsoil of site III had pH value in this range, the solubility of Cu and Zn is unlikely in these sites.

The concentrations of Co in these soil profiles were in the range of 2.0 to 11.1 mg kg^{-1}. The highest concentrations of Co were observed in the soil profile of site II (Table 4). Like other metals, the concentrations of Co were higher in the soil samples collected within the asphalt plants than those collected at 500 m distance from the plants. The Department of Petroleum Resources of Nigeria permissible limit of Co in soil is 20 mg kg^{-1} (DPR, 2002). The concentrations of Co, found in our sites, were below the specified limit of Co in soil by the Nigerian regulation. The concentrations of Co observed in these sites were lower than concentrations of Co in soils around industrial sites in southern India (Krishna and Govil, 2008). However, Co concentrations in the range of 3.55 to 58.9 mg kg^{-1} have been reported in urban soils of different cities in China (Zhang and Ke, 2004; Lu and Bai, 2006; Lee et. al., 2006; Liao et. al., 2006; Luo et. al., 2012b).

The concentrations of Fe in these soil profiles ranged from 58.0 to 247 mg kg^{-1}. The highest concentration of Fe was observed in the soil profile of site II. The concentrations of Fe observed in these soil profiles were below global average value (Alloway, 2005) and crustal abundance value of Fe of 47000 mg kg^{-1}. The concentrations of Fe in these soils samples were lower than the concentrations of Fe previously reported for the Niger Delta soils (Iwegbue et. al., 2006; Nwajei and Iwegbue, 2010; Iwegbue et. al., 2009a; Iwegbue, 2013).

The concentrations of Mn in these soil samples ranged between 54.1 and 278 mg kg^{-1} for all sites and depths. The highest concentration of Mn was observed in the topsoil of site II. The distribution patterns of Mn in the topsoil of these sites follow the order II > V > I > III > IV. The concentrations of Mn found in these soil profiles were below the crustal abundance and global average values (Alloway, 2005; Turiekian and Wedepohl, 1961). The concentrations of manganese were about 1.13 to 1.84 times higher than levels observed at 500m distance from the asphalt plants. However, the concentrations of Mn in the soil profiles of these asphalt plants were comparable to the concentrations of Mn observed in soils in the vicinity of gas plant (Iwegbue et. al., 2006) and crude oil impacted soils (Iwegbue et. al., 2009b) but were lower than the concentrations of Mn found in soils around

a cement industry in Nigeria (Maina et. al., 2009). The concentration of Mn in soils is of significance because of its high mobility. It migrates easily and contaminates surface streams and ground water.

The concentrations of Zn in all sites and depths varied from 32.0-102 mg kg^{-1} within the asphalt plants and from 21.2 to 92.9 mg kg^{-1} at 500 m distance from the asphalt plants. The higher concentrations of Zn were observed in sites I and III than other sites investigated. The Department of Petroleum Resources of Nigeria permissible limit for Zn in soil is 140 mg kg^{-1} (DPR, 2002). The concentrations of Zn observed in soils collected from all sites and depths were below the DPR limit. Similar Zn concentrations have been reported in soils in the vicinity of industrial activities in Nigeria (Iwegbue et. al., 2006; Iwegbue et. al., 2009; Maina et. al., 2009) and other regions of the world (Kabala and Singh, 2001).

3.1. Contamination/Pollution Index

As shown in Table 5, the index values for Cd, Cu, Fe, Mn and Zn were in the contamination range (i.e., less than unity), whereas that of Cr and Ni were in the pollution range (i.e., greater than unity). The multiple pollution index value for these sites ranged from 1.6 to 5.5 with a significant contribution from Ni and Cr. The MPI values decreased with increasing depths of the profiles, which indicated that the surface soils were more polluted than the subsurface soils. Again, the MPI values can be used to rank the various sites and depths in order of magnitude of pollution. In this case, the magnitudes of pollution by these metals followed the order: II > V > IV > III > I.

Table 5: Contamination/Pollution index for soils within the plants and 500 m from the Asphalt plant

Within the asphalt plant									
Site	**Depth (cm)**	**Cd**	**Pb**	**Ni**	**Cr**	**Cu**	**Co**	**Zn**	**MPI**
I	0-15	0.4	0.0	3.2	1.6	0.8	0.4	0.7	4.7
	15-30	0.2	0.0	2.4	0.1	0.3	0.2	0.5	2.4
	30-60	0.1	0.0	1.8	0.1	0.3	0.1	0.4	2.3
II	0-15	0.5	0.1	3.3	1.5	0.9	0.5	0.2	4.8
	15-30	0.4	0.0	3.0	1.9	0.3	0.1	0.6	4.9
	30-60	0.2	0.0	2.5	0.1	0.3	0.2	0.4	2.5
III	0-15	0.4	0.0	3.6	1.7	0.7	0.5	0.7	5.2
	15-30	0.2	0.0	2.9	1.5	0.6	0.4	0.6	4.4
	30-60	0.1	0.0	1.6	0.0	0.3	0.1	0.4	1.6
IV	0-15	0.4	0.0	4.0	1.8	0.3	0.6	0.4	2.6
	15-30	0.1	0.0	3.3	1.5	0.2	0.3	0.3	4.8
	30-60	0.1	0.0	2.7	1.2	0.1	0.2	0.2	3.9
V	0-15	0.4	0.0	3.9	1.7	0.3	0.5	0.4	5.5
	15-30	0.3	0.0	3.1	1.5	0.2	0.2	0.3	4.6
	30-60	0.1	0.0	2.6	1.3	0.1	0.1	0.3	3.9
500 m distance from the asphalt plant									
I	0-15	0.2	0.0	1.9	1.0	0.5	0.3	0.7	1.9
	15-30	0.2	0.0	1.2	0.6	0.2	0.2	0.4	1.2
	30-60	0.1	0.0	1.1	0.5	0.1	0.1	0.4	1.1
II	0-15	0.2	0.0	3.7	0.9	0.8	0.3	0.6	3.7
	15-30	0.2	0.0	3.6	0.6	0.4	0.2	0.4	3.6
	30-60	0.1	0.0	3.0	0.5	0.3	0.1	0.4	3.0
III	0-15	0.2	0.0	1.1	1.1	0.3	0.4	0.3	2.2
	15-30	0.1	0.0	2.1	0.6	0.3	0.2	0.4	2.1
	30-60	0.1	0.0	3.0	0.5	0.3	0.1	0.4	3.0
IV	0-15	0.2	0.0	2.2	0.9	0.2	0.2	0.3	2.2
	15-30	0.1	0.0	1.1	0.6	0.1	0.1	0.2	1.1
	30-60	0.1	0.0	0.6	0.4	0.1	0.1	0.2	0.0
V	0-15	0.2	0.0	2.0	1.0	0.3	0.4	0.3	2.0
	15-30	0.2	0.0	2.1	0.9	0.2	0.3	0.3	2.1
	30-60	0.9	0.0	0.6	0.4	0.1	0.1	0.0	0.6

3.2. Enrichment factor and Geoaccumulation index

The estimated Enrichment Factors (EF) for metals in soils within the asphalt plants and at 500 m distance from the plant are displayed in Table 6. Apart from Cd, Cr and Ni other metals had EF values less than 1. The enrichment factors decreased in the order; Ni > Cr > Cd > Cu > Co > Pb > Mn > Fe. In the present study, the soil collected within the asphalt plants had higher EF values than those collected at 500 m distance from the asphalt plants. EF values for the metals in these soils decreased with depth and lateral distance from the plant which indicated that surface horizons of these sites were more enriched with metals than subsurface horizon and moreso, soils within the plants were enriched with metals than those collected at a distance away from the plant. From contamination categorisation based on the enrichment factor values, the soils within and at a distance from the asphalt plants fall within the deficiency to minimal enrichment to moderate enrichment categories.

The geoaccumulation index (Igeo) for the examined metals in these soils are displayed in Table 7. The Igeo values of the examined metals for all sites, depths and 500 m distance from the asphalt plants were negative which also indicated that these sites were not polluted with the studied metals. Igeo values observed in these sites, depths and distance from the plants indicate that the examined soils fall within the class 1 (no pollution) of the Igeo categorization.

Table 6: Enrichment factor of soils within the plants and 500 m distance from the asphalt plants

		Within the asphalt plant					500 m distance from the asphalt plant				
Metals	**Depth (cm)**	**I**	**II**	**III**	**IV**	**V**	**I**	**II**	**III**	**IV**	**V**
Cd	0-15	1.07	1.27	1.07	0.97	1.03	0.57	0.50	0.43	0.50	0.47
	15-30	0.50	0.93	0.47	0.33	0.67	0.40	0.43	0.37	0.37	0.43
	30-60	0.37	0.47	0.37	0.23	0.37	0.33	0.37	0.33	0.27	0.23
Pb	0-15	0.17	0.20	0.15	0.15	0.15	0.10	0.14	0.09	0.08	0.07
	15-30	0.05	0.10	0.11	0.07	0.08	0.06	0.05	0.05	0.05	0.08
	30-60	0.04	0.06	0.05	0.05	0.05	0.05	0.04	0.04	0.04	0.03
Ni	0-15	1.69	1.75	1.88	2.10	2.03	0.96	1.93	1.41	1.13	1.03
	15-30	1.29	1.58	1.56	1.76	1.66	0.62	1.86	1.06	0.55	1.10
	30-60	0.93	1.34	0.87	1.43	1.38	0.56	1.52	1.55	0.31	0.30
Cr	0-15	1.73	1.66	1.83	1.95	1.85	1.08	0.98	1.19	1.00	1.13
	15-30	0.14	2.10	1.63	1.66	1.66	0.68	0.67	0.62	0.63	0.97
	30-60	0.10	0.13	0.10	1.35	1.40	0.56	0.55	0.56	0.41	0.46
Cu	0-15	0.64	0.69	0.58	0.23	0.27	0.42	0.62	0.20	0.13	0.27
	15-30	0.28	0.24	0.47	0.14	0.18	0.16	0.27	0.25	0.09	0.13
	30-60	0.22	0.20	0.23	0.04	0.10	0.09	0.22	0.22	0.04	0.04
Co	0-15	0.43	0.50	0.50	0.55	0.49	0.32	0.33	0.37	0.34	0.35
	15-30	0.21	0.49	0.43	0.31	0.09	0.20	0.21	0.15	0.21	0.30
	30-60	0.11	0.20	0.10	0.20	0.10	0.10	0.10	0.10	0.11	0.10
Fe	0-15	0.01	0.01	0.00	0.00	0.01	0.00	0.00	0.00	0.00	0.00
	15-30	0.00	0.00	0.00	0.00	0.00	0.00	0.00	0.00	0.00	0.00
	30-60	0.00	0.00	0.00	0.00	0.00	0.00	0.00	0.00	0.00	0.00
Mn	0-15	0.22	0.33	0.19	0.18	0.23	0.19	0.18	0.09	0.08	0.11
	15-30	0.08	0.09	0.09	0.08	0.10	0.10	0.07	0.08	0.07	0.07
	30-60	0.07	0.07	0.07	0.06	0.07	0.06	0.05	0.05	0.06	0.06
Zn	0-15	1.07	0.34	1.05	0.53	0.64	0.98	0.95	0.49	0.43	0.44
	15-30	0.69	0.85	0.84	0.45	0.44	0.60	0.64	0.59	0.28	0.42
	30-60	0.55	0.63	0.62	0.34	0.38	0.51	0.52	0.53	0.22	0.01

3.3. Principal Component Analysis

The PCA factor loading after Varimax rotation with Kaiser Normalization of metals in the soil profiles within the asphalt plants and at 500 m distance from the plants are displayed in Tables 8 and 9, respectively. PCA factor loading for soils within the asphalt plants have been previously described (Iwegbue, 2013). Briefly, two factors were obtained accounted for 91.33% of the total variance at 0-15 cm depth of the immediate vicinity of the plant. Factor 1 accounted for 59.07% of the total variance and was dominated by total organic carbon, Cd, Fe, Cu, and Pb. This suggests that the mechanism for the retentions of these metals in the topsoil is due to complexation to organic matter (Romic et. al., 2004). Copper has a higher loading of 0.993 than the other metals, which might be explained by the chalcophilic characters of these elements (they form sulphide which is poorly soluble minerals, e.g., Cu_2S, CuS and CdS etc). In contrast to Cd, most colloidal particles in soil strongly adsorb Cu. Copper

forms a stable complex with organic matter than other bivalent transition metals and, therefore, soil, which is rich in organic matter, can retain more copper without causing plant toxicity. Bipolarity of factor with a higher negative loading for Cr and Ni and somewhat lower loading for Mn and Co were observed. Factor 2 explained 32.26% of the total variance with significant loading in Mn, Zn, pH and conductivity. Again, the retention of these metals (Mn and Zn) in the soil is pH dependent. Mn and Zn are associated with traffic activities. Zn may be derived from mechanical abrasion of vehicles. Zinc in these soils may therefore be related, in part, to traffic movement within these sites. Zinc compounds have been employed extensively as antioxidants, e.g., (zinc carboxylate complexes and zinc sulphonates) and as detergent dispersant improvers for lubricating oil (Miguel et. al., 1997). It was reported that tire wear contributes significant amounts of Zn to the environment. However, Mn is a fuel additive, especially in diesel which is used to run the plants and truck used haulage of the processed asphalt. At the 15-30 cm depth, the PCA results showed that 3 principal components were extracted, accounting for 46.13%, 30.98% and 19.53% of the total variance. Factor 1had a significant positive loading in Cu, Mn, Zn, Cd, Pb and conductivity. Chemisorption on the Mn and Al oxides may explain this association. Factor 2 had a significant loading in Fe, Cd, Zn and organic matter while factor 3 had significant loading in Cr and conductivity. The bipolarity factor of the second factor with a high negative factor loading for Ni and somewhat lower loading for Co, Cr, Pb and Cu, was observed as well (Table 8). At the 30-60 cm depth, the PCA results indicated that three components were extracted. Factor 1 had a significant positive loading for Zn, Cu, Cd and Ni consisting of 78.38% of total variance. The bipolarity of the first factor with high negative factor loading for Fe and Mn and a negative loading for TOC and electrical conductivity. Factor 2 accounted for 13.95% of the total variance with the dominance of metal such as Pb, Cr, Co and electrical conductivity, and a high negative bipolar factor in Zn, Mn, Cu and pH and TOC. Factor 3 constitutes 8.55% the total variance comprising Pb, Cd, Cr, Co and with high negative bipolar factor in pH and TOC.

Table 7: Geoaccumulation index for soils within the plants and 500 m distance from the asphalt plants

		Within the asphalt plant					500 m distance from the asphalt plant				
Metals	**Depth (cm)**	**I**	**II**	**III**	**IV**	**V**	**I**	**II**	**III**	**IV**	**V**
Cd	0-15	-0.49	-0.24	-0.49	-0.63	-0.54	-1.40	-1.59	-1.79	-1.59	-1.68
	15-30	-1.59	-0.68	-1.68	-2.17	-1.17	-1.91	-1.79	-2.03	-2.03	-1.79
	30-60	-2.03	-1.68	-2.03	-2.68	-2.03	-2.17	-2.03	-2.17	-2.49	-2.68
Pb	0-15	-3.11	-2.88	-3.32	-3.29	-3.33	-3.89	-3.45	-4.13	-4.31	-4.46
	15-30	-4.88	-3.92	-3.83	-4.34	-4.27	-4.61	-4.88	-4.92	-4.94	-4.22
	30-60	-5.12	-4.73	-4.97	-4.86	-4.86	-4.97	-5.14	-5.12	-5.40	-5.57
Ni	0-15	0.17	0.22	0.33	0.49	0.44	-0.65	0.36	-0.09	-0.41	-0.55
	15-30	-0.21	0.07	0.05	0.23	0.15	-1.28	0.31	-0.50	-1.45	-0.45
	30-60	-0.70	-0.16	-0.79	-0.06	-0.12	-1.43	0.02	0.04	-2.27	-2.34
Cr	0-15	0.21	0.15	0.29	0.38	0.30	-0.48	-0.61	-0.33	-0.59	-0.40
	15-30	-3.45	0.49	0.12	0.14	0.15	-1.14	-1.17	-1.28	-1.26	-0.62
	30-60	-3.91	-3.49	-3.90	-0.16	-0.10	-1.43	-1.45	-1.43	-1.86	-1.70
Cu	0-15	-1.23	-1.12	-1.37	-2.74	-2.46	-1.82	-1.26	-2.91	-3.49	-2.49
	15-30	-2.44	-2.66	-1.68	-3.44	-3.08	-3.21	-2.45	-2.61	-4.03	-3.56
	30-60	-2.79	-2.91	-2.69	-5.08	-3.85	-3.99	-2.77	-2.76	-5.09	-5.18
Co	0-15	-1.80	-1.58	-1.58	-1.44	-1.62	-2.24	-2.19	-2.01	-2.14	-2.09
	15-30	-2.83	-1.62	-1.80	-2.29	-4.10	-2.91	-2.87	-3.29	-2.87	-2.33
	30-60	-3.78	-2.91	-3.91	-2.90	-3.92	-3.91	-3.88	-3.91	-3.80	-3.93
Fe	0-15	-8.10	-8.10	-8.25	-8.30	-8.18	-8.55	-9.16	-9.09	-8.70	-8.87
	15-30	-9.49	-9.44	-9.29	-9.35	-9.25	-9.62	-10.03	-9.60	-9.67	-9.63
	30-60	-9.81	-9.68	-9.75	-9.82	-9.76	-10.02	-10.22	-10.25	-10.13	-9.95
Mn	0-15	-2.80	-2.20	-2.95	-3.08	-2.71	-2.98	-3.07	-4.11	-4.18	-3.80
	15-30	-4.15	-4.11	-4.06	-4.19	-3.91	-3.87	-4.50	-4.19	-4.35	-4.33
	30-60	-4.51	-4.38	-4.39	-4.56	-4.38	-4.76	-4.89	-4.91	-4.73	-4.54
Zn	0-15	-0.49	-2.16	-0.51	-1.51	-1.23	-0.62	-0.67	-1.60	-1.79	-1.76
	15-30	-1.13	-0.82	-0.84	-1.73	-1.79	-1.33	-1.22	-1.34	-2.40	-1.84
	30-60	-1.45	-1.25	-1.27	-2.15	-1.98	-1.55	-1.52	-1.51	-2.75	-7.17

  - Volume 7, (Number 1), (ISSN 1995-6681)

Table 8: PCA Factor loadings after varimax rotation with Kaiser Normalization for heavy metals in soil profile within asphalt plants

	0-15 cm		15-30 cm			30-60 cm		
Parameter	**Factor 1**	**Factor 2**	**Factor 1**	**Factor 2**	**Factor 3**	**Factor 1**	**Factor 2**	**Factor 3**
Fe	.871	.105	-.6.17E-02	.996	-2.91E-02	-.829	.002	.371
Mn	-.548	.784	.963	.227	8.79E-02	-.605	-.637	.458
Zn	-1.28E-03	.952	.979	.174	4.78E-02	.586	-.737	.337
Cu	.933	.177	.961	-.211	-4.38E-02	.790	-.556	-.018
Pb	.879	-.408	.914	-.302	-.190	-.083	.513	.843
Cd	.882	-.420	.610	.769	-.186	.639	.301	.529
Cr	-.984	1.318E-02	-.443	-.142	.885	.080	.681	.724
Co	-.577	-.734	-.715	-.575	.363	.036	.793	.518
Ni	-.943	-.314	.479	-.797	-.288	.999	.029	.013
pH	-.666	.683	-.117	-.8.23E-02	-.988	.152	-.214	-.933
Conductivity	.319	.938	.668	-.324	.669	-.218	.792	.562
TOC%	.920	6.97E-02	5.50E-02	.868	-.128	-.151	-.332	-.691
Var. (%)	**59.07**	**32.26**	**46.13**	**30.98**	**19.53**	**76.38**	**13.95**	**8.55**

At 500 m distance from the asphalt plants, only three components were extracted from the data set for the 0-15 cm depth (Table 9). Factor 1 expresses about 58.12% of the total variance which was dominated by Cd, Cr, Cu, Ni and Zn which had no association with the soil physicochemical characteristics. The PCA results indicate that these metals are of anthropogenic origin. Factor 2 expresses about 23.94% of total variance including Co, conductivity and TOC and factor 3 expresses 15.73% of the total variance with a significant loading in Fe and pH. Factors 2 and 3 explain the fact that the presence of Fe and Co in soils was purely of pedogenic and lithogenic origin. However, the retention mechanisms of these metals in these soils are entirely different. The association of Fe and pH suggested that Fe was retained in the exchange sites while organic complexation is the prevailing retention mechanism for Co in this depth. At the 15-30 cm depth, four principal components were extracted. Factor 1was dominated by Mn, Pb, Cr, Co, Ni which accounts for 44% of the total variance. Factor 2 was comprised of Zn, Cu, Pb, Cd, Co and conductivity, and accounted for 29.9 % of the total variance. Factor 3 consisted of Fe and conductivity and factor 4 was dominated by Ni, TOC and conductivity accounting for 9.33% of the total variance. At 30-60 cm depth three principal components were extracted accounting for 49.33%, 27.98% and 15.71% of the total variance. Factor 1 included Cu, Zn and organic matter. Complexation to organic matter explained the retention of Zn and Cu in the soil. Factor 2 comprised of Fe, Pb, Mn and somewhat low loading for Cd which indicated that Pb was associated Fe-Mn oxides and factor 3 was dominated by Co, Pb, Ni and pH, which indicated that these metals occurred at the exchangeable sites. Bipolarity of factor 1 showed high negative loading for Cr and Ni while the bipolarity of factor 3 showed a high negative loading for Cd.

Table 9: PCA Factor loadings after varimax rotation with Kaiser Normalization for heavy metals in soil profile at 500 m from asphalt plant

	0-15 cm			15-30 cm				30-60 cm		
Parameter	**Factor 1**	**Factor 2**	**Factor 3**	**Factor 1**	**Factor 2**	**Factor 3**	**Factor 4**	**Factor 1**	**Factor 2**	**Factor 3**
Fe	-.749	-.238	.617	.346	1.20E-02	.934	9.055E-02	.313	.817	.478
Mn	-.951	-9.53E-02	.283	.864	-3.61E-02	.495	8.292E-02	.193	.911	-2.23E-02
Zn	.984	-.112	5.941E-02	.184	.774	-.494	-.350	.934	.343	7.710E-02
Cu	.814	-.333	-.455	-8.22E-02	.961	.129	-.230	.955	.218	-.147
Pb	.872	-.201	.373	.830	.541	.126	-4.72E-02	-.355	.621	.664
Cd	.977	-.163	4.476E-02	.140	.920	.367	-4.15E-03	.414	.469	-.673
Cr	.754	-.648	.105	.980	-9.67E-02	.142	.139	-.994	-6.99E-02	-2.84E-02
Co	3.256E-02	.989	-.101	.763	.553	-.335	1.38E-02	-.218	-.113	.785
Ni	.778	-.322	-.516	.688	-.312	.379	.534	-.775	.125	.620
pH	9.199E-02	.255	.941	-6.70E-02	-.232	-.967	8.262E-02	.335	.134	.887
Conductivity	-.485	.832	.256	.450	.604	9.403E-02	.658	-.244	-.913	.299
TOC%	6.220E-02	.533	-.838	3.22E-02	-.314	-.3.46E-02	.948	.923	.271	-.175
Var. (%)	**58.12**	**23.94**	**15.73**	**44.00**	**29.94**	**17.64**	**9.33**	**49.33**	**27.98**	**15.71**

3.4. Ecological Risk Assessment

The ecological risk (RI) is a measure of the sensitivity of various biological communities to toxic substances and illustrates the potential ecological risk caused by metals (Benhaddya and Hadjel, 2014). The ecological risks of metals in the studied soil profiles are displayed on Table 10. The ecological risk index (RI) of metals in these soil profiles ranged from 13.0 to 58.0 with significant contributions from Cd, Ni and Cr. The highest ecological risk index value was obtained in the premises of site II. The ecological risk index of metals in these soil profiles were less than 150 which suggests low ecological risks.

Table 10: Ecological risk assessment of metals in soil in the vicinity of asphalt plants.

Sites	Depth (cm)	Cd	Pb	Ni	Cr	Cu	Co	Zn	RI
Within Plant									
I	0-15	30.0	0.88	8.46	3.47	3.20	0.91	1.07	48.0
	15-30	20.0	0.25	6.46	0.28	1.38	0.44	0.69	29.5
	30-60	10.0	0.23	4.63	0.20	1.08	0.23	0.55	16.9
II	0-15	40.0	1.03	8.76	3.33	3.46	1.06	0.34	58.0
	15-30	30.0	0.50	7.88	4.21	1.19	1.03	0.85	45.7
	30-60	10.0	0.28	6.71	0.27	1.00	0.42	0.63	19.3
III	0-15	30.0	0.75	9.42	3.67	2.90	1.06	1.05	48.9
	15-30	10.0	0.53	7.78	3.27	2.33	0.91	0.84	25.6
	30-60	10.0	0.25	4.35	0.20	1.16	0.21	0.62	16.8
IV	0-15	30.0	0.78	10.52	3.91	1.12	1.17	0.53	48.0
	15-30	10.0	0.38	8.82	3.32	0.69	0.65	0.45	24.3
	30-60	10.0	0.25	7.18	2.69	0.22	0.42	0.34	21.1
V	0-15	30.0	0.75	10.15	3.69	1.37	1.03	0.64	47.6
	15-30	20.0	0.40	8.32	3.33	0.89	0.19	0.43	33.6
	30-60	10.0	0.25	6.90	2.80	0.52	0.21	0.38	21.1
500 m away									
I	0-15	20.0	0.50	4.78	2.15	2.12	0.67	0.98	31.2
	15-30	10.0	0.30	3.10	1.36	0.81	0.42	0.60	16.6
	30-60	10.0	0.25	2.79	1.12	0.48	0.21	0.51	15.4
II	0-15	20.0	0.70	9.63	1.96	3.12	0.69	0.95	37.1
	15-30	10.0	0.25	9.29	1.34	1.38	0.43	0.64	23.3
	30-60	10.0	0.23	7.58	1.10	1.10	0.21	0.52	20.7
III	0-15	10.0	0.43	7.07	2.38	1.00	0.78	0.49	22.1
	15-30	10.0	0.25	5.30	1.24	1.23	0.33	0.59	18.9
	30-60	10.0	0.23	7.73	1.11	1.11	0.21	0.53	20.9
IV	0-15	20.0	0.38	5.65	2.00	0.67	0.72	0.43	29.8
	15-30	10.0	0.25	2.74	1.25	0.46	0.43	0.28	15.4
	30-60	10.0	0.18	1.55	0.82	0.22	0.23	0.22	13.2
V	0-15	10.0	0.35	5.13	2.27	1.33	0.74	0.44	20.3
	15-30	10.0	0.40	5.49	1.95	0.63	0.63	0.42	19.5
	30-60	10.0	0.15	1.48	0.93	0.21	0.21	0.01	13.0

3.5. Non-carcinogenic hazard and carcinogenic risks

The non-carcinogenic and carcinogenic risks, evaluated based on the total metal concentrations for the children and adult scenarios, are displayed in Tables 11 and 12, respectively. The non-carcinogenic hazards of the different exposure pathways indicated that HQing>>HQderm>>HQinh for the children-which is possible due to hand-to-mouth habits of children, whereas, in the case of adult, HQinh>>HQing>>HQderm. Cumulatively, the HI for the children scenario ranged from 0.17 to 1.37 and 0.28 to 0.86 within the asphalt plant and 500 m distance from the asphalt plants, respectively. The HI of

metal for adult's case ranged from 0.27 to 1.26 for all sites and depths. Although, the HI values were slightly greater than 1 in 53% of the samples for the children scenario and 33% of the samples for the adult scenario within the asphalt plants. The cumulative HI for exposure via the three major exposure pathways at 500 m distance from the asphalt plant were less than 1 for the adult and children scenarios. Overall, the non-carcinogenic risks of metals in soil were higher at the premises of the asphalt plants than at 500 m distance from the plants.

Table 11: Non-carcinogenic hazard exposure to metals in soil in the vicinity of asphalt plant.

		CHILD				ADULT			
Within Plant	**Depth(cm)**	HQ_{ing}	HQ_{inh}	HQ_{derm}	HI	HQ_{ing}	HQ_{inh}	HQ_{derm}	HI
I	0-15	1.03	0.0017	0.13	1.17	0.17	0.83	0.025	1.03
	15-30	0.28	0.0007	0.01	0.29	0.05	0.34	0.003	0.39
	30-60	0.17	0.0005	0.01	0.18	0.03	0.24	0.002	0.27
II	0-15	1.08	0.0021	0.13	1.21	0.18	1.05	0.024	1.26
	15-30	1.18	0.0013	0.16	1.34	0.20	0.65	0.030	0.87
	30-60	0.27	0.0006	0.01	0.28	0.04	0.32	0.003	0.36
III	0-15	1.13	0.0017	0.14	1.27	0.19	0.84	0.027	1.06
	15-30	0.97	0.0012	0.13	1.10	0.16	0.58	0.024	0.77
	30-60	0.16	0.0005	0.01	0.17	0.03	0.24	0.002	0.27
IV	0-15	1.21	0.0017	0.15	1.36	0.20	0.86	0.028	1.09
	15-30	0.89	0.0011	0.13	1.02	0.15	0.55	0.024	0.72
	30-60	0.68	0.0009	0.10	0.78	0.12	0.42	0.019	0.55
V	0-15	1.12	0.0019	0.14	1.27	0.19	0.91	0.027	1.13
	15-30	0.72	0.0010	0.13	0.85	0.12	0.50	0.024	0.64
	30-60	0.62	0.0008	0.11	0.73	0.11	0.40	0.020	0.53
500 m away									
I	0-15	0.68	0.0013	0.08	0.77	0.12	0.63	0.016	0.76
	15-30	0.43	0.0007	0.05	0.48	0.07	0.36	0.010	0.44
	30-60	0.30	0.0005	0.04	0.34	0.05	0.23	0.008	0.29
II	0-15	0.70	0.0014	0.08	0.78	0.12	0.67	0.015	0.81
	15-30	0.47	0.0008	0.05	0.53	0.08	0.40	0.010	0.49
	30-60	0.34	0.0006	0.05	0.38	0.06	0.30	0.008	0.36
III	0-15	0.76	0.0010	0.09	0.86	0.13	0.51	0.017	0.65
	15-30	0.39	0.0007	0.05	0.44	0.07	0.34	0.009	0.42
	30-60	0.34	0.0006	0.05	0.39	0.06	0.30	0.009	0.36
IV	0-15	0.66	0.0009	0.08	0.74	0.11	0.45	0.015	0.58
	15-30	0.40	0.0006	0.05	0.45	0.07	0.30	0.009	0.38
	30-60	0.25	0.0004	0.03	0.28	0.04	0.20	0.006	0.25
V	0-15	0.71	0.0010	0.09	0.80	0.12	0.50	0.016	0.64
	15-30	0.62	0.0008	0.08	0.70	0.10	0.41	0.014	0.53
	30-60	0.26	0.0004	0.04	0.29	0.04	0.22	0.007	0.27

Table 12: Carcinogenic risk associated with metal exposure in soils in the vicinity of the asphalt plants

		CHILD				ADULT			
	Depth(cm)	$RISK_{ing}$	$RISK_{inh}$	$RISK_{derm}$	TOTAL CANCER RISK	$RISK_{ing}$	$RISK_{inh}$	$RISK_{derm}$	TOTAL CANCER RISK
I	0-15	8.25E-03	1.57E-04	1.92E-04	8.60E-03	1.40E-03	7.70E-02	3.60E-05	7.84E-02
	15-30	1.62E-03	8.87E-05	1.50E-05	1.73E-03	2.75E-04	4.35E-02	2.90E-06	4.38E-02
	30-60	1.41E-03	6.64E-05	1.10E-05	1.49E-03	2.39E-04	3.28E-02	2.10E-06	3.30E-02
II	0-15	8.91E-03	1.71E-04	1.84E-04	9.27E-03	1.51E-03	8.37E-02	3.45E-05	8.53E-02
	15-30	7.00E-03	1.25E-04	2.33E-04	7.36E-03	1.19E-03	6.13E-02	4.37E-05	6.25E-02
	30-60	1.75E-03	9.32E-05	1.50E-05	1.86E-03	2.96E-04	4.57E-02	2.80E-06	4.60E-02
III	0-15	7.79E-03	1.59E-04	2.03E-04	8.15E-03	1.32E-03	7.79E-02	3.81E-05	7.93E-02
	15-30	6.17E-03	1.25E-04	1.81E-04	6.48E-03	1.04E-03	6.12E-02	3.39E-05	6.23E-02
	30-60	1.55E-03	6.54E-05	1.10E-05	1.63E-03	2.62E-04	3.21E-02	2.10E-06	3.23E-02
IV	0-15	8.17E-03	1.73E-04	2.16E-04	8.56E-03	1.38E-03	8.48E-02	4.06E-05	8.62E-02
	15-30	5.41E-03	1.26E-04	1.84E-04	5.72E-03	9.17E-04	6.17E-02	3.44E-05	6.26E-02
	30-60	4.10E-03	9.85E-05	1.49E-04	4.35E-03	6.95E-04	4.83E-02	2.79E-05	4.90E-02
V	0-15	7.81E-03	1.67E-04	2.04E-04	8.18E-03	1.32E-03	8.19E-02	3.83E-05	8.33E-02
	15-30	5.56E-03	1.22E-04	1.84E-04	5.87E-03	9.42E-04	5.98E-02	3.46E-05	6.08E-02
	30-60	4.22E-03	9.55E-05	1.55E-04	4.47E-03	7.14E-04	4.68E-02	2.91E-05	4.76E-02
500 m away									
I	0-15	4.89E-03	8.92E-05	1.19E-04	5.10E-03	8.28E-04	4.38E-02	2.23E-05	4.46E-02
	15-30	3.00E-03	5.61E-05	7.52E-05	3.13E-03	5.08E-04	2.75E-02	1.41E-05	2.80E-02
	30-60	2.49E-03	4.91E-05	6.18E-05	2.60E-03	4.21E-04	2.41E-02	1.16E-05	2.45E-02
II	0-15	5.77E-03	1.56E-04	1.09E-04	6.04E-03	9.77E-04	7.67E-02	2.04E-05	7.77E-02
	15-30	2.71E-03	1.21E-04	7.40E-05	2.91E-03	4.59E-04	5.92E-02	1.39E-05	5.97E-02
	30-60	2.34E-03	9.99E-05	6.09E-05	2.50E-03	3.95E-04	4.90E-02	1.14E-05	4.94E-02
III	0-15	4.72E-03	1.09E-04	1.32E-04	4.96E-03	7.99E-04	5.36E-02	2.47E-05	5.44E-02
	15-30	2.61E-03	7.67E-05	6.86E-05	2.76E-03	4.42E-04	3.76E-02	1.29E-05	3.81E-02
	30-60	2.35E-03	1.02E-04	6.17E-05	2.51E-03	3.98E-04	4.98E-02	1.16E-05	5.02E-02
IV	0-15	4.06E-03	9.00E-05	1.11E-04	4.26E-03	6.87E-04	4.41E-02	2.07E-05	4.48E-02
	15-30	2.62E-03	4.86E-05	6.93E-05	2.74E-03	4.44E-04	2.38E-02	1.30E-05	2.43E-02
	30-60	1.78E-03	3.00E-05	4.57E-05	1.86E-03	3.01E-04	1.47E-02	8.60E-06	1.50E-02
V	0-15	4.21E-03	8.27E-05	1.26E-04	4.41E-03	7.12E-04	4.06E-02	2.36E-05	4.13E-02
	15-30	4.14E-03	8.99E-05	1.08E-04	4.34E-03	7.01E-04	4.41E-02	2.02E-05	4.48E-02
	30-60	1.76E-03	2.75E-05	5.13E-05	1.83E-03	2.97E-04	1.35E-02	9.60E-06	1.38E-02

For the carcinogenic risk assessment, only Cd, Pb, Ni and Cr were used. As shown in Table 10, the total cancer risk for the children scenario ranged from 1.63×10^{-3} to 9.27×10^{-3} with significant impact from the ingestion pathway. In the case of adults, the total cancer risk from exposure to metals in these soil profiles ranged from 1.38×10^{-2} to 8.6×10^{-2} with the highest impact from the inhalation pathway. The cancer risks for different exposure routes follow the order $Risk_{ingestion} >> Risk_{dermal} >> Risk_{inhalation}$ for the children scenario and $Risk_{inhalation} >> Risk_{ingestion} >> Risk_{dermal}$ in the case of adults. The carcinogenic risks of metals due to exposure to these soils through ingestion, inhalation and dermal contact exceeded the target value of 10^{-6} which indicates serious cancer risks for persons working within the asphalt plant and those whose farms are located within 1 km distance from the plants.

4. Conclusions

The concentrations of Cr and Ni in the soil profiles exceeded the maximum allowed levels in soils as specified by the Department of Petroleum Resources of Nigeria. The multiple pollution indexes indicate that the examined sites fall with the "slight pollution" to "severe pollution" ranges with significant contributions from Cr and Ni. The present study indicates that asphalt plants are a possible source of elevated concentrations of metal species (particularly Cd, Ni and Cr) in these soil profiles. The total ecological risk (RI) values of metals in these soil profiles were <150, which suggested low ecological risks for these soils. However, the total cancer risk of metals in these soil profiles exceeded the target value of ($1/10^6$) one in a million population of the risk of developing cancer. If this trend is allowed to continue unabated, it is most likely that the local food web complexes in the vicinity of these plants might be at the highest risk of the induced metals contamination.

References

[1] Abollino, O., Aceto, M., Malandrino, M., Menstasti, E., and Sarzanini, C., Petralla F. 2002. Heavy metals in agricultural soils from Piedmont, Italy: Distribution, speciation and chemometric data treatment, Chemosphere, 49: 545-557.

[2] Aina G.R.E., and Sridhar M.K.C. 2004. Soil quality near a chemical industry at Port-Harcourt, Nigeria, AJEAM-REGEE, 8:19-26.

[3] Alloway, B.J., 2005. Bioavailability of Trace metals in soil. In Selinus O., Alloway, B.J., Centero, J.A., Finkelman, R.B., Fuger, Lindh U., Smedly, P. (eds). Essential of Medical Geology. The Impact of the natural environmental on Public Health Elsevier. London, pp. 347 - 372.

[4] Benhaddya M.L., and Hadjel M. 2014. Spatial distribution and contamination assessment of heavy metals in surface soils of Hassi Messaoud, Algeria, Environmental Earth Sciences, 71:1473-1486.

[5] Bhattacharya, P., Mukherjeb, A.B., Jack, G., and Nordguist, S., 2002. Metal contamination at a wood preservation site: Characterization and experimental studies on remediation, Science of Total Environment, 290:165-180.

[6] Department of Petroleum Resources (DPR). 2002. Environmental guidelines and standard for the petroleum industry in Nigeria (revised edition. Department of Petroleum Resources, Ministry of Petroleum and Mineral Resources, Abuja Nigeria.

[7] Dudka, S., Piotrowska, M., and Terelk, H., 1996. Transfer of Cadmium, lead and zinc from industrially contaminated soils to crop plants, Environmental Pollution, 1996, 94: 151 – 158.

[8] Guney, M., Zagury, G.J., Dogan, N. and Onay, T.T., 2010. Exposure assessment and risk characterization from trace elements following soil ingestion by children exposed to playgrounds, parks and picnic areas, Journal of Hazard Materials, 182:656–664.

[9] Hakanson, L. 1980. An ecological risk index for aquatic pollution control. A sedimentological approach, Water Research, 14: 975–1001.

[10] Inuwa, M., Abulrahman, F.W., Birnin Yauri, U.A., and Ibrahim, S.A., 2007. Analytical Assessment of some trace metals in soil around the major industrial areas of north-western Nigeria, Trends in Applied Science Research, 2(6): 515 – 521.

[11] Itana, F. 1998. Comparative study on soil pollution with toxic substances on farmland close to old and new industrial sites in Ethiopia, Bulletin of Chemical Society of Ethiopia, 2(2): 105 – 112. 67.

[12] Iwegbue, C.M.A. 2013. Chemical fractionation and mobility of heavy metals in soils in the vicinity of asphalt plants in Delta State, Nigeria. Environmental Forensics 14:248-259

[13] Iwegbue, C.M.A., Egobueze, F.E., and Opuene, K., 2006 Preliminary assessment of heavy metals levels of soil of an oil field in the Niger Delta, Nigeria, International Journal Environmental Science Technology, 3(2): 167 – 172.

[14] Iwegbue, C.M.A., Williams, E.S., and Isirimah, N.O. 2009. Study of heavy metal distribution in soil impacted with crude oil in southern Nigeria, Soil and Sediment Contamination, 18(2): 136 – 143.

[15] Iwegbue, C.M.A., Nwajei, G.E., Ogala, J.E., and Overah, C.L., 2010. Determination of trace metal concentrations in soil profiles of municipal waste dumps in Nigeria. Environmental Geochemistry and Health, 32:415-430. doi:10.1007/s10653-010-9285-y.

[16] Kabala, C., and Singh, B.R. 2001. Fractionation and mobility of copper, lead and zinc in soil profiles in the vicinity of a copper smelter, Journal of Environmental Quality 30:485 – 492.

[17] Krishna, A.K., and Govil P.K. 2008. Assessment of heavy metals contamination in soils around Manalic industrial area, Chennai, Southern India, Environmental Geology 54:1465-1472.

[18] Lacatusu, R. (2000). Appraising levels of soil contamination and pollution with heavy metals: In Heinike, H.J., Eckrelman, W., Thomasson, A.J., Jones, R.J.A., Montanarella, L. and Buckley, B. (eds). Land information system for planning the sustainable use of land resources. European Soil Bureau. Research Report No 4, Office for Official Publication of the European Communities, Luxembourg, pp. 393 – 402.

[19] Lai, H.Y., Hseu, Z.Y., Chen, T.C., Chen, B.C., Guo, H.Y., and Chen, Z.S., 2010. Health risk-based assessment and management of heavy metals-contaminated soil sites in Taiwan, International Journal of Environmental Research and Public Health, 7: 3595–3614.

[20] Lee, C.S., Li, X.D., Shi, W.Z., Cheung, S.C., and Thornton, I. 2006. Metal contamination in urban, suburban and country park soils of Hong Kong: a study based on GIS and multivariate statistics, Science of the Total Environment, 356:45-61.

[21] Liao X.Y, Chen T.B., Wu, B., Yan X.L., Nie C.J., Xie H et. al., 2006. Mining urban soil pollution: concentrations and patterns of heavy metals in the soils of Jinchang, China. Geographical Research 25:843-852.

[22] Lieben, J., Mohrherr, C.J, and Ranga, R.O.K., 2012. Trace metals assessment in soils in a small city and its rural surroundings, Pensacola, FL, USA, Environmental Earth Sciences, 65:1781-1793.

[23] Loska, K. and Wiechula, D. 2003. Application of principle components analysis for the estimation of source of heavy metal contamination in surface sediments from the Rybnik Reservoir, Chemosphere, 51:723-733.

[24] Lu S.G. and Bai S.Q. 2006. Study on the correlation of magnetic properties and heavy metals concentration in urban soils of Hangzhou city, China, Journal of Applied Geophysics, 60:1-12.

[25] Luo, X.S., Ding, J., Xu, B., Wang, Y.J., Li, H.B. and Yu, S., 2012a. Incorporating bioaccessibility into human health risk assessments of heavy metals in urban park soils, Science of the Total Environment, 424: 88–96.

[26] Luo, X.S., Yu, S., Zhu Y.G., Li X.D., 2012b. Trace metal contamination in urban soils of China, Science of the Total Environment, 421-422:17-30.

[27] Maina, H.M., Barminas, J.T., Nkafamiya, I.I., 2009. Levels and distribution of some heavy metals in soils in the vicinity of Ashaka cement factory, Gombe State, Journal of Chemical Society of Nigeria, 34(1): 15- 25.

[28] Man, Y.B., Kang, Y., Wang, H.S., Lau, W., Li, H., Sun, X. l., Geisy, J.P., Chow, K.L and Wong, M. H., 2013. Cancer risk assessments of Hong Kong soils contaminated by polycyclic aromatic hydrocarbons, Journal Hazardous Materials, http://dx.doi.org/10.1016/j.jhaznat.2012.11.067.

[29] Miguel, E.D., Llmas, J.F., Chaco, E., Berg, T., Larssen S., and Royset, O., 1997. Origin and patterns of distribution of trace elements in street dust: Unleaded petrol and urban lead, Atmospheric Environment, 31(17): 2733-2740.

[30] MOEE (Ministry of Environment and Energy).2008. Ontario's Ambient Air Quality Criteria. Standard Development Branch, Ontario Ministry of Environment and Energy. http://www.ene.gov.on.ca/publications/6570e-chem.pdf accessed on 10 November 2014.

[31] Muller, G. 1969. Index of geoaccumulation in sediment of the Rhine River, Geological Journal, 2:108-118.

[32] Onianwa, P.C and Fakayode, S.O. 2000. Lead contamination of the topsoil and vegetation in the vicinity of a battery factory in Ibadan, Environmental Geochemistry and Health, 22:211-218.

[33] Radojevic, M. and Bashkin, V.M. 1999. Practical Environmental Analysis. Royal Society of Chemistry, Cambridge, United Kingdom.

[34] Reimann, C and De Caritat, P. 2000. Intrinsic flaws of element enrichment factor (EF's) in environmental geochemistry, Environmental Science and Technology, 34:5084-5091.

[35] Rogan, N., Dolenec, T., Serfimovski, T., Tasev, G. and Dolenec, M., 2010. Distribution and mobility of heavy metals in puddy soils of the Kocani field in Macedonia, Environmental Earth Science, 61:899 – 907 doi: 10.1007.s12665-009-0405-x.

[36] Romic, M., Romic, D., Dolanjski D and Stricevic I., 2004. Heavy metal accumulation in topsoils from wine growing regions, Agriculturae Conspectus Scientificus, 69 (1): 1-10.

[37] Shi, P., Xiao, J., Wang, Y., and Chen, L. 2014. Assessment of ecological and human health risks of heavy metal contamination in Agriculture soils disturbed by pipeline construction, International Journal of Environmental Research and Public Health, 11: 2504-2520.

[38] Sutherland, R.A. 2000. Bed sediment associated trace element in urban stream Oahu, Hawaii, Environmental Geology, 39:361-627.

[39] Turekian, K.K., and Wedepohl, K.H. 1961. Distribution of the elements in some major units of earth crust. Bulletin Geological Society of America, 72:175-192.

[40] US DOE (United States Department of Energy) 2011. The Risk Assessment Information System (RAIS); U.S. Department of Energy's Oak Ridge Operations Office (ORO): Oak Ridge, TN, USA.

[41] Umoren, I.U., and Onianwa, P.C. 2005. Concentrations and distribution of some heavy metals in urban soils of Ibadan, Nigeria, Pakistan Journal of Science and Industrial Research, 48(6): 397 – 403.

[42] US EPA (United States Environmental Protection Agency) 2001. Risk assessment guidance for superfund. Volume 1: Human evaluation Manual (Part E, Supplemental guidance for defined risk assessment). EPA/540/R/99/005.7. Washington, DC, USA: Office of Emergency and Remedial response, United states Environmental Protection Agency.

[43] US EPA (United States Environmental Protection Agency). 2011. Regional Screening Level Table (RSL) for Chemical Contaminants at Superfund Sites. U.S. Environmental Protection Agency: Washington, DC, USA.

[44] US EPA (United States Environmental Protection Agency). 1989. Risk Assessment guidance for superfund, Vol. 1: Human health Evaluation Manual EPA/se0/1-89/002, office of solid waste and emergency Response, Washington, DC.

[45] US EPA (United States Environmental Protection Agency) 1997. Exposure Factors Handbook. EPA/600/P-95/002F. Environmental Protection Agency, Office of Research and Development, Washington, DC.

[46] Zhang, M.K., and Ke Z.X. 2004. Heavy metals, phosphorus and some other elements in urban soil of Hangzhou city, Pedosphere, 14:177-185.

JJEES
Jordan Journal of Earth and Environmental Sciences

Volume 7, (Number 1), June, 2015
ISSN 1995-6681
Pages 65 - 70

Evaluation of Heavy Metal Contents in Road Dust of Jalingo, Taraba State, Nigeria

Maxwell O. Kanu[1*], O. C. Meludu[2], and S. A. Oniku[2]

[1]Department of Physics, Taraba State University, P.M.B.1167, Jalingo, Nigeria
[2]Department of Physics, ModibboAdama University of Technology, Yola, Nigeria

Received 25 August, 2014; Accepted 19 May 2015

Abstract

The investigation of the anthropogenic contamination by heavy metals on road surface is very necessary for environmental planning and monitoring in urban towns. In the presentstudy, the concentration of five heavy metals (Fe, Pb, Cd, Cu and Zn) in dust samples, from two major township roads -Hammaruwa Way (HW) and Palace Way (PW) in Jalingo metropolis, were analyzed using Atomic Absorption Spectrophotometer. The pollution status was assessed using Sediment Quality Guidelines (SQG), Geo-accumulation index (Igeo), Degree of Contamination (CD), Pollution Load Index (PLI) and Enrichment Factor (EF). Results of SQG, Igeo, CD and PLI show that these urban roads are not polluted. Analysis of the Enrichment Factor shows that apart from Pb, all other metals analyzed are enriched and the enrichment comes from anthropogenic activities. This implies that the soils are contaminated to some degree but not polluted. It is evident that the concentration of these heavy metals may increase and pose health hazards at the long run if proactive steps are not taken to check vehicular pollution.

Keywords: heavy metals, pollution, road dusts, anthropogenic, contamination

1. Introduction

Heavy metals occur either naturally in the soil through a pedogenic process of weathering of parent materials or by anthropogenic activities. However, naturally occurring heavy metals are rarely toxic and pose little or no threat to the soil ecosystem. Increased concentrations of heavy metals are caused by anthropogenic activities and may lead to high risks to human health, plants and animals, among others. Anthropogenic heavy metals pollution may occur through different diffuse and point sources (El-Hassan *et. al.*, 2006). Traffic activities are examples of diffuse sources, while industrial emissions (e.g., from power plants, coal combustion, chemical plants, etc.) are examples of point sources. Traffic activities on roads can lead to elevated levels of heavy metals in the environment through vehicular exhaust and non-exhaust emissions. Exhaust emissions are produced during incomplete combustion of vehicle fuel which is a mixture of hydrocarbons and compounds that improve combustion properties. Several types of pollutants such as Carbon monoxide, Nitrogen dioxide, polycyclic aromatic hydrocarbons (PAHs) and particulate matter are generated during this process. Non-exhaust emissions are generated through mechanical (e.g., braking, clutch usage, tire wear and road abrasion) and chemical processes (e.g., corrosion of vehicle elements). It was reported that topsoil and road side soils near heavy traffic in urban areas are indicators of heavy metal contamination from atmospheric deposition (Arowolo *et. al.*, 2000). Metals such as Cd, Cu, Pb and Zn are good indicators of contamination in soils because they appear in gasoline, car component, oil lubricants and industrial incinerators emissions (Popoola*et. al.*, 2012). The degree of emissions of pollutants originating from road traffic are affected by vehicle age, fuel type and quality, wide variety of vehicle (e.g., passenger cars, trucks, etc.) and engine types (e.g., diesel or gasoline powered engine), type of tire, road conditions and traffic conditions (e.g., heavy or light traffic), etc.

Regular monitoring and assessment of heavy metals pollution in our environment are necessary in order to study the impact of developmental projects on the environment. To assess the severity of soil contamination and to distinguish between natural and anthropogenic inputs in the soil, several approaches have been applied,such as Enrichment Factor (EF), Geo-accumulation Index (Igeo), Pollution Load Index (PLI) and Sediment Quality Guidelines (SQG) (Barakat *et. al.*, 2012; Manoj and Padly, 2012; Salah *et. al.*, 2012).

Jalingo witnessed vehicular traffic congestion on the major roads in the past decade and vehicular pollution has not been checked by environmental regulatory authorities, leading to elevated levels of pollution. The situation is worrisome and might be attributed to the poor economic disposition of Nigerians, large importation of old and fairly-used cars, the poor vehicle maintenance culture causes an increase in the emissions of dangerous substances through the exhaust

* Corresponding author. e-mail: maxiexpress007@gmail.com

pipes of vehicles; and a large number of irreparable and decomposing car parts litter the road surfaces and roadsides. These expose the residents to serious health risks. In Nigeria, the State Environmental Protection Agency (SEPA) and the Federal Environmental Protection Agency (FEPA) are saddled with the responsibility of enforcing environmental laws, regulations and standards in order prevent people, industries and organizations from polluting the environment. Unfortunately, these bodies have not lived up to expectation as their impact is not felt. Presently, there is neither a legislative frame work nor a set standard in the state to monitor emissions from mobile sources. Therefore, there is a need to investigate the extent of pollution from vehicular sources in this town. Furthermore, despite the vast majority of studies on metal contents of street dust done in developed countries with long histories of industrialization, relatively very few of such studies were done in developing countries like Nigeria. Little interest has been focused on metal contamination of street dust despite its direct contact with a great part of the population. The present study aims at using the various contaminant assessment indices to assess the pollution levels in road dusts. The expected results of the present study will assist the public and the concerned authorities in planning adequate pollution control measures.

2. Materials and Methods

2.1. Study Area

Jalingo is a rapidly growing city in the North-Eastern region of Nigeria. It is the administrative headquarters of Taraba State which is located between latitude 6°30′ and 8°30′ N and between Longitude 9°00′ and 12°00′ E (Figure 1). The state has a tropical wet and dry climate, the dry season lasts for a minimum of five months (November to March) while the wet season spans from April to October. It has an annual rainfall of about 8000 mm. According to the 2006 census figures released by the National Population Commission, Nigeria, Jalingo has a total population of 118,000 inhabitants. Jalingo is a city with no major industry. The major pollution source is the emission from traffic and power generating sets and human activities such as indiscriminate dumping of waste.

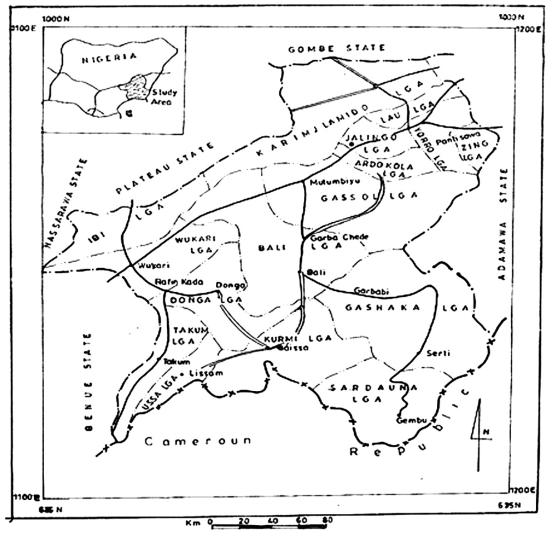

Figure 1. Map of study area

2.2. Sample Collection, Preparation and Analysis

Two major roads, namelyHammaruwa way (about 5 km) and Palace Way (about 3 km) were chosen for this study. The roads were chosen because of the considerable high traffic density of about 10,000 vehicles including tricycles per day. Figure 2 shows the traffic congestion in Hammaruwa way. Dust samples were collected along the roads on the tarred surface by sweeping with a broom and a plastic scoop and were transferred into a clean, self-sealing polythene bags to avoid contamination. The samples were collected during the dry season (February, 2013) when it was assumed that enough dust would have accumulated on the road surface. In the laboratory, the samples were air dried at room temperature for some days to reduce mass contribution of water and to avoid any chemical reactions. The samples were sieved using a 1 mm sieve mesh (Zhang *et. al.*, 2011) to remove particles such as glass, plant debris, refuse and small stones.

For the analysis of the total concentration of heavy metals (Fe, Pb, Cd, Cu and Zn), 0.5 g of samples were digested in 20 ml freshly prepared aqua regia (a mixture of concentrated Hydrochloric acid and Nitric acid in the ratio 3:1) in a microwave digestion oven, then evaporated and analyzed for metal concentration. The contents of Fe, Pb, Cd, Cu and Zn were analyzed using a Flame Atomic Absorption Spectrophotometer (Buck 210 Model) at the Adamawa State University, Mubi, Nigeria.

Table 1: Heavy Metal Concentration

Hammaruwa Way					
sample	**Fe (mg/kg)**	**Pb (mg/kg)**	**Cd (mg/kg)**	**Cu (mg/kg)**	**Zn (mg/kg)**
HW 3	22.56	0.003	0.002	0.58	2.26
HW 9	20.89	0.002	0.002	0.35	2.57
HW 15	21.69	0.001	0.001	0.62	2.55
HWL1 1m	23.40	0.017	0.003	6.02	3.36
HWL1 2m	22.79	0.003	0.003	0.46	2.78
Mean	22.27	0.005	0.002	1.61	2.70
S.D	0.98	0.007	0.0008	2.47	0.41
Palace Way					
sample	**Fe (mg/kg)**	**Pb (mg/kg)**	**Cd (mg/kg)**	**Cu (mg/kg)**	**Zn (mg/kg)**
PW 3	22.97	0.019	0.003	1.64	3.41
PW 8	20.77	0.002	0.002	0.36	2.50
PW 10	19.54	0.008	0.003	0.67	1.58
PW 12	21.49	0.002	0.001	0.37	2.54
PW 14	23.98	0.033	0.003	2.16	3.68
Mean	21.75	0.013	0.0024	1.04	2.74
S.D	1.76	0.01	0.0009	0.82	0.83

Figure 2. View of vehicular congestion releasing pollutants in Jalingo metropolis

3. Results and Discussion

The concentrations of heavy metals (Fe, Pb, Cd, Cu and Zn) in samples from the two Jalingo urban roads are presented in Table 1. Results showed comparable values of the concentrations of heavy metals in both road surfaces, suggesting similar sources of emissions. Mean concentrations of heavy metals in these roads in mg/kg are 22.27 ± 0.98 and 21.75 ± 1.76 Fe, 0.005 ± 0.007 and 0.013 ± 0.01 Pb, 0.002 ± 0.0008 and 0.0024 ± 0.0009 Cd, 1.61 ± 2.47 and 1.04 ± 0.82 Cu and 2.70 ± 0.41 and 2.74 ± 0.83 for HW and PW, respectively. This indicates that the concentration of heavy metals in these urban roads exist in the following order: Fe > Zn > Cu >Pb> Cd.

Fe, Cu and Zn are the most concentrated in the urban roads dusts. High concentration of Fe was found in car exhaust particulates and other car derivatives such as corrosion of body parts (Hopke *et. a*l., 1980; Lu *et. a*l., 2005) as well as soils (Robertson *et. a*l., 2003). The concentration of Fe in Jalingo urban road dust is comparable to roadside sediment from London (mean, 27.332 ± 5.930 mgg^{-1}) and Halton (mean Fe, 22.630 ±7.983 mgg^{-1}) in UK (Crosby, 2012). Studies conducted on roadside soils from selected locations in Lagos Metropolis, Nigeria, revealed higher concentrations of heavy metals (Olukanmi *et. a*l., 2012). This higher value is attributed to the higher traffic density in Lagos, being a mega city and a major industrial and commercial hub in Nigeria. Since there is no major industry in the study area, such as smelting operations, the primary sources of Zn might be derived from fragmented vehicle tires (Hopke *et. a*l., 1980), lubricating motor oil in which Zn compounds are used extensively as anti-oxidants and as detergent/dispersant improving agents (Lu *et. a*l., 2005). Cu is a common element in automobile thrust bearing, brake lining and other parts of the engine. Corrosion causes metal wear in the automobile engine and releases heavy metals to the environment and, eventually, accumulation in the topsoil (Lu *et. a*l., 2005). Cu replaced asbestos and has been used as a brake friction material since the 1930's (Hopke *et. a*l., 1980; Robertson *et. a*l., 2003). The concentration of Cu obtained in this study is consistent with values obtained for low traffic volume areas of road side soils of Ijebu-North Local Government Area, Ogun State, Nigeria (Adedeji *et. a*l., 2013). According to the latter study, Cu ranged between 0.92 and 2.01 mg/kg with a mean value of 1.41 mg/kg. The concentration of lead was found to be low. The low Pb level of the Jalingo road dust might be due to the drop in the use of Pb as additives in fuel.

The correlation between certain geochemical concentration parameters can establish influencing factors and indicate potential sources (Robertson *et. a*l., 2003; Crosby, 2012). The results of the correlation analysis between heavy metals performed using Microsoft Excel 2007 is shown in Tables 2 and 3 for the HW and PW, respectively. The strong positive correlation between almost all the metals indicates similar sources in most cases enhanced geochemical concentrations compared to background levels indicates anthropogenic influences (Crosby, 2012).

Table 2: Pearson correlation Coefficients between with heavy metals contents of Hammaruwa Way

	Fe	Pb	Cd	Cu	Zn
Fe	1				
Pb	0.703391	1			
Cd	0.678469	0.620239	1		
Cu	0.658394	0.990023	0.514673	1	
Zn	0.572983	0.881208	0.644508	0.883236	1

Table 3: Pearson correlation Coefficients between heavy metals contents of Palace Way

	Fe	Pb	Cd	Cu	Zn
Fe	1				
Pb	0.821533	1			
Cd	0.238381	0.68321	1		
Cu	0.851579	0.987095	0.692028	1	
Zn	0.983614	0.75762	0.216757	0.802339	1

3.1. Assessment of Heavy Metals Contamination Status in Jalingo Road Dusts

A. Assessment According to United States Environmental Protection Agency (USEPA) Standards

The level of heavy metal contamination is assessed by a comparison with the Sediment Quality Guidelines (SQG) proposed by USEPA since Nigerian Federal Environmental Protection Agency (FEPA) does not currently have SQG for land pollution. These criteria for the measured heavy metals are presented in Table 4. The result of the present study shows that the samples from the urban roads are not polluted.

Table 4: EPA Guidelines for Sediments

Metal (mg/kg)	Not Polluted	Moderately Polluted	Heavily Polluted	Present Study
Fe	<30	-	-	19.54 - 23.98
Pb	< 40	40 - 60	> 60	0.001- 0.033
Cd	-	< 6	> 6	0.001- 0.003
Cu	< 25	25 – 50	> 50	0.35- 2.16
Zn	< 90	90 - 200	> 200	1.58- 3.68

(Barakat et. al., 2012; Saha and Hossain, 2011)

B. Assessment According to Geo-accumulation Index (Igeo)

The Geo-accumulation index is usually employed in order to determine the metal contamination in sediments by comparing the current concentration with background levels (pre-industrial levels). The Igeo is determined following Muller (1979) as:

$$I_{geo} = log_2 \left(\frac{C_n}{1.5\ B_n} \right) \quad (1)$$

where Cn is the concentration of the examined metal n in the sample, Bn is the geochemical background concentration of the metal n and the factor 1.5 is background matrix correction factor due to lithogenic effects (Manoj and Padhy, 2012). In this study, the world average shale values for heavy metals

given by Turakin and Wodepohl (1961), where Fe = 47200 mg/kg, Pb= 20 mg/kg, Cd = 0.3 mg/kg, Cu = 45 mg/kg and Zn = 95 mg/kg, was used as Bn.

Based on the Igeo values, Muller (1981) distinguished seven classes of sediments as presented in Table 5. The results of the Igeo for the road dust samples from the two roads are presented in Table 6. All the samples show that Igeo< 0 for each heavy metal determined indicating that the samples are unpolluted.

Table 5: Index Classification of Sediment Quality

Igeo Values (Muller, 1981)	**Class**	**Sediment Quality**
≤ 0	0	Unpolluted
0 – 1	1	Unpolluted to moderately polluted
1 – 2	2	Moderately polluted
2 – 3	3	Moderately polluted to highly polluted
3 – 4	4	Highly polluted
4 – 5	5	Highly polluted to very highly polluted
>5	6	Very highly polluted
CF Values (Hakanson, 1980)	**Class**	**Sediment Quality**
CF <1	1	Low contamination
1≤ CF < 3	2	Moderate contamination
3 ≤ CF < 6	3	Considerable contamination
CF ≥ 6	4	Very high contamination
CD Values (Ahdy and Khaled, 2009)	**Class**	**Sediment Quality**
CD < 6	1	Low degree of contamination
6 ≤ CD <12	2	Moderate degree of contamination
12 ≤ CD < 24	3	Considerable degree of contamination
CD ≤ 24	4	Very high degree of contamination

Table 6: Geo-accumulation Index (Igeo) for HW and PW

Sample	**Fe**	**Pb**	**Cd**	**Cu**	**Zn**
Hammaruwa Way					
HW 3	-11.62	-12.70	-7.81	-6.86	-5.98
HW 9	-11.73	-13.87	-7.81	-7.59	-5.79
HW 15	-11.67	-14.87	-8.81	-6.77	-5.80
HWL1 1m	-11.56	-10.79	-7.23	-3.49	-5.41
HWL1 2m	-11.60	-12.70	-7.23	-7.20	-5.68
Mean	-11.64	-12.99	-7.78	-6.38	-5.73
S.D	0.07	1.53	0.65	1.65	0.21
Palace Way					
sample	**Fe**	**Pb**	**Cd**	**Cu**	**Zn**
PW 3	-11.59	-10.63	-7.23	-5.36	-5.39
PW 8	-11.74	-13.87	-7.81	-7.55	-5.83
PW 10	-11.82	-11.87	-7.23	-6.66	-5.42
PW 12	-11.69	-13.87	-8.81	-7.51	-5.81
PW 14	-11.53	-9.83	-7.23	-4.97	-5.28
Mean	-11.67	-12.01	-7.66	-6.41	-5.55
S.D	0.12	1.84	0.69	1.20	0.26

C. Assessment According to Contamination Factor (CF) and Degree of Contamination (CD)

The contamination factor and the degree of contamination are used to assess the pollution load of the sediments with respect to heavy metals. The CF for each metal is calculated following Manoj and Padhy (2012) as follows:

$$CF = \frac{\textit{Measured concentration of metal}}{\textit{Background concentration of the same metal}} \quad (2)$$

The CD for each sample is calculated as the sum of all contamination factors (Ahdy and Khaled, 2009). The CF and CD values for the two road samples are shownin Table 7. Results show that CF in all samples is < 1, indicating low heavy metal contamination and CD is < 6 in all samples implying low degree of contamination (Table 7).

Table 7: Results of Contamination Factor, Degree of Contamination and Pollution Load Index PLI for Jalingo Urban Roads

Sample	**Contamination Factor (CF)**					**CD**	**PLI**
	Fe	**Pb**	**Cd**	**Cu**	**Zn**		
Hammaruwa way							
HW 3	0.00048	0.00015	0.0067	0.013	0.024	0.044	0.0027
HW 9	0.00044	0.0001	0.0067	0.0078	0.027	0.042	0.0028
HW 15	0.00046	0.00005	0.0033	0.0138	0.027	0.045	0.0031
HWL1 1m	0.00050	0.00085	0.0100	0.1380	0.035	0.184	0.0073
HWL1 2m	0.00048	0.00015	0.0100	0.0100	0.029	0.050	0.0029
Mean	0.00047	0.00026	0.0073	0.0370	0.028	0.073	0.0038
S.D	0.00002	0.00030	0.0030	0.0600	0.004	0.060	0.0020
Palace Way							
Sample	**Contamination Factor (CF)**					**CD**	**PLI**
	Fe	**Pb**	**Cd**	**Cu**	**Zn**		
PW3	0.00049	0.00095	0.0100	0.036	0.036	0.083	0.0057
PW8	0.00044	0.00010	0.0067	0.008	0.026	0.041	0.0023
PW 10	0.00041	0.00040	0.0100	0.015	0.017	0.043	0.0034
PW 12	0.00046	0.00010	0.0033	0.008	0.027	0.039	0.0020
PW 14	0.00051	0.00170	0.0100	0.048	0.039	0.099	0.0070
Mean	0.00046	0.00065	0.0080	0.023	0.029	0.061	0.0040
S.D	0.00004	0.00070	0.0030	0.020	0.009	0.030	0.0020

D. Assessment according to Pollution Load Index (PLI)

The Tomlison Pollution Load Index (Tomlinson *et. a*l., 1980) indicates how much a sample exceeds the heavy metal concentrations for the natural environments and gives an assessment of overall toxicity status for a sample (Angulo, 1996). In this study, PLI is determined following the method proposed by Tomlinson *et. a*l., (1980)as follows:

$$PLI = \sqrt[n]{(CF1\ x\ CF2\ x \ldots\ldots\ldots\ldots CFn)} \quad (3)$$

where CF is the contamination factors and n is the number of parameters. The results of PLI are shown in Table 7. The results of our measurements show that the samples are not polluted. PLI values vary from 0 (unpolluted) to 10 (highly polluted) as follows: PLI = 0 (background concentration); 0 < PLI ≤ 1 (unpolluted); 1 < PLI ≤ 2 (moderately to unpolluted); 2 < PLI ≤ 3 (moderately polluted); 3 < PLI ≤ 4 (moderately to

highly polluted); 4 < PLI ≤ 5 (highly polluted) and PLI > 5 (very highly polluted) (Zhang et al, 2011; Singh et al, 2003).

E. Assessment According to Enrichment Factor (EF).

The EF is a convenient measure of geochemical trends and is used for making comparisons between areas (Sinx and Helz, 1981). It is used to distinguish between anthropogenic and natural sources of metals. The values of EF are obtained using the following equation:

$$EF =: \frac{(M/Fe)sample}{(M/Fe)background} \quad (4)$$

where is the ratio of metal to Fe concentrations of the sample of interest. The is the ratio of the natural background value of the metal to Fe concentration. As we do not have a metal background value for our study area, we used the world average shale values Turakin and Wedepohl (1961). EF values, less than 1.5, suggest that heavy metals are derived mainly from natural (crustal) source such as weathering process while EF values greater than 1.5 suggest that the sources are more likely to be anthropogenic (Zhang and Liu, 2002). The results of EF for this study are shown in Table 8. Results show that all the metals, except for Pb, have been enriched. The mean EF value of Pb in both HW and PW are < 1.5 indicating crustal influence such as weathering process as source of Pb. Other metals - Zn, Cd and Cu - all indicated anthropogenic influx, which is likely from vehicular activities.

Table 8: Table 8. Enrichment factors EF for Jalingo Urban Roads

Sample	Pb	Cd	Cu	Zn
Hammaruwa Way				
HW 3	0.31	13.95	26.97	49.77
HW 9	0.23	15.06	17.57	61.12
HW 15	0.11	7.25	29.98	58.41
HWL1 1m	1.72	20.17	269.84	71.34
HWL1 2m	0.31	20.71	21.17	60.61
Mean	0.54	15.43	73.11	60.25
S.D	0.67	5.47	110.08	7.70
Palace Way				
Sample	**Pb**	**Cd**	**Cu**	**Zn**
PW3	1.95	20.55	74.89	73.76
PW 8	0.23	15.15	18.18	59.80
PW 10	0.97	24.16	35.96	40.18
PW 12	0.22	7.32	18.06	58.72
PW 14	3.25	19.68	94.48	76.25
Mean	1.32	17.37	48.31	61.74
S.D	1.29	6.47	34.69	14.43

4. Conclusion

The concentrations of five heavy metals (Fe, Pb, Cd, Cu and Zn in dust samples collected from two major road from Jalingo metropolis were analyzed. Among the major conclusions of this study are the following:

1. The concentration of heavy metals determined decreased in the order Fe < Zn < Cu <Pb< Cd. This showed Fe, Zn and Cu are the most abundant elements in the dust samples. Based on the USEPA sediment quality guidelines, the concentrations of these metals are within the acceptable level and thus the dust samples were not polluted.
2. The strong positive inter-correlation between Fe, Pb, Cd, Cu and Zn suggests that the metals originate from similar sources.
3. Results of geo-accumulation index, degree of contamination and PLI points to the low contamination and unpolluted nature of the dust samples.
4. Analysis of the Enrichment factor, however, showed that apart from Pb, all other metals analyzed are enriched and the enrichment comes from anthropogenic activities. It is evident that these heavy metals may increase over time if proactive steps are not taken to check pollution sources like vehicular emissions, which may pose serious health risks in the near future.
5. It is necessary to conduct further studies on the accumulation of heavy metals to ensure effective protection and management of urban environment. Finally, the results obtained from the present work may hopefully provide a significant reference value for future studies of these areas and other regions in Taraba State, Nigeria

References

[1] Adedeji, O. H., Olayinka, O.O., Oyebanji, F. F. (2013): Assessment of traffic related heavy metals pollution of roadside soils in emerging urban centres in Ijebu-North Area of Ogun State, Nigeria, J. Appl. Sci. Environ. Manage. Vol. 17 (4): 509-514.

[2] Ahdy, H. H. H. and Khaled, A. (2009): Heavy metals contamination in sediments of the Western Part of Egyptian Mediterranean Sea. Aust. J. Basic and Applied Sci. 3: 3330-3336.

[3] Angulo, E. (1996): The Tomlison Pollution Load Index Applied to Heavy Metal "Mussel-watch"Data: A useful Index to Assess Coastal Pollution. Sci. Total Environ., 187: 49-56.

[4] Arowolo, T. A., Bamgbose, O. and Odukoya, O. O. (2000): The chemical forms of lead in roadside dust of metropolitan Lagos, Nigeria. Global J. Pure and Applied Sci., Vol. 6, No. 3, 483-487.

[5] Barakat, A., El Baghdadi, M., Rais, J. and Nadem, S. (2012): Assessment of Heavy Metal in Surface Sediments of Day River at Beni-Mellal Region, Morocco. Research Journal of Environmental and Earth Sciences, 4 (8): 797-806

[6] Crosby, C. J. Application of mineral magnetic measurements as a pollution proxy for urban road deposited sediment. PhD Thesis, University of Wolverhampton. 353 pp, 2012

[7] El-Hasan, T., Batarseh, M., Al-Omari, H., Ziadat, A., El-Alali, A., Al-Naser, F., Berdainer, B. W. and Jiries, A. (2006): The distribution of heavy metals in urban street dusts of Karak City, Jordan. Soil and Sediment Contamination, 15: 357- 365

[8] Hakanson, L. (1980): Ecological Risk Index for Aquatic pollution Control. A Sedimentological Approach Water Res. 14: 975-1001.

[9] Hopke, P. K., Lamb, R. E., and Natush, D. F. S. (1980): Multielemental Characterization of Urban Roadway Dust. Env. Sci. Technol. 14: 164 – 172.

[10] Lu, S. G., Bai, S. Q., Cai, J. B., C. and Xu, C. (2005): Magnetic properties and heavy metal contents of automobile emission particulates. J.Zhejiang Univ. Sci. B. V. 6(8): 731-735. Doi: 10.1631/jzus.2005.B0731.

[11] Lu, S. G., Bai, S. Q. and Xue, Q. F. (2007): Magnetic Particles as Indicators of Heavy Metals Pollution in Urban Soils: A case Study from the City of Luoyang, China. Geophys. Journ. Inter. 171: 603 – 612.

[12] Manoj, K., Kumer, B. and Padhy, P. K. (2012): Characterization of materials in water and sediments of Subarnarekha River along the projects sites in Lower Basin, India. Universal Journal of Environmental Research and Technology, vol.2 issue 5: 402-410.

[13] Muller, G. (1979): Heavy metals in the sediments of the Rhine Changes Seity. Umsch. Weiss. Tech., 79: 778-783.

[14] Muller, G. (1981): The heavy metal pollution of the sediments of Neckars and its tributary: An Inventory. Chem. Zeitung, 105: 157-164.

[15] Olukanni, D. O. and Adeoye, D. O. (2012): Heavy metal concentrations in roadside soils from selected locations in the Lagos metropolis, Nigeria. International Journal of Engineering and Technology, Vol. 2, No. 10, 1743-1751.

[16] Popoola, O. E., Bamgbose, O., Okonkwo, O. J., Arowolo, T. A., Odukoya, O. and Popoola, A. O. (2012): Heavy metals contents in playground topsoil of some public primary schools in metropolitan Lagos, Nigeria. Research Journal of Environmental Earth Sciences. Vol. 4, No. 4, 434-439

[17] Robertson, D. J., Taylor, K. G. and Hoon, S. R. (2003): Geochemical and mineral magnetic characterization of urban sediments particulates, Manchester, UK. Applied Geochemistry 18: 269-282.

[18] Saha, P. and Hossain, M. D. (2011): Assessment of heavy metal contamination and sediment quality in the Buriganga River, Bangladesh. 2nd International Conference on Environmental Science and Technology IPCBEE, Vol. 6, IACSIT Press, Singapore.

[19] Salah, E. A. M., Zaidan, T. A. and Al-Rawi, A. S. (2012): Assessment of heavy metals pollution in the sediments of Euphrates River, Iraq. Journal of Water Resources and Protection, 4, 1009-1023.

[20] Singh, A. K., Hasnain, S. I. and Banerjee, D. K. (2003). Grain size and geochemical portioning of heavy metals in sediments of the Danoder River - a tributary of the lower Ganga India, Environmental Geology, 39, 90-98.

[21] Sinx, S. A. and Helz, G. R. (1981): Regional geochemistry of trace elements in Chesapeake Bay sediments. Environ. Geol., vol. 3: 315-323.

[22] Tomlinson, D. L., W ilson, J. R., Harris, C. R. and Jeffrey, D. W. (1980): Problems in the assessment of heavy metals levels in estuaries and the formation of a pollution index. Helgol. Wiss. Meeresunters, 33: 566-575.

[23] Turakin, K. K. and Wedepophl, K. H. (1961): Distribution of the elements in some major units of the Earth's Crust. Geol. Soc. Am. Bull., 72: 175-192.

[24] Zhang, J. and Liu, C. L. (2002): Riverine composition and estuarine geochemistry of particulate metals in China-weathering features, anthropogenic impact and chemical fluxes. Estuar. Coast. Shelf. S. 54: 1051-1070.

[25] Zhang, C., Qiao, Q., Piper, J. D. A. and Huang, B. (2011) Assessment of heavy metal pollution from Fe- smelting plant in urban river sediments using environmental magnetic and geochemical methods. Environ. Poll. 159: 3057 – 3070

The Jordan Journal of Earth and Environmental Sciences (JJEES)

INSTRUCTIONS TO AUTHORS:

The Jordan Journal of Earth and Environmental Sciences (JJEES) is the national journal of Jordan in earth and environmental sciences. It is an internationally refreed journal dedicated to the advancement of knowledge. It publishes research papers that address both theoritical and applied valuable subjects and matters in both Arabic and English languages in the various fields of geoscience and environmental disciplines. JJEES is published quarterly by the Hashemite University.

Submitted articles are blindly and rigorously reviewed by distinguished specialists in their respected fields.

The articles submitted may be authenitic research papers, scientific reviews, technical/scientific notes.

SUBMISSION OF PAPERS

Online: For online submission upload one copy of the full paper including graphics and all figures at the online submission site, accessed via http://jjees.hu.edu.jo. The manuscript must be written in MS Word Format. All correspondence, including notification of the Editor's decision and requests for revision, takes place by e-mail and via the Author's homepage, removing the need for a hard-copy paper trail.

By Mail: Manuscripts (1 original and 3 copies) accompanied by a covering letter may be sent to the Editor-in-Chief. However, a copy of the original manuscript, including original figures, and the electronic files should be sent to the Editor-in-Chief. Authors should also submit electronic files on disk (one disk for text material and a separate disk for graphics), retaining a backup copy for reference and safety.

Note that contributions may be either submitted online or sent by mail. Please do NOT submit via both routes. This will cause confusion and may lead to delay in article publication. Online submission is preferred.

FORMATE GUIDE:

1. The research papers should be printed on one side of the paper, be duoble-line spaced, have a margin of 30 mm all around, and no more than 30 pages (7,500 words, font size 13). The title page must list the full title and the names and affiliations of all authers (first name, middle name and last name). Also, their addresses, including e-mail, and their ranks/positions must be included. Give the full address, including e-mail, telephone and fax, of the author who is to check the proof.

2. The research must contain the title and abstract, keywords, introduction, methodology, results, discussion, and recommendations if necessary. The system of international units must also be used. Scientific abbreviations may be used provided that they are mentioned when first used in the text. Include the name(s) of any sponsor(s)of the research contained in the paper, along with grant number(s).

3. Authors should submit with their paper two abstracts, one in the language of the paper and it should be typed at the beginning of the paper followed by the keywords before the introduction. As for the other abstract, it should be typed at the end of the paper on a separate sheet. Each abstract should not contain more than 200 words.

4. Captions and tables should be numbered consecutively according to their occurrence in the research with headings. When mentioned in the text, the same consecutive numbers should be used. Captions and tables must be typed on separate sheets of paper and placed at the end of the paper.

5. The author(s) should submit a written consent that he or she will not publish the paper in any other journal at the same time of its publication in JJEES. After the paper is approved for publication by the editorial board, the author does not have the right to translate, quote, cite, summarize or use the publication in the other mass media unless the editor-in-chief submits a written consent according to the policy of JJEES. Submitted material will not be returned to the author unless specifically requisted.

6. DOCUMENTATION:

- References:

a. To cite sources in the text, use the author-date method; list the last name(s) of the author(s), then the year. Examples: (Holmes, 1991); (Smith and Hutton 1997).

b. In the event that an author or reference is quoted or mentioned at the beginning of a paragraph or sentence or an author who has an innovative idea, the author’s name is written followed by the year between two brackets. Example: Hallam(1990).

c. If the author’s name is repeated more than once in the same volume, alphabets can be used. Example: (Wilson, 1994 a; Wilson, 1994 b).

d. Footnotes may be used to solve any ambiguity or explain something as in the case of a term that requires illustration. In this case, the term is given a number and the explanation is written in a footnote at the bottom of the page.

e. If the number of authors exceeds two, the last name of the first author followed by et. al. is written in the text. Example: (Moore et. al.). Full names are written in the references regardless of their number.

f. Prepare a reference section at the end of the paper listing all references in alphabetical order according to the first author's last name. This list should include only works that been cited.

- Books:

Hunt, J. 1996. Petroleum Geochemistry and Geology. 2nd Ed., H. W. Freeman and Company, New York.

- Chapter in a book:

Shinn E. A., 1983. Tidal Flat Environment, In: Carbonate Depositional Environments, edited by Scholle, P. A., Bebout, D. G., and Moore, C. H., The American Association of Petroleum Geologists, Tulsa, Oklahoma, U.S.A. pp. 171-210.

- Periodicals:

Sexton, P. F., Wilson, P. A.,and Pearson, P. N., 2006. Paleoecology of Late Middle Eocene Planktonic Foraminifera and Evolutionary Implication, Marine Micropaleontology, 60(1): 1-16.

- Conferences and Meetings:

Huber, B. T. 1991. Paleogene and Early Neogene Planktonic Foraninifer Biostratigraphy of Sites 738 and 744, Kerguelen Plateau (southern Indian Ocean). In: Barron, J., Larsen, B., et. al. (Eds.), Proceedings of the Ocean Drilling Program. Scientific Results, vol. 119. Ocean Drilling Program, College station, TX, pp. 427-449.

- Dissertations:

Thawabteh, S. M. 2006. Sedimentology, Geochemistry, and Petrographic Study of Travertine Deposits along the Eastern Side of the Jordan Valley and Dead Sea, M. Sc. Thesis, The Hashemite University.

- Unpublished:

Makhlouf, I. M. and El-Haddad, A. 2006. Depositional Environments and Facies of the Late Triassic Abu Ruweis Formation, Jordan, J. Asian Earth Sciences, England, in Press.

- Illustrations:

a. Supply each illustration on a separate sheet, with the lead author's name, the figure number and the top of the figure indicated on the reverse side.

b. Supply original photographs; photocopies and previously printed material are not acceptable.

c. Line artwork must be high-quality laser output (not photocopies).

d. Tints are not acceptable; lettering must be of reasonable size that would still be clearly legible upon reduction, and consistent within each figure and set of figure.

e. Electronic versions of the artwork should be supplied at the intended size of printing; the maximum column width is 143 mm.

f. The cost of printing color illustrations in the Journal may be charged to the author(s).

7. Arranging articles in JJEES is based on the editorial policy.

8. The author should submit the original and two copies of the manuscript, together with a covering letter from the corresponding author to the Editor-in-Chief.

9. The editorial board's decisions regarding suitability for publication are final. The board reserves the right not to justify these decisions.

10. In case the paper was initially accepted, it will be reviewed by two specialized reviewers.

11. The accepted papers for publication shall be published according to the final date of acceptance.

12. If the author chooses to withdraw the article after it has been assessed, he/she shall reimburse JJEES the coast of reviewing the paper.

13. The author(s) will be provided with one copy of the issue in which the work appears in addition to 20 off prints for all authors. The author(s) must pay for any additional off prints of the published work.

14. Statement transferring copyright from the authors to the Hashemite University to enable the publisher to disseminate the author's work to the fullest extent is required before the manuscript can be accepted for publication. A copy of the Copyright Transfer Agreement to be used (which may be photocopied) can be found in the first issue of each volume of JJEES.

15. Articles, communications or editorials published by JJEES represent the sole opinion of the authors. The publisher bears no responsibility or liability whatsoever for the use or misuse of the information published by JJEES.

16. Submission address:

Prof. Dr. Eid A. Al-Tarazi
Editor-in-Chief,
Jordan Journal of Earth and Environmental Sciences,
The Hashemite University,
P.O. Box 150459, Zarqa, 13115, Jordan.
Phone: 00962-5-3903333 / Ext. 4229
Fax: 00962-5-3826823
E-Mail: jjees@hu.edu.jo
http:// jjees.hu.edu.jo/

المملكة الأردنية الهاشمية

صندوق دعم البحث العلمي

الجامعة الهاشمية

المجلة الأردنية
لعلوم الأرض والبيئة

JJEES

مجلة علمية عالمية محكمة

المجلد (٧) العدد (١)

http:// jjees.hu.edu.jo/

ISSN 1995-6681

المجلة الأردنية لعلوم الأرض والبيئة
مجلة علمية عالمية محكمة

المجلة الأردنية لعلوم الأرض والبيئة: مجلة علمية عالمية محكمة ومفهرسة ومصنفة، تصدر عن الجامعة الهاشمية وبدعم من صندوق البحث العلمي– وزارة التعليم العالي والبحث العلمي، الأردن.

هيئة التحرير

ترسل البحوث إلى العنوان التالي:

أ. د. عيد عبد الرحمن الطرزي

رئيس تحرير المجلة الأردنية لعلوم الأرض والبيئة

عمادة البحث العلمي والدراسات العليا

الجامعة الهاشمية

الزرقاء ١٣١٣٣ – الأردن

هاتف ٣٩٠٣٣٣٣–٥–٩٦٢+ فرعي ٤٢٢٩

Email: jjees@hu.edu.jo, Website: www.jjees.hu.edu.jo

المملكة الأردنية الهاشمية
صندوق دعم البحث العلمي
الجامعة الهاشمية

المجلة الأردنية لعلوم الأرض والبيئة

JJEES

مجلة علمية عالمية محكمة

تصدر بدعم من صندوق دعم البحث العلمي

http://jjees.hu.edu.jo/

المجلد (٧) العدد (١) ISSN 1995-6681 حزيران ٢٠١٥ / شعبان ١٤٣٦